# MODELLING AND TESTING SMART AILERON SERVO TABS: DEVELOPING SIMULATION TOOLS FOR SMART MATERIALS

VELAPHI MSOMI

Submitted in partial fulfilment of the requirements for the degree

of

DOCTOR OF TECHNOLOGY IN MECHANICAL ENGINEERING

at the

CAPE PENINSULA UNIVERSITY OF TECHNOLOGY

May, 2015

**To my wife, Simphiwe Nancy, who supported and encouraged me**

**To my son, Ayabonga, who motivated me**

**To my daughter, Jesunathi, who brought smile to my face**

## ACKNOWLEDGEMENTS

As this dissertation represents the culmination of lifetime spent learning, it seems inappropriate to begin by acknowledging anyone other than my Creator and the Lord Jesus Christ for strengthening me during tough times.

Many thanks go to my advisor, Professor G.J. Oliver for the directions he gave me during this difficult level of study. I would like most of all his patience with me during the hard time of my life and his tolerance is incomparable. I would also like to thank my co-supervisor, Associate Professor O. Philander, for opening this study opportunity and the confidence he had on me. I would also like to thank Professor J. Gryzagoridis for his encouraging words and the facts that he gave me during the no-hope moments. I am thankful to the CPUT Mechanical Engineering Workshop staff by their support they provided to me. I am thankful to Mr Vuyani Moni (Senior Technician) for allowing and assisting me in performing the experiments of this thesis.

Ngithi ngasekugcineni angibonge umndeni wami obungeseka njalo nokungipha isibindi sokuqhubeka nalapho ithemba seliphela. Ikakhulukazi unkosikazi wami obehlezi engipha amazwi enduduzo uma isimo salomsebenzi singabonakali. Ngingelibala umama wethu, M.Z. Msezane, obehlezi evuma ngasosonke isikhathi uma kukhona esikucelayo kuye.

**Disclaimer**

I would also like to thank Airbus Company for their financial support and for initiating the project. It should be noted that there are no experimental or numerical data in this work verified by Airbus Company.

**MODELLING AND TESTING SMART AILERON SERVO TABS: DEVELOPING SIMULATION TOOLS FOR SMART MATERIALS.**

Supervisor: Professor G.J. Oliver

Co-supervisor: Associate Professor O. Philander

## ABSTRACT

This dissertation addresses the development and the testing of a simulation tool to be used to predict the behaviour of smart material/structures. Along with the development of the simulation tool, a new form of the model describing the behaviour of shape-memory alloy was developed and implemented. The proposed model was developed based on the existing cosine model, conventionally used in literature, but it uses hyperbolic tangent functions. The hyperbolic tangent function was chosen so as to allow the simulation of any range of temperatures. Experiments were performed to obtain the parameters to be used in the simulation and to validate the numerical results. Two different simulations were performed: a one dimensional FEA analysis with a two dimensional orientation (NiTi SMA wire simulation) and a three dimensional FEA analysis (NiTi SMA plate) [Msomi and Oliver, 2015]. Alongside the FEA analysis, two experiments were performed with the purpose of obtaining the material parameters to be used in FEA analysis and to compare the FEA results to the experimental results.

A steel beam SMA experiment and a smart aileron deflection experiment were performed. The one dimensional FEA analysis was performed using a C++

program implementing combined beam and bar elements. The displacement was calculated using a prescribed thermal history causing a phase change in the SMA material which produces equivalent nodal forces. The solution variable for this particular analysis is only displacement with an associated solution of the phase kinetic equations and the temperature field is input from experimental data, not solved for.

The smart aileron deflection FEA analysis was performed on the ABAQUS simulation package using C3D8T elements, and the developed material algorithm was incorporated into ABAQUS using the available FORTRAN user written material subroutine (UMAT). The user material subroutine was for a coupled thermo-mechanical solution with associated phase kinetic equations and was solved as a coupled temperature-displacement problem in ABAQUS. For the implementation into ABAQUS, the algorithmic tangent moduli for the non-linear solution needed to be prescribed in the user material subroutine along with the determination of the state of stress for a total strain and temperature state. The temperature state is also dependent on the phase kinetics through the latent heat effect. There is no dissipation of elastic strain energy considered in the material implementation, in keeping with the research goals.

The experimental and numerical results are compared in the text and the FEA results show good correlation with the experimental results in both types of analysis following the material parameter estimation within the one dimensional finite element solution.

## TABLE OF CONTENTS

**Page**

# LIST OF TABLES

**Table** **Page**

## LIST OF FIGURES

**Figure** **Page**

# CHAPTER 1

## INTRODUCTION

### 1.1 Problem statement

Shape-memory alloys (SMAs) are widely used in applications that don't make use of actuation, especially in Medical Applications [Otsuka and Wayman, 1999]. However, in order to use SMAs for actuation we need an improvement of control, requiring well-defined models. These models are needed in the design of controllers to account for the non-linear behaviour that can arise from the shape-memory effect or pseudo-elasticity present in SMAs which will be explored later. So far, different types of commercial finite element software packages have been used to mimic the behaviour of different structures, but few of these FE packages can be used to simulate the behaviour of shape-memory alloys without user written additions [Auricchio and Taylor, 1997; Seelecke and Papenfuss, 2000; Auricchio et al., 2003; Dong et al., 2008]; which brings us to the purpose of developing a simulation tool.

### 1.2 Objectives

This thesis is aimed at developing an engineering tool that can be used as the basis of designing the complex shape/structure of a 'smart' aileron. The following procedure is used to accomplish the objective:

- The finite elements analysis (FEA) that represents a 'smart' aileron was developed through Solidworks drawing software.

- The developed FEA was integrated into a commercially available FEA package called ABAQUS.
- A comparative study between predicted and experimental results was conducted.

## 1.3 Background

Smart materials are said to be smart due to their response to external stimuli. They are materials that have one or more properties that can be changed in a controlled manner by external stimuli. Some of the external stimuli that can act upon these materials include stress, temperature, moisture, pH, electric or magnetic fields, hydrostatic pressure, etc. “Smart materials receive, transmit or process a stimulus and respond by producing a useful effect that may include a signal that the materials are acting upon it” [Myer Kutz ,1990]. Smart materials are divided into various groups such as:

- Piezoelectric materials - change shape in response to an applied electric field.
- Electrostrictive materials - change dimensions in response to an applied electric field.
- Magnetostrictive materials - change dimensions in response to an applied magnetic field.
- Rheological materials (solids or fluids) - change states instantly through the application of magnetic or electric fields.

- Thermo-responsive materials (Shape-memory Alloys) - change shape in response to heat or cold.
- pH-sensitive materials - change colour as a result of change in pH.
- Electrochromic materials - change optical properties with the application of voltage.
- Smart gels - absorb or release fluids in response to any chemical or physical stimuli.

Most of the well-known materials have been investigated for complex applications. The predominant smart materials used are shape-memory alloys (SMAs) due to their simple operation. Due to their unique properties, smart materials are also termed as 'intelligent' materials. Shape-memory alloys fall in the sphere of being 'intelligent' materials due to the unique properties they exhibit i.e. shape-memory effect and pseudo-elastic effect. SMAs exhibit these effects by temperature variations.

- Shape-memory effect (SME): The SMA is loaded at low temperature (normally at room temperature or below austenitic start temperature) such that an apparent plastic deformation is caused, which is maintained until an increase in temperature causes the deformation to disappear completely.
- Pseudo-elastic (super-elastic) effect: The SMA is loaded at a high temperature (above austenitic finish temperature) to full transformation at

the de-twinned martensitic state and then unloaded fully transforming back to the austenitic state, while recovering the entire transformation strain [Duerig et al.,1990, Brinson,1993].

These two unique properties that SMA materials exhibit are illustrated graphically in **figure 1.1**. These properties, which are functions of temperature,T, and stress,σ, allow SMAs to be the best candidates in many innovative engineering applications, such as active shape and vibration control, shape-memory sensors and actuators, aerospace industries and medical implants [Duerig et al. 1990]. The symbols $\varepsilon$, $M_s$, $M_f$, $A_s$ and $A_f$ shown in figure 1.1 represent strain, martensite start temperature, martensite finish temperature, austenitic start temperature and austenitic finish temperature, respectively. SMAs have high stiffness which gives sufficient energy densities, and their fast response times provide high bandwidth. SMAs exhibit these unique properties due to transformation that occurs at microstructural level i.e. martensite transforms to austenite and the reverse [Brinson, 1993]. In the stress-free state, an SMA material at high temperature exists in austenite/parent phase. An austenitic phase has a body centred cubic crystal structure. When the temperature of the material decreases, the parent phase transforms into

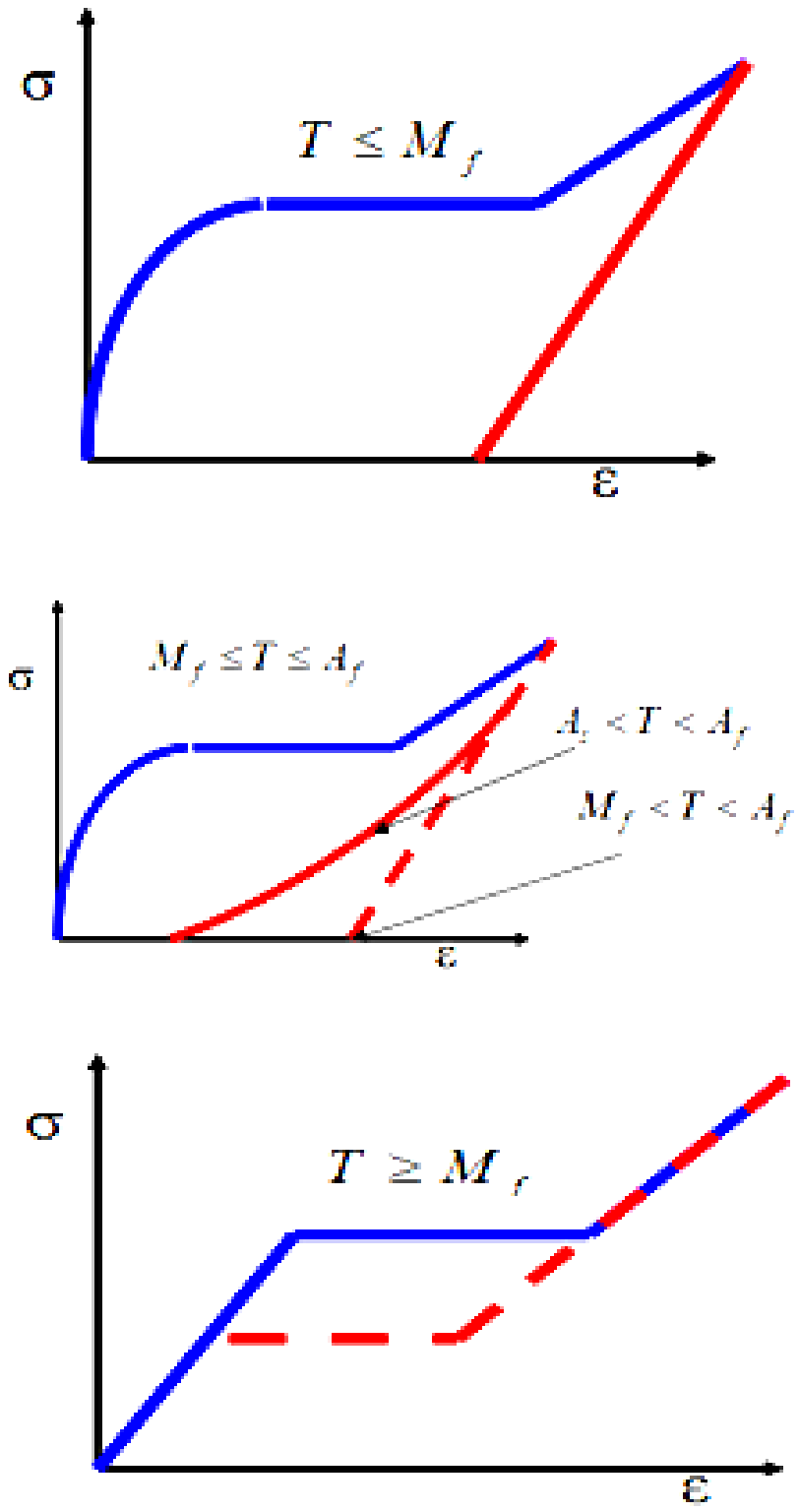


**Figure 1. 1:Schematic representation of (a) Shape-memory effect, (b) Partial Pseudo- elastic effect and (c) Pseudo-elastic effect [Brinson,1993].**

Martensite which is normally a face-centred cubic crystal structure. In the stress-free state the martensite phase exists in multiple variants that are crystallographically similar, but are oriented in different planes. Since the behaviour of the SMA material depends on stress and temperature and is intimately connected with the crystallographic phase of the material and thermodynamics underlying the transformation process, the formulation of adequate macroscopic laws is necessarily complex [Brinson and Huang, 1996].

## 1.4 Related Literature survey

### 1.4.1 Review on Shape-memory alloy models

Shape-memory alloy (SMA) is a material that can configure its original shape upon heating after plastic deformation. In the past, SMA behaviour has been modelled from various perspectives such as thermomechanical, thermodynamics, phenomenological and finite element analysis models. Achenbach [1989] has developed thermodynamic models which break down the SMA into small elements called lattice particles. The lattice particles are arranged in layers whose shape and potential energy are temperature or stress dependent.

Achenbach's model was further extended by Seelecke and Mueller [2004]. The model extension was made so as to make quantitative predictions in the use of Helmholtz free energy and further to simulate SMA mechanical behaviour such

as residual and elastic deformation, resulting from shape recovery and flipping of layers when martensite layers convert to austenite. Tanaka et al. [1994] used the Claussius-Duhem inequality to develop a phenomenological model which derives thermomechanical equations and kinetics of transformation.

A phenomenological model refers to an attractive choice which directly describes the material behaviour and also is used to control experiments. It is faster (computationally), simpler and more conducive in controlling loops. Furthermore, to model pseudo-elasticity, an exponential function is used to qualify the relationship of the martensite fraction to the stress and temperature to reproduce SMA behaviour in the stress-temperature and stress-strain planes. Liang and Rogers [1990] used a similar approach to Tanaka but with cosine functions added.

Brinson and Lammering [1993] and Amalraj et al. [2000] developed finite element models. A micromechanics model derived by Goo and Lexcellent [1997] is based on Helmholtz free energy. They developed equations describing kinetic relationships in SMA, martensite nucleation and the reorientation of martensite variants. The pseudo-elastic behaviour can be described using their model.

The separation of the martensite fraction into temperature-induced and stress-induced parts and the introduction of twinned and de-twinned martensite was created by Brinson [1993] by extending Tanaka's, and Liang and Roger's work.

This separation was done so as to model low temperature shape-memory effect (SME) in addition to pseudo-elasticity. A phenomenological model similar to Tanaka's was developed by Ikuta [1990] where variables are added so as to define minor loops but no extension to minor loop behaviour.

Madill and Wang [1994] extended Ikuta's [1990] work by using *switching conditions* to describe the SMA behaviour under partial temperature cycling. This model deals with constant stress. Madill further developed equations describing the loading behaviour of martensite and austenite. Auricchio and Taylor [1997], and Auricchio [2001] proposed a phenomenological model including large deformations.

The macroscopic free energy function depending on internal variables was introduced by Auricchio and Taylor [1997], and Auricchio [2001], which describes the state of the phase transition. This transformation coincides with a martensitic volume fraction where only one single phase variant is considered. The activation of the transition is ruled by a Druger-Prager flow criterion known from plasticity in soil and concrete materials.

The micromechanically based model of Thamburaja and Anand [2001] is able to describe the effect of super-elasticity (pseudo-elasticity). It is based on crystal plasticity whereas the polycrystalline structure of SMA is approximated by the Taylor model. Reese and Christ [2008] presented new concepts for the modelling

of the super-elastic effect in the finite strains regime. The assumption is that the deformation gradient can be split into three parts: an elastic deformation gradient, a second part accounting for the deformation occurring during the phase transition and a third one correlating with the energy dissipation. Moreover, a numerical algorithm was suggested which uses the spectral decomposition, allowing the numerical computation of the model variables in a closed form.

Fremond [1996] developed a three-dimensional model that is able to reproduce the pseudo-elastic and shape-memory effects by using three internal variables that should obey internal constraints related to the coexistence of the different phases. Afterwards, a new one-dimensional model, based on the original Fremond's model, is developed and reported in CISM Courses and Lectures [James,2000;Savi et al.,2002].

This new model allows the description of more phenomena including the effect of thermal and plastic strains, and including a plastic phase transformation coupling, which makes the two-way shape-memory effect (*TWSME)* description possible. This model also describes tension-compression asymmetry—a point of great relevance to actuator design.

In one of the early numerical implementations of SMA models, Brinson and Lammering [1993] studied the finite element analysis of the behaviour of SMA and their applications using 1-D truss elements. Newton's method was applied on both the weak form of momentum balance and the SMA law, and thus,

replaced the materially and geometrically non-linear problem into a sequence of linear problems solved numerically. In another study, Trochu and Qian [1997] performed a numerical simulation of pseudo-elasticity using geometrically non-linear finite elements. Panahandeh and Kasper [1997] presented a general formulation for coupled thermomechanical simulations of SMAs in the context of the finite element method. They proposed a SMA model composed of a set of non-linear algebraic equations that did not require integration of rate type evolution equations.

They employed the isothermal fractional-step (staggered) method to additively separate the coupled thermomechanical problem into a thermal and mechanical problem. Each problem is then cast into its weak form and discretized in space using the finite element method. The resultant set of algebraic equations is solved globally using the Newton-Raphson iteration scheme.

Numerical simulations are performed in the context of the truss finite element and its extension to multiple dimensions is shown. Govindjee and Kasper [1998] simulated a 1-D SMA model of Uranium-Niobium alloy accounting for plastic strains using the radial return mapping algorithm, which is a special case of the closest point projection algorithm.

Numerous studies have been performed based on 1-D computational implementation of SMA models. With regard to 3-D implementation, Reisner et al. [1998] utilized a return mapping algorithm based on the forward Euler

(explicit) time discretization of the relations. Lagoudas and co-workers [2003] have reported a 3-D numerical implementation of SMA models. During their study an SMA model was implemented using the forward Euler integration scheme. In 1996, Lagoudas et al. presented and implemented the 3-D unified thermodynamic model based on the work of Boyd and Lagoudas [1994].

They analysed the response of an active metal matrix composite with different geometric arrangements of embedded SMA fibres using the finite element method. The explicit time discretization of the transformation strain flow rule is carried out using the convex cutting plane return mapping algorithm proposed by Simo and Ortiz [1985]. Lagoudas et al. [1994] further modelled the thermomechanical response of general active laminates with SMA strips using the layer-wise finite element method based on the same time integration algorithm.

Sottos et al.[1996] and Jonnalagadda et al. [1996, 1997 and 1999] have carried out a series of studies based on a 3-D fully coupled temperature-displacement analysis of the transformation of embedded shape-memory alloy wires and ribbons. They employed the commercially available FEA software ABAQUS which solves the field equations associated with mechanical and heat conduction problems simultaneously, using implicit integration for unconditional convergence. Bo and Lagoudas [1999] proposed an extensive 3-D thermomechanical model based on micromechanics, where they also simulated, predicted and compared the cyclic behaviour, minor loops, TWSME and material

identification of 1-D SMA wires with experiments. Moss [1984] emphasised that the return mapping algorithms are driven by strain, making them directly adaptable to the displacement based finite element method. The idea of using the return mapping algorithm is typical for integrating the SMA thermomechanical response.

Qidwai and Lagoudas [2000] have shown that the rate independence and loading history dependence allow the thermomechanical behaviour to be possibly defined by a stress-elastic strain state relation that includes the transformation strain as an internal state variable, differential evolution equation for the transformation strain and a transformation function to determine the onset of phase transformation.

This structure implies that any proven numerical algorithm designed to integrate the rate independent elasto-plastic behaviour can be used to integrate the SMA thermomechanical elastic-transformation model. Return mapping algorithms have been studied extensively over the years in the context of elasto-plasticity for integration of relations.

They are also called elastic predictor-plastic corrector algorithms, where a purely (thermo) elastic *principal (trial) state* is followed by transformation corrector phase (return mapping). The purpose of the corrector part is to enforce continuity in a manner consistent with the prescribed flow rule.

Return mapping algorithms may differ on the basis of the kind of discretization employed to numerically integrate the evolution equations, and the numerical procedure adopted to solve the resultant set of non-linear algebraic equations in the corrector part. Ortiz and Popov [1985] pointed out that most of the return mapping algorithms employ integration rules that are particularly cased of the trapezoidal and midpoint rules, suitably generalized to facilitate satisfaction of the transformation consistency condition.

### 1.4.2 Shape-memory Alloys in Aero-morphing

The following section gives a brief background of the application of smart material in Aero-morphing. The word morphing can be defined as ‘to cause a change in shape’. Morphing aircraft (aero-morphing) design has been reported since 1903 by the Wright brothers when they built their first aircraft. Morphing technology on aircrafts has found increased interest over the last decade because it is likely to enhance performance and efficiency over a wide range of flight conditions.

Dong et al. [2008] designed and manufactured a changeable aerofoil model. They developed a finite element model of skins and simulated the deformation of skins under the control of the discrete points (see Figure 1.2). They measured the deformation of the skins actuated by SMA springs and compared the simulated and experimental results.

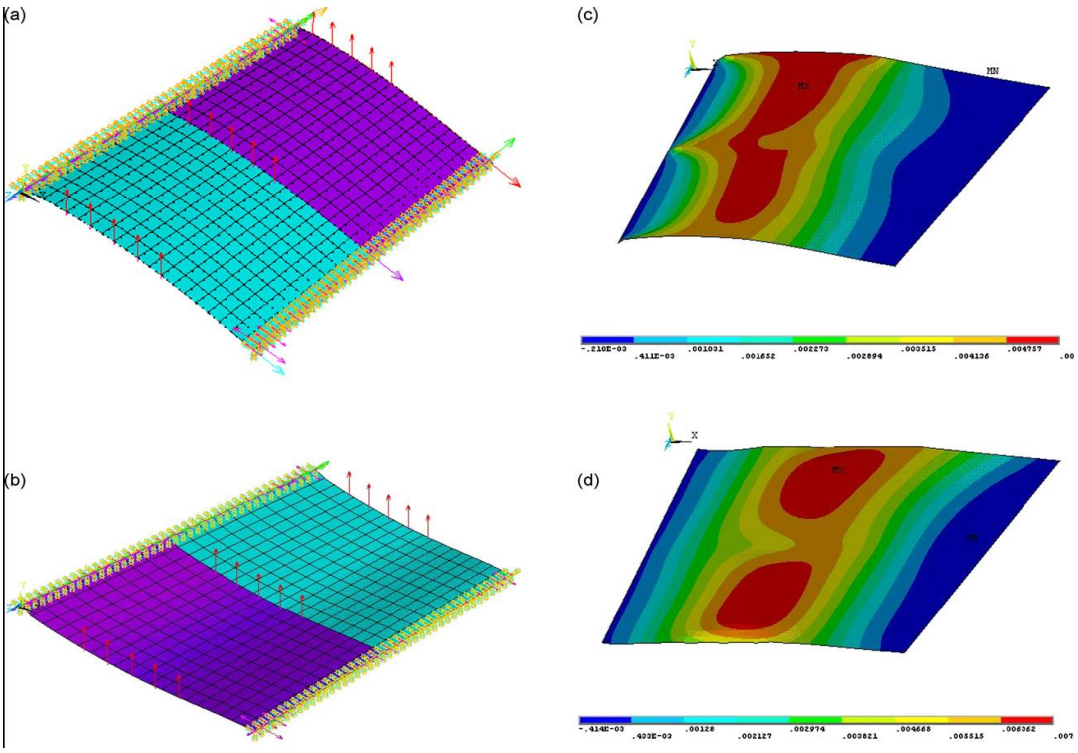


**Figure 1. 2:(a) Finite element model of the upper skin. (b) Finite element model of the lower skin. (c) Deformation displacements of the upper skin. (d) Deformation displacements of the lower skin [Dong et al, 2008].**

Lagoudas et al. [2008] developed a direct numerical simulation to study active material based actuation to develop an active skin for turbulent drag reduction. They used dynamic finite element analysis to investigate the responses of the skin designs to complicated loading sequences. SMA wires have been used for morphing because they can produce considerable deformation but they need to be heated to produce deformation and need to be cooled to return to their original shape.

Flight control surfaces need to have quick response times, while mission adaptive morphing needs to have large deflections, however the response time

for SMAs is slow because of the heating and cooling processes where the heating process is usually much faster than the cooling process for practical implementations, unless there is a convenient heat sink, such as the low temperatures of the atmosphere at high altitude.

The present doctoral research is aimed to develop a very simple computational tool for the analysis of shape-memory alloys through an exploration of the applicability of generalized plasticity to the representation of their behaviour. Specifically, some models that reproduce the shape-memory effect are to be developed and numerically implemented into a finite-element setting. Some applications will be presented in order to show the viability of the proposed approach as an effective tool for the design of devices based on shape-memory alloys. The implementation of the model in the FE code should lead to an actuator design that can be cycled through both heating and cooling phases which therefore might need to account for the two way shape-memory effect.

### 1.4.3 SMA FINITE ELEMENT SIMULATION.

In the past, numerous shape-memory alloys models have been reported [Brinson and Huang, 1996]. Early efforts go back to Tanaka and Tanaka et al. [1986 and 1994]. Their model uses the fraction of martensite as an internal variable and gives a phenomenological equation of state for its dependence on stress and temperature in the form of an exponential function. Liang and Rogers [1990] later modified the model by using a cosine law for the martensite fraction.

However, both versions are only applicable to predict the super-elastic behaviours of the SMAs. Brinson [1993] improved the model by introducing a separation of the martensite fraction into twinned and de-twinned martensites such that the quasiplastic behaviour can be predicted as well. The model was further refined by Bekker and Brinson [1997 and 1998] by using a phase diagram based approach. Boyd and Lagoudas [1996] have developed a model that is derived from irreversible thermodynamics. The model follows the guidelines of the classical theory of rate-independent plasticity with yield conditions triggering the phase transformations and is formulated in a three-dimensional setting. Closed form solutions for damping capacity and actuator efficiency are obtainable from the model. A drawback, however, is the large number of material parameters to be determined. Furthermore, due to its origin from the classical theory of plasticity, the dissipation potential is not chosen from physical reasoning but rather from mathematical arguments like convexity properties. Based on generalized plasticity theory, Aurichio and Taylor [1997] developed a model to predict the super-elastic behaviour of SMA materials. All these models above are rate independent and their suitability for the practical simulation of SMA actuator applications is limited by complexity. The same holds for the recent micromechanical models [Lu and Weng, 1998, Patoor et al,1996, Gao and Brinson, 2002], which, based on the self-consistent average methods, are too complex to be used for the simulation of mostly one-dimensional SMA actuators. In this work, the focus is on a one-dimensional model accounting for both thermodynamic and mechanical aspects. A notable model in this respect has

been developed by Ivshin and Pence [1994] and Wu and Pence [1998]. The model evolves from careful thermodynamic consideration. Despite a lack of physical reasoning, the model appears to be quite powerful with respect to the simulation of SMA actuator behaviour. It includes an energy balance with contributions from convective heat exchange, latent heats and external heat sources, and a number of interesting simulations are displayed in the article titled "Two variant modeling of shape memory materials: Unfolding a phase diagram triple point" (name of journal/article) [Wu and Pence, 1998]. One of the latest models for SMA wires is developed by Shaw [2002]. The model is capable to simulate both super-elastic and shape-memory behaviours of SMAs. The model also takes into account the unstable phase transformation behaviour by including the strain gradient effects and by allowing softening transformation paths. The energy balance and latent heat effects are also included in the model, which also makes it suitable for the simulation of SMA actuators. Another model that has recently been applied to SMA actuator applications has originally been developed by Achenbach and Müller [1985], Achenbach [1989] and Seelecke and Müller [2004]. It uses ideas from statistical thermodynamics and describes the evolution of two martensite fractions based on the theory of thermally activated processes. The coupling with the balance of energy, including latent heat effects due to the phase transformation, makes it possible to reproduce the time-dependent length change of an electric current heated SMA wire under an arbitrary time-dependent load. The attractiveness of the model is based on the fact that the complete load- and temperature-dependent hysteretic behaviour of

SMAs is derived from the energy function alone without any additional loading/unloading criteria. The model can represent both the shape-memory effect and super-elasticity of SMA materials. A very limited number of material parameters, used to construct the free energy, can be identified from only two tensile experiments conducted at two different temperatures. Together with a convenient mathematical structure in the form of an ODE system, allowing for robust numerical integration, these features make the model an attractive candidate for the simulation of SMA actuators and their control behaviour. Due to their complex temperature-dependent and hysteretic behaviour, numerical methods like the finite element method must be used in order to predict the responses of SMA structures and devices. Many simulations of SMA structures and devices using FEM have been reported in many literatures (see, e.g. Auricchio,2004, Trochu and Qian,1997, Lagoudas et al, 2003, Patoor et al, 2006, Amalraj et al, 2000, Krevet & Kohl, 2004, Achenbach & Muller,1985, Achenbach, 1989 & Zhou et al, 2009). However, most of these simulations have been conducted under the assumption of isothermal or homogenous temperature fields without including the non-linear transient heat transfer into the problems. By neglecting the latent heat effects, Amalraj et al. [2000] studied the phase transformation of an SMA wire by solving the heat transfer equation and equation of mechanical deformation separately, using the Galerkin finite element method. Using a very simplified SMA model, Krevet and Kohl [2004] conducted a 3-D finite element simulation of an SMA micro-actuator by solving an electro-thermo-mechanically coupling problem sequentially. Typically, SMA actuators are driven

by electric current heating and convective cooling with the environment, therefore the latent heats due to the phase transformation have to be taken into account if the fully coupled thermo-mechanical problem is to be solved. In order to simulate SMA actuator behaviour that includes both the solution of temperature and displacement, a non-linear transient thermo-mechanically coupled problem needs to be solved. If the variation of the resistivity of SMAs with temperature and mechanical loading is also considered, the problem will become an electro-thermo-mechanically coupled problem.

## 1.5 ORGANIZATION OF THE DISSERTATION.

The dissertation is organized as follows:

- Chapter 1 gives an introduction and literature survey of SMA based on developed models and applications.
- Chapter 2 highlights the available SMA models and the development of the proposed model.
- Chapter 3 describes the experimental performance.
- Chapter 4 gives solution algorithms for the implementation of SMA material into FE programs.
- Chapter 5 describes the experimental setup, performance and equipment used.

# CHAPTER 2

## 2.0 MODELS FOR SHAPE-MEMORY ALLOYS.

Numerous SMA models have been reported since the late ‘80s and ‘90s, all of which are trying to analyse the SMA’s behaviour using different mathematical approaches; Brinson [1993], Brinson & Huang [1996], Seelecke & Müller, [2004], Seelecke & Papenfuss [2000], Auricchio & Taylor [1997], Auricchio [2001], Thamburaja & Anand [2001], Reese & Christ [2008] and Fremond [1996]. Since shape-memory alloy material behaviour depends on stress, temperature is connected with the phase of the material and the thermodynamics underlying the transformation process, the formulation of possible macroscopic laws, is complicated. One feature of many of the descriptions of shape-memory alloy’s behaviour is that the models can generally be separated into two laws governing the transformation behaviour: a mechanical law which establishes the relation between stress, strain and temperature, and a kinetic law which formulates the degree of transformation. The models can be roughly summarized into the following categories:

- Phenomenological models based on the volume fraction of martensite as the internal state variable. These models take into account the dependence of the transformation behaviour on temperature, including shape-memory effect and pseudo-elasticity;
- Models derived from a special free energy formulation;

- Models based on thermodynamic laws;
- Laws based on a model for hysteresis;
- Models based on non-linear thermo-plasticity theory, generalized plasticity, or visco-plastic theory;
- Mathematical models for the dynamics of phase boundary motion;
- Models based on deformation of crystal structure during phase transformation;
- Laws that allow for micro-structural deformation during phase transformation and free energy concept, using an energy dissipation or energy balance approach.

The aim of each of the above models is to describe the behaviour of the SMA from a certain aspect and on a different scale. However, in spite of all these efforts, no single model exists that is able to quantitatively describe the shape-memory alloy's behaviour. This may be due to the very strong effect of micro-structure and processing on the mechanical properties. From an engineering application perspective, the most practical and productive approach is based on phenomenological models, which fit the uniaxial experimental data, without attempting to capture the detailed underlying thermomechanical behaviour. The models selected in this study are frequently used models in the literature and they are all based on the model proposed by Tanaka [1986]. Some frequently used models include Zhou et al. [2009] and Qidwai and Lagoudas [2000]. These

models are known as the models with assumed phase kinetics that consider pre-established simple mathematical functions to describe phase transformation kinetics. These two models are presented in this chapter. The advantage of using one model over another only depends upon the level of complexity required. In general, more extensive models capture a wider range of macroscopic behaviour, but also require additional material testing for the determination of the material's constants. Implementation of the models into engineering codes plays a vital role in the model choice due to possible numerical problems or increased coding and solving times. Thus, the model to be adopted should be chosen according to the application's requirements and experimental capabilities. For this study the model by Liang and Rogers [1990] is chosen and modified as presented in the next sections.

## 2.1 SHAPE-MEMORY ALLOY MODEL

### 2.1.1 PROPOSED SHAPE-MEMORY ALLOY MODEL

This section discusses the formulation of the shape-memory alloy model. The formulated model was based on the model published in the proceedings of the International Conference of Computational Science and its Applications 2011 (ICCSA). It was discovered that some temperature ranges are not catered by the published model, hence the need for the modification.

#### 2.1.1.1 PHASE TRANSFORMATION MECHANISM OF SHAPE-MEMORY ALLOY

The mechanical properties of shape-memory effect and super-elasticity are the results of reversible phase transformation in SMA. There are three kinds of solid phases associated with SMA at different temperatures and stress i.e. austenite, twinned martensite and de-twinned martensite. The illustration [adapted from Bo et al., (2009)] of the microscopic mechanism of the SMA phase transformation is shown in figure 2.1. The phase transformation occurring at a stress-free state is shown in figure 2.1 (A), where austenite transforms to twinned martensite upon cooling and is the reverse upon heating. This type of transformation is also known as a self-accommodating phase transformation because there is no notable macroscopic strain occurring during the transformation.

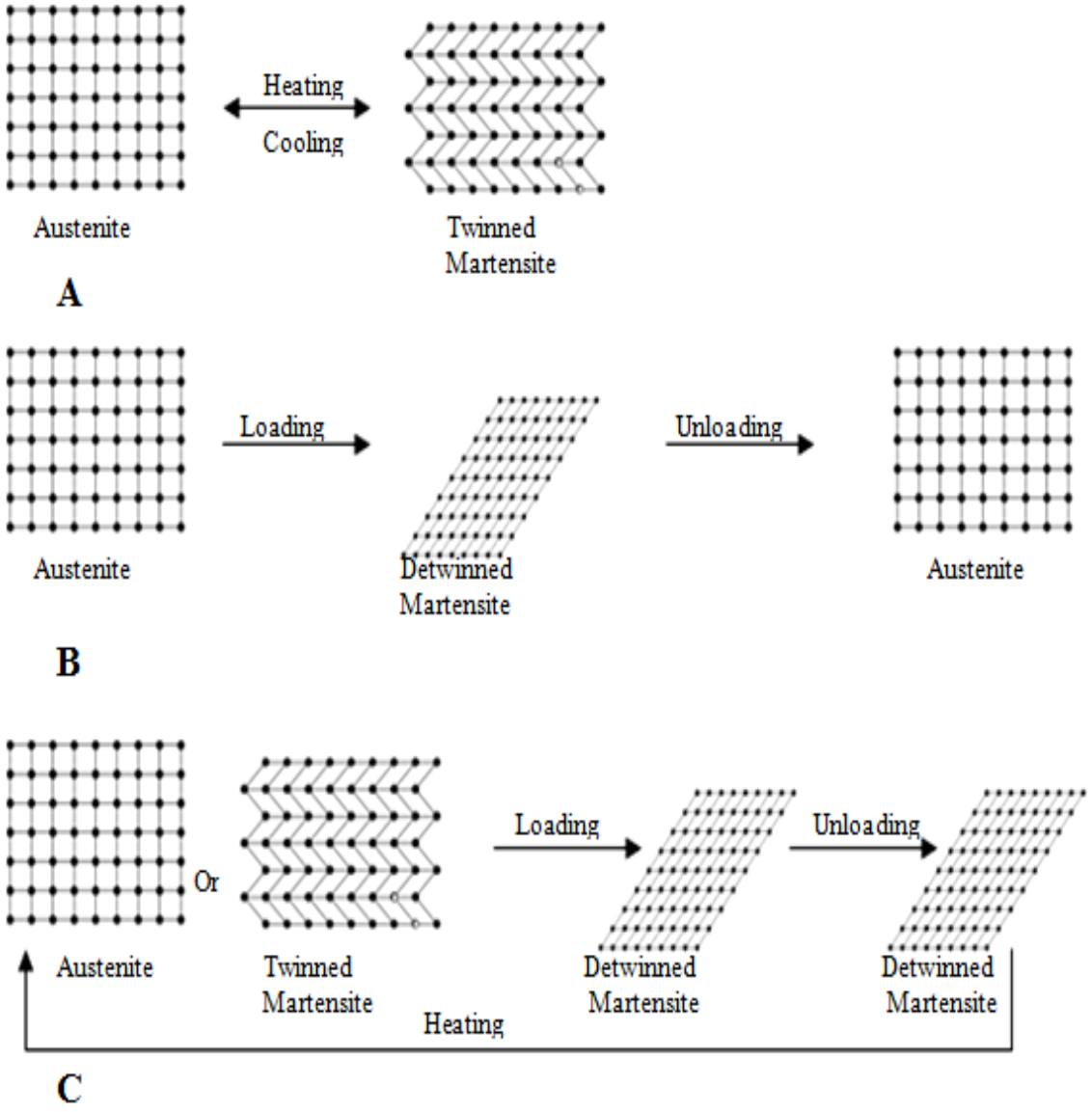


**Figure 2.1: Microscopic mechanism of phase transformation in SMA (A) The phase transformation of self-accommodating, (B) The phase transformation of superelasticity, (C) The phase transformation due to the shape-memory effect [Bo et al. , 2009].**

Figure 2.1 (B) shows the transformation occurring at high temperature (above austenite finish temperature) where austenite transforms to de-twinned martensite during loading and reverse during unloading. The shape-memory

effect mechanism induced by the loading-unloading cycle at temperature below austenite start temperature is shown by figure 2.1 (C). In this case, the twinned martensite transforms to de-twinned martensite upon loading and the de-twinned martensite transforms to austenite upon heat application. Figure 1 reveals that martensite has two states i.e. twinned martensite and de-twinned martensite. Thus, the total martensite volume fraction, ξ, is given by de-twinned martensitic volume fraction, $\xi_s$, and twinned martensite volume fraction, $\xi_t$,

$$\xi = \xi_S + \xi_t \tag{2.1}$$

Brinson [1993] named these transformations as the stress-induced martensite volume fraction and temperature induced volume fraction respectively. Bo et al. [1999] named them as de-twinned martensite volume fraction and twinned martensite volume fraction which accords well with the microscopic mechanism of SMA phase transformation.

#### 2.1.1.2 LIANG AND ROGERS MODEL

The law adopted in their model by Liang and Rogers [1990] is the same as in Tanaka's model. The difference comes in the transformation fraction estimation functions. This model presents an alternative evolution law for the martensite fraction based on a cosine function.

The phase transformation kinetics equation for heating is

$$\xi = \frac{\xi_M}{2}\cos\left[a_A\left(T - A_s\right) + b_A\sigma\right] + \frac{\xi_M}{2} \tag{2.2}$$

The phase transformation for cooling is

$$\xi = \frac{1-\xi_A}{2}\cos\left[a_M\left(T - M_f\right) + b_M\sigma\right] + \frac{1+\xi_A}{2} \tag{2.3}$$

where T is the input temperature

$$a_A = \frac{\pi}{A_f - A_s}, a_M = \frac{\pi}{M_s - M_f} \tag{2.4}$$

are two material constants, and $A_f$, $A_s$, $M_s$ and $M_f$ are austenite final, austenite start, martensite final and martensite start temperatures, respectively. The other two material constants are defined as

$$b_A = -\frac{a_A}{C_A}, b_M = -\frac{a_M}{C_M} \tag{2.5}$$

$C_A$ and $C_M$ indicate the influence of stress on the four transformation temperatures. Furthermore $\xi_M$ and $\xi_A$ are the martensite fractions reached before heating and cooling, respectively.

#### 2.1.1.3 PROPOSED PHASE TRANSFORMATION EQUATION FORMULATION

The law adopted for the proposed model is based on the one adopted by Liang and Rogers [1990] with the difference on the phase transformation estimation functions. In this work we formulated an alternative way to estimate the phase transformation behaviour i.e. hyperbolic tangent functions. The newly formulated phase transformation equations can give a final bound of phase transformation of

ξ = 0.999 which is similar to Tanaka's model. The author discovered that the temperature range used to test the existing model must have a maximum difference of 10°C (i.e. the difference between the martensite start temperature and martensite end temperature, or austenite start temperature and austenite end temperature). When the difference is beyond the maximum temperature difference, the model yields meaningless information. In our case, the difference between the austenite start and finish is about 17°C, so we cannot use the existing model for our application. The model proposed in this work caters for all the temperature ranges. The transformation of martensite to austenite (heating) is described by the following equation:

$$\xi_{M-A} = \xi_M \left\{1 - \tanh\left[\iota_A \left(T - A_s\right) + \vartheta_A\right]\right\}_j \tag{2.6}$$

where $\iota_A$ and $\vartheta_A$ are the material constants that can be calculated as follows

$$\iota_A = \frac{\pi}{4\left(A_f - A_s\right)} \tag{2.7}$$

$$\vartheta_A = \frac{b_A \sigma}{5\pi} \tag{2.8}$$

$A_s, A_f, \sigma$ are austenitic start and austenitic end temperatures and applied stress, respectively. The material constant $b_A$ can be calculated as follows

$$b_A = \frac{-\iota}{C_A} \tag{2.9}$$

Where $C_A$ is the representative of the change in transformation temperatures, $A_s$ and $A_f$, with the applied stress. The transformation of austenite to martensite is described by the following equation

$$\xi_{A-M} = \beta - B\tanh\left[\iota_M\left(T - M_f\right) + \vartheta_M\right] \tag{2.10}$$

Where the material constants, $\beta, B, \iota_M, \vartheta_M$ can be calculated as follows:

$$\beta = 2\left(\frac{1+\xi_A}{2}\right) \tag{2.11}$$

$$B = 1 - \xi_A \tag{2.12}$$

$$\iota_M = \frac{\pi}{4\left(M_s - M_f\right)} \tag{2.13}$$

$$\vartheta_M = \frac{b_M \sigma}{5\pi} \tag{2.14}$$

$M_s, M_f$ are martensitic start and martensitic finish temperatures, respectively. The material constant $b_M$ can be calculated as follows:

$$b_M = \frac{-\iota_M}{C_M} \tag{2.15}$$

where $C_M$ represents the change in transformation temperatures, $M_s$ and $M_f$, with the applied stress. The transformation strain during heating and cooling can be easily be obtained by multiplying equation (2.6) and (2.10) with the maximum recovery strain, $\varepsilon_L$. The value of $\varepsilon_L$ is measured experimentally. However, the transformation strain associated with heating is given by:

$$\varepsilon_{M-A} = \varepsilon_L \xi_{M-A} \tag{2.16}$$

The transformation strain associated with cooling is given by:

$$\varepsilon_{A-M} = \varepsilon_L \xi_{A-M} \tag{2.17}$$

The analytical and numerical formulation together with the corresponding description for this model are presented in the next chapters.

# CHAPTER 3

## 3.1 EXPERIMENTAL PROCEDURES

This chapter describes four types of experiments that were conducted during the study. These experiments were conducted to determine material parameters, test a concept and validate the finite element-based simulation tool developed in this work. A tensile test was conducted with the purpose of analysing the behaviour of a NiTi SMA plate. This experiment was undertaken after a brittle fracture failure occurred during the first attempt at manufacturing a smart aileron. A second set of experiments was aimed at determining the maximum load for the NiTi SMA wire. This experiment was performed so as not to overload the NiTi SMA wire during the simulation as well as providing useful data on the maximum force per volume of NiTi wire. A third type of experiment was performed using NiTi wire deflecting a steel beam with the purpose of obtaining material parameters, and also for the comparison with 1-D analysis finite element analysis for the same thermal history. The last experiment was performed on a smart aileron with the purpose of obtaining material parameters for the plate and for comparison with the 3-D aeromorphing simulation in ABAQUS.

## 3.2 BEAM DEFLECTION TEST EXPERIMENT (1-D ANALYSIS)

This experiment was performed using the following equipment:

- Explorer GLX Data logger

- Nickel Titanium shape-memory alloy wire of 0.5mm diameter
- ISO-TECH IPS 2303 Laboratory DC Power Supply
- Linear variable differential transformer (LVDT)
- Fluke 190C Scope meter
- Rectangular steel beam
- Rectangular steel frame

The steel beam used was 300mm long with a 25mm breadth and 1.2mm thickness. Both ends of the steel beam were fixed on top of the vertical rectangular steel frame. The effective length for the steel beam after installation to the vertical rectangular steel frame was 243mm. Figure 3.1 shows the complete experimental setup.

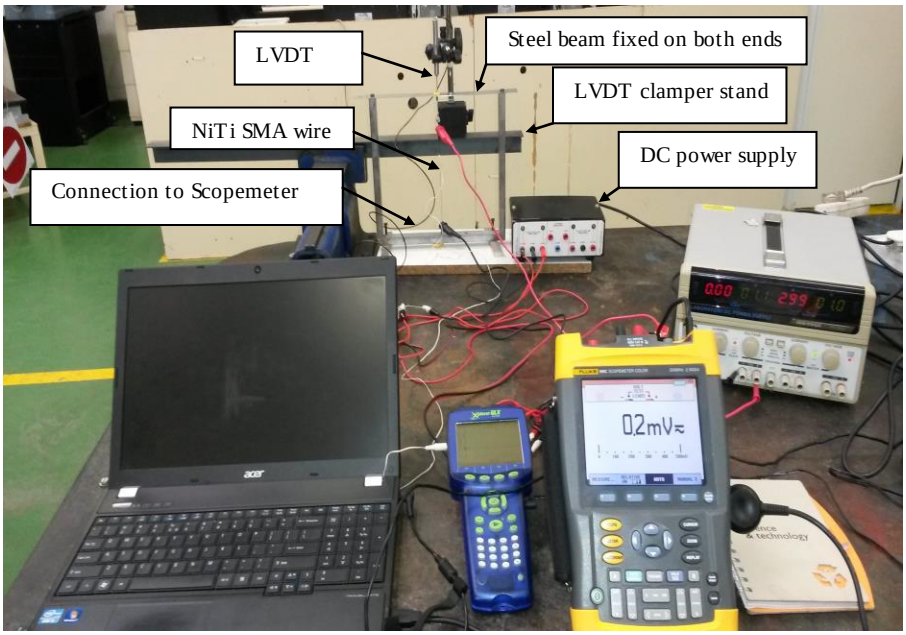


**Figure 3.1: Beam test experiment setup**

A 184mm long NiTi SMA wire with 0.5mm diameter was attached with one end at the centre of the steel beam and the other end at the centre foot of the steel frame. The attachment of the NiTi SMA wire to the frame and to the beam was isolated using high melting temperature plastic tubes. The isolation was required since the NiTi SMA wire was heated through the joules heating method. The NiTi SMA wire was attached at the centre of the beam so as to get the maximum deflection. During the performance of the experiment, two types of data was being logged i.e. beam deflection and the NiTi SMA wire temperature. The beam deflection was recorded through the LVDT which was powered by the DC power supply (shown in the figure 3.1). The LVDT data was logged in the form of output voltage and it was translated into millimetres using the method described below. The temperature was recorded using a GLX explorer data logger. A 1.54 A was supplied to the NiTi SMA wire and the temperature of the wire increased from the room temperature to a maximum temperature. The wire was allowed to cool down after reaching the maximum deflection of the beam and then the beam could go back to its rest position. This process was repeated several times so as to get stable results.

### 3.3 DEFLECTION TRANSDUCER'S CALIBRATION

Figure 3.2 shows the experimental setup used to calibrate the deflection transducer. It was mentioned in the previous section that the Scope meter was logging deflection in the form of voltage, therefore the output voltage was translated into millimetres using a vertical height Vernier gauge.

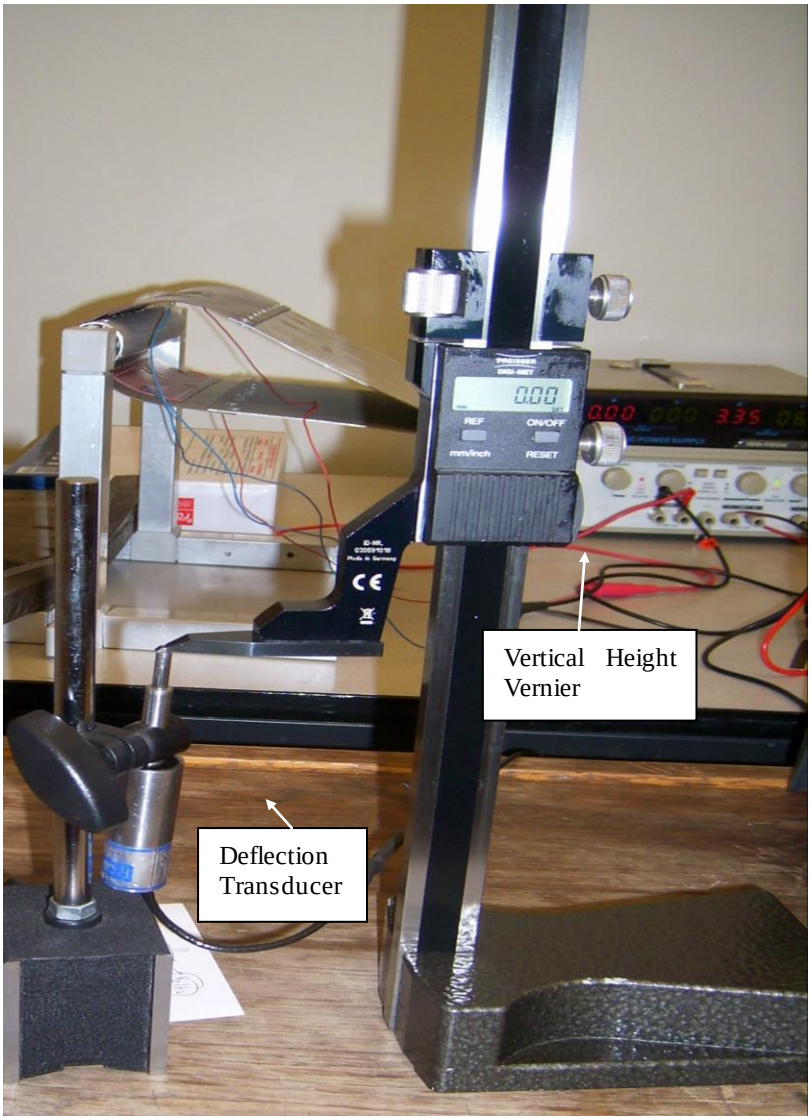


**Figure 3.2: Deflection transducer calibration setup**

The vertical height Vernier gauge was displaced and the corresponding output voltage from the transducer was logged through the Scope meter. The graph was plotted as a means to convert voltage change into millimetres moved. The slope of the graph was used to develop the relationship between the deflection in

millimetres and the equivalent deflection in volts. It was found that 1mm was equivalent to 156.99 mV.

### 3.4 DEFLECTION TRANSDUCER CALIBRATION RESULTS

Figure 3.3 is the plot of the data obtained when the deflection transducer was calibrated. It should be noted that the deflection transducer relaxes at full extension. So the zero deflection is read as a maximum deflection value by the Scope meter and similarly the maximum deflection is read as a minimum value. The data was presented as such, hence the graph in figure 3.3 shows an inverse linear relationship.

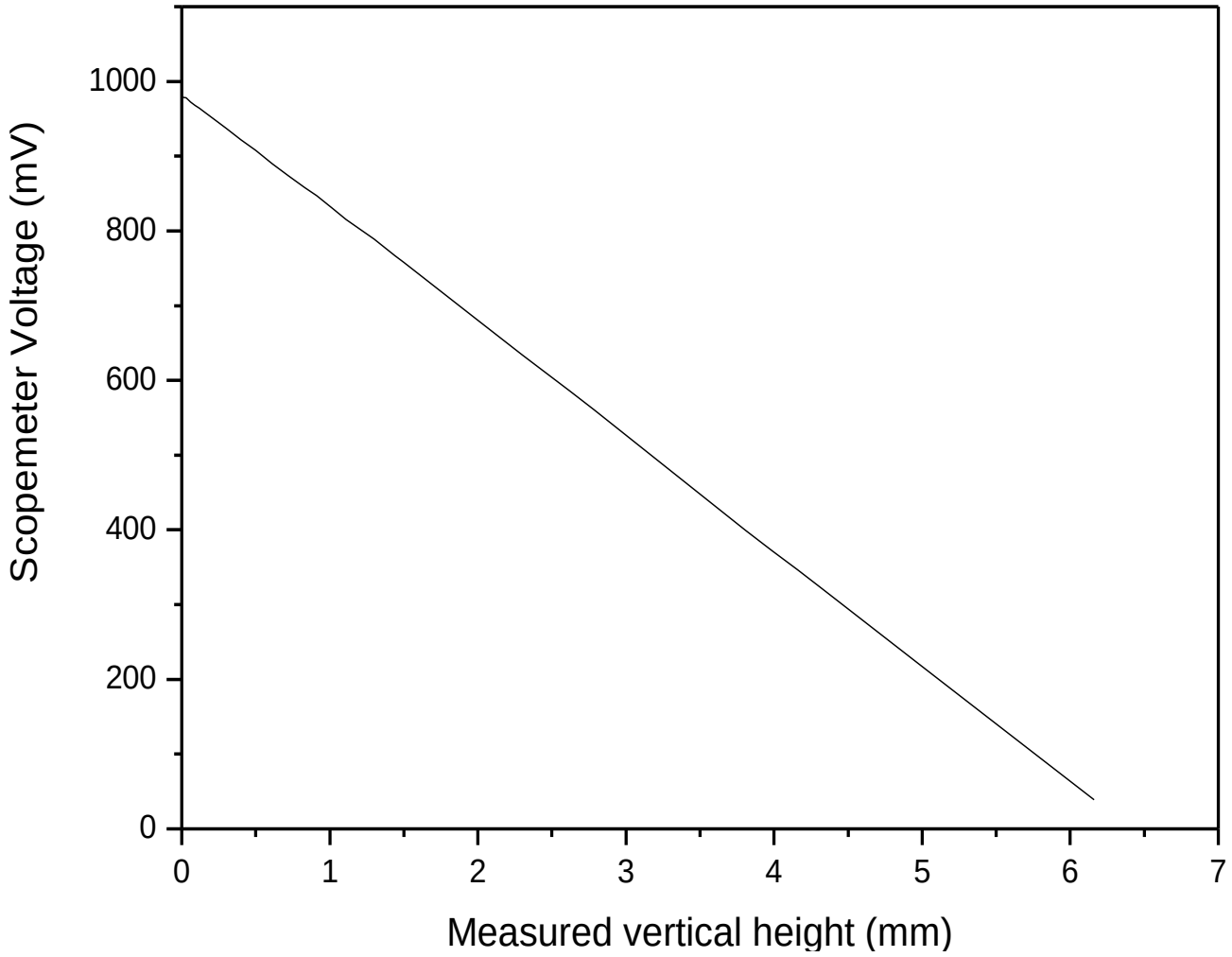


**Figure 3.3: Measured vertical height – Scope meter voltage graph**

### 3.5 DEFLECTION TEST RESULTS

The following figures show the experimental results for the beam deflection test and these results will be used in the following chapter to validate FEA results. Although there were several tests conducted, only one graph is presented to avoid repetition. It should be noted that the results presented are already translated into millimetres using the previously mentioned method. Figure 3.4 shows the time it takes for a beam to finish the full deflection cycle i.e. the

deflection from the rest position to the final position or maximum deflection and from the final position back to rest position.

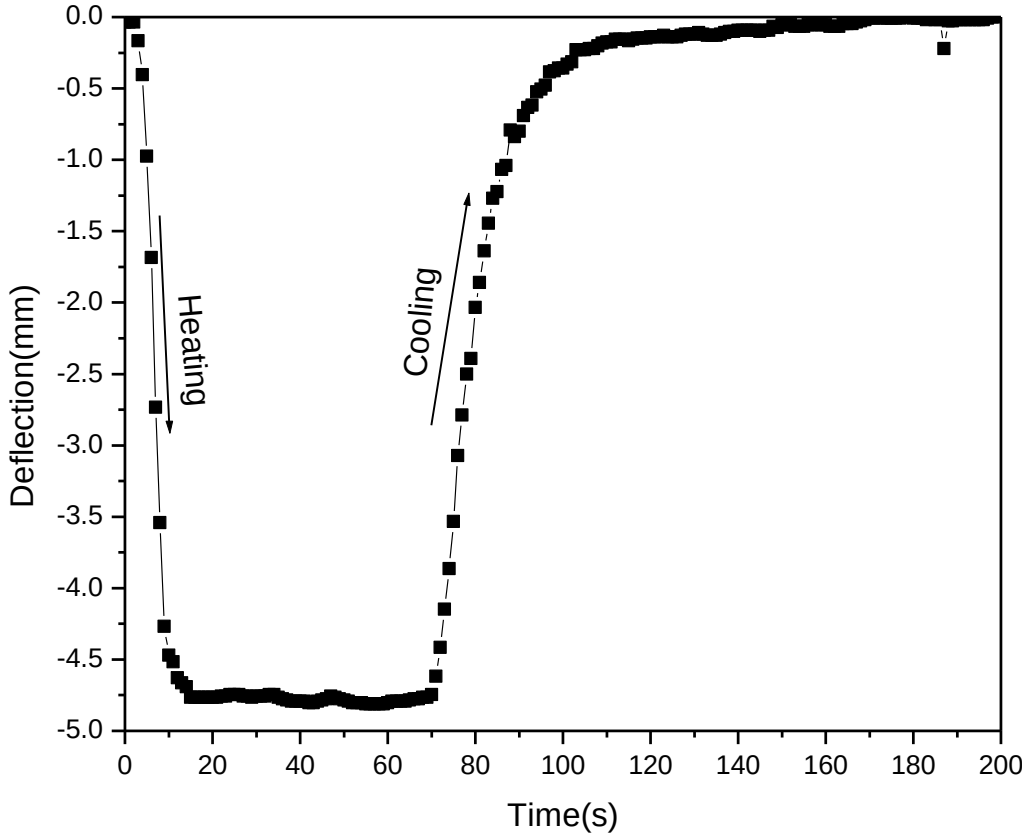


**Figure 3.4: Time – deflection curve**

During heating, the beam deflects from rest position to the maximum deflection, and the reverse during cooling. It is clearly seen from the figure that the beam's maximum deflection is reached in less than ten seconds which is very quick. This quickness is suggested to be related to the wire diameter. The smaller the diameter the faster the response of the wire. It is noted in the figure that there is a flatness of the graph between ten seconds and seventy seconds. This flatness shows the beginning of the cooling cycle. It should be remembered that the driving force behind this graph is the NiTi SMA wire phase transition as

discussed in the previous chapter. The martensite phase transforms to austenite phase between zero and ten seconds upon heating. The austenite phase is the dominant phase between ten and seventy seconds and then the nucleation of martensite starts to occur after seventy seconds. Martensite start occurs after seventy second and finishes after 140 seconds. The flatness behaviour is seen after 140 seconds which depicts the domination of martensite phase. The number of data points between zero and ten seconds are few compared to the rest of the graph and this caused by the fact that the sampling rate was not easy to control.

The SMA wire force which produced the maximum deflection of the steel beam is shown in figure 3.5. The maximum force produced by the current SMA wire (184mm long) was found to be approximately 35.87517 N (~ 3.5kg).

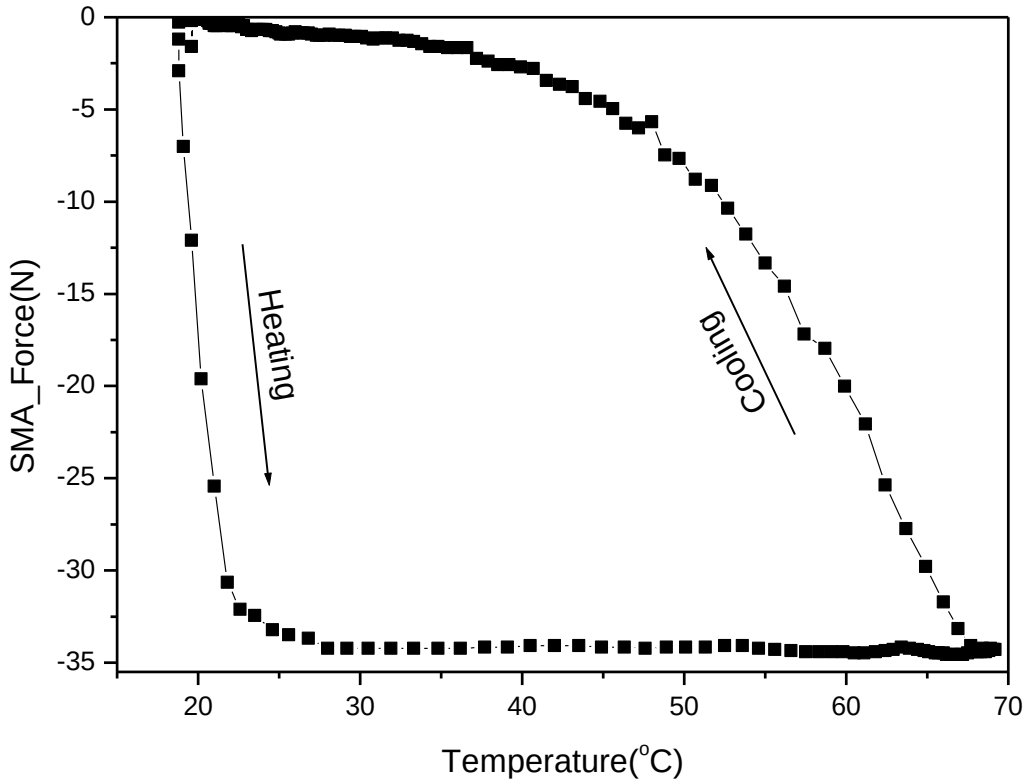


**Figure 3.5: SMA wire force – temperature graph**

Figure 3.6 shows the deflection of the beam to the negative vertical (y) direction as the temperature increases and the reverse during cooling. It is noted that all the values on the y-axis of each figure is negative. This indicates that the direction of steel beam is to the negative y- direction. It is noted also that the curves (from figure 3.4 - 3.6) are not smooth, caused by the uncontrolled environmental conditions. The maximum deflection is taken with consideration of the sign of the value since it symbolizes the axis direction.

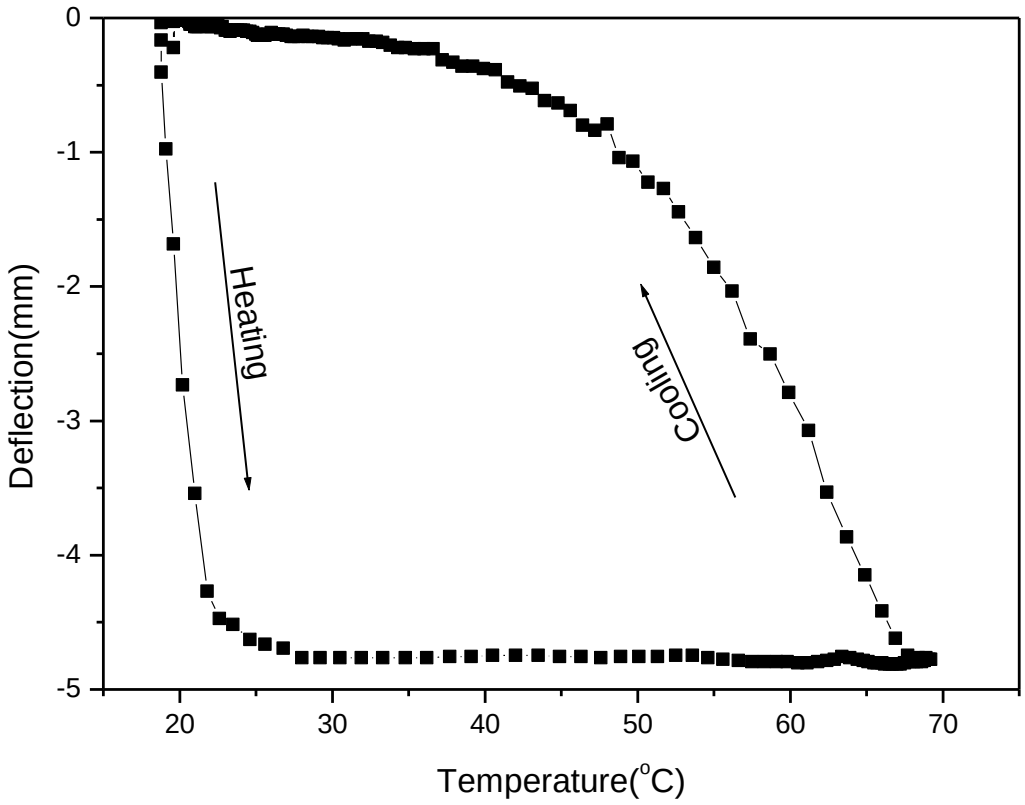


**Figure 3.6: Steel beam deflection – temperature graph**

The deflection test results seem to be in agreement with the general behaviour of shape-memory alloy material. So these results will be used as the benchmark for simulation results and will be compared with FEA results in the succeeding/following chapter.

## 3.6 CHARACTERIZATION OF THE SHAPE-MEMORY ALLOY PLATE

The mechanical properties of the NiTi plate were characterized using the equipment available at the Mechanical Engineering Department, of the Cape Peninsula University of Technology. The NiTi SMA plate broke when it was bent using the bending machine, hence its mechanical properties were investigated.

The stress-strain curve (see fig. 3.7) shows that the plate fails as a brittle material. Based on the results, it was concluded that a NiTi SMA plate should not be bent beyond a certain point. The point or angle of fracture/failure was determined using a $90^{o}$ engineering ruler together with the bending machine. It was found that the SMA plate should be bent at an angle more than $30^{o}$.

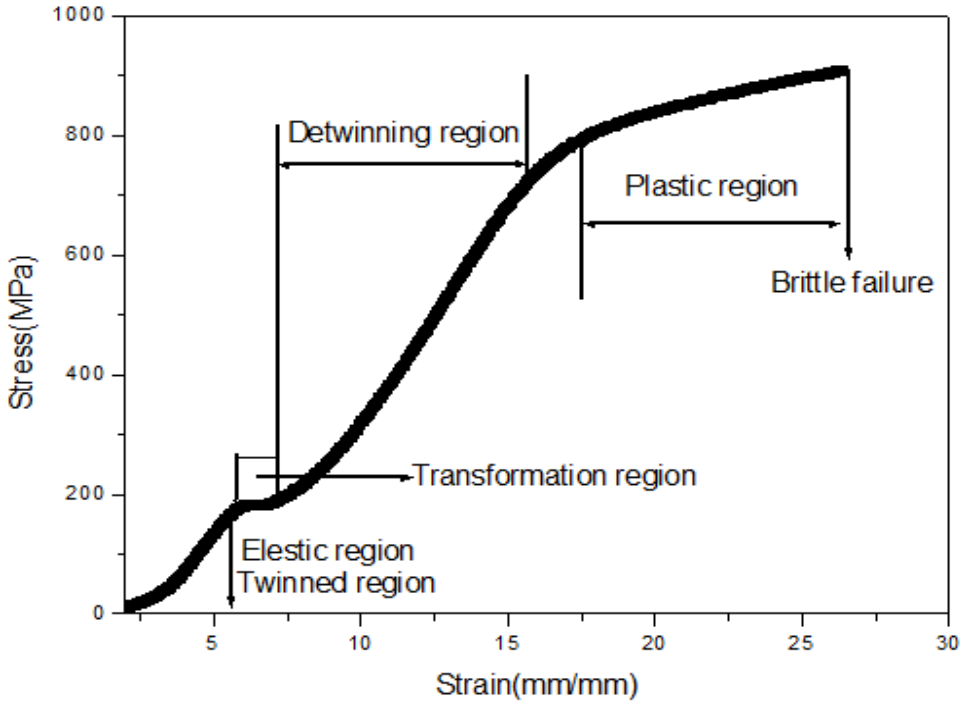


**Figure 3.7: The stress-strain curve for the NiTi plate.**

This investigation was used as a guideline in developing the training dies used in introducing airfoil shapes to the SMA plates used in smart aileron construction.

## 3.7 SMART AILERON EXPERIMENT (3-D ANALYSIS)

Prior to the performance of the experiment, the equipment used is being listed and described. An experiment was performed using the following apparatus and equipment:

- Nickel Titanium plates (NiTi),
- Silicone self-adhesive heater mat kit.
- Short Brush Aluminium plates
- Rivet gun and pop rivets

The detailed description of some of the above mentioned apparatus follows underneath.

### 3.7.1 NICKEL TITANIUM SHAPE-MEMORY PLATES

The manufacturer of the NiTi plates used to perform the experiment is Sea Bird Metal Company based in China. The plates had different dimensions but uniform thickness (1.2mm). The transformation temperature of the plates was $90^{o}C$ (austenitic finish temperature). The martensitic finish temperature was $50^{o}C$. These temperatures are factory transformation temperatures and they can be changed depending on the training procedure

### 3.7.2 SHORT BRUSH ALUMINIUM PLATES

These plates were cut to 180 x110 mm to meet our requirements from the sheet that was available in the CPUT stores. The plate's thickness was uniform 1.2mm.

### 3.7.3 SILICONE SELF-ADHESIVE HEATER MAT KIT

The silicone self-adhesive heater mat kit was supplied by RS Components, based in Johannesburg, South Africa. The heater mat kit specified above was chosen for this experiment because of its bending feature at high temperature.

**Table 3.1: Heater Mat Kit specifications**

| Number | Dimensions (mm x mm) | Voltage (V) | Power (W) |
|---|---|---|---|
| **1** | 150 x 300 | 30 | 150 |
| **2** | 150 x 100 | 30 | 50 |
| **3** | 150 x 75 | 30 | 38 |
| **4** | 150 x 50 | 30 | 25 |
| **5** | 75 x 75 | 30 | 18.5 |
| **6** | 75 mm diameter | 30 | 18.5 |

## 3.8 EXPERIMENTAL RESULTS FOR THE SMART AILERON

The smart aileron (hingeless) structure used to perform the experiments was constructed using NiTi and aluminium plates. The leading edge was constructed with NiTi plates and the trailing edge with aluminium plates. The NACA 0015 (symmetrical) aero foil shape was used for the smart aileron. The NiTi plates were cut into rectangular 180 x 110 mm shapes so that they could fit into the training dies. The SMA plates were trained for two shapes i.e. un-actuated and actuated shapes of the aileron.

Figure 3.8 shows images of the actuated and un-actuated dies. The two dies were equipped with screws for clamping the NiTi plate to the desired shape during training. Figures 3.9 and 3.10 show dies with NiTi plates ready for training (ready to be placed inside the furnace).

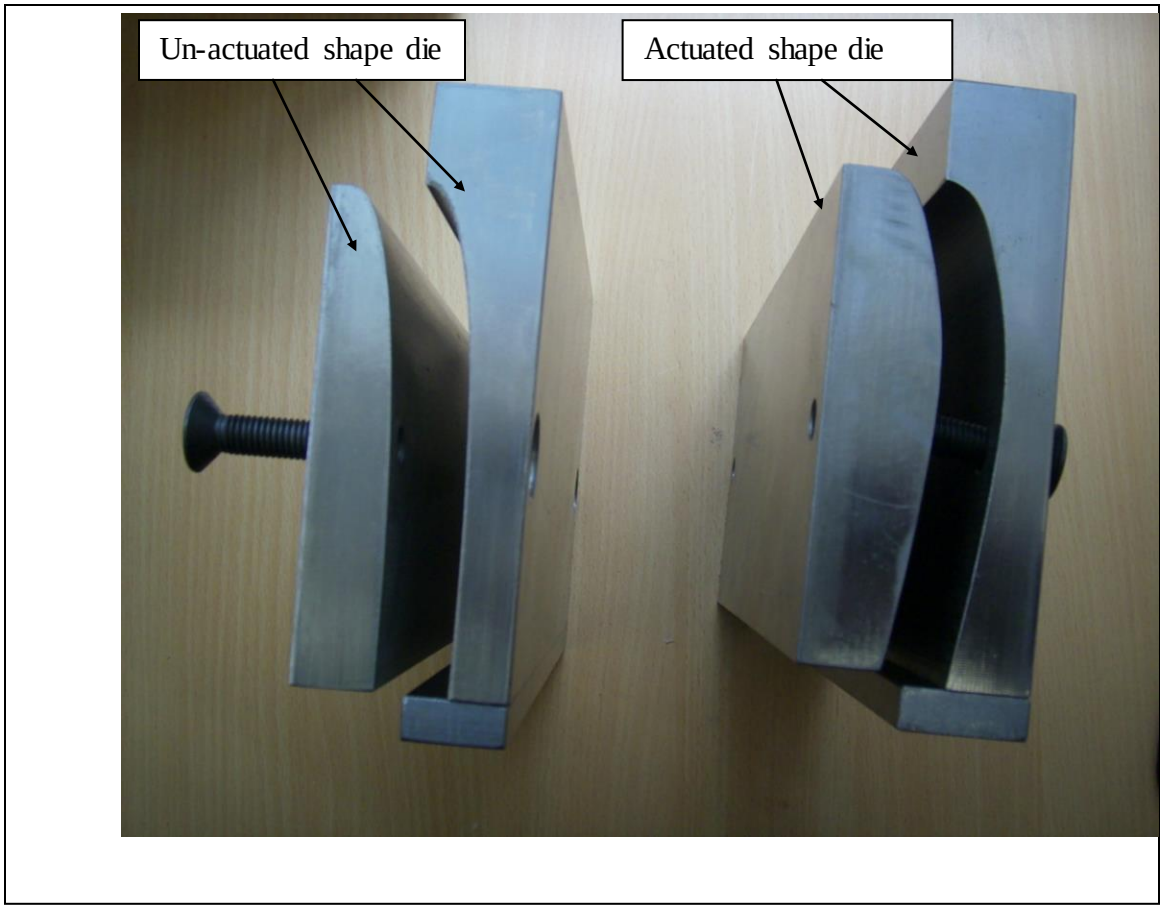


**Figure 3.8: The two opened dies used to train NiTi plates as airfoil shapes.**

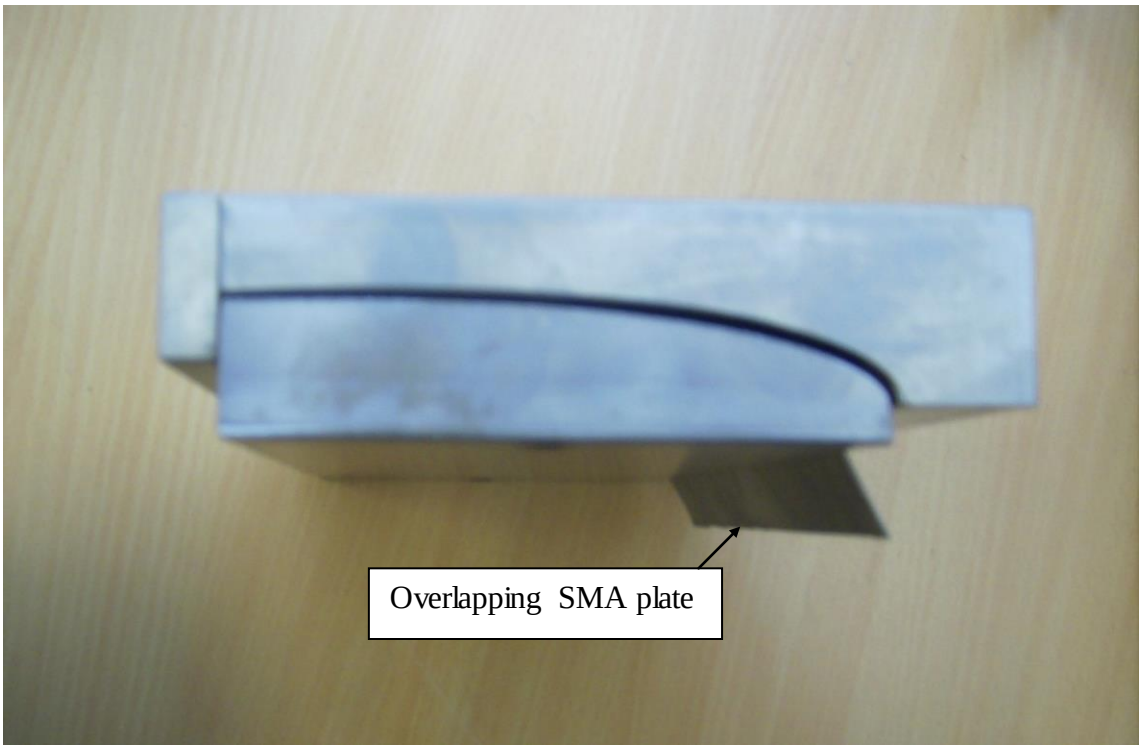


**Figure 3.9: A NiTi plate closed inside an un-actuated shape die.**

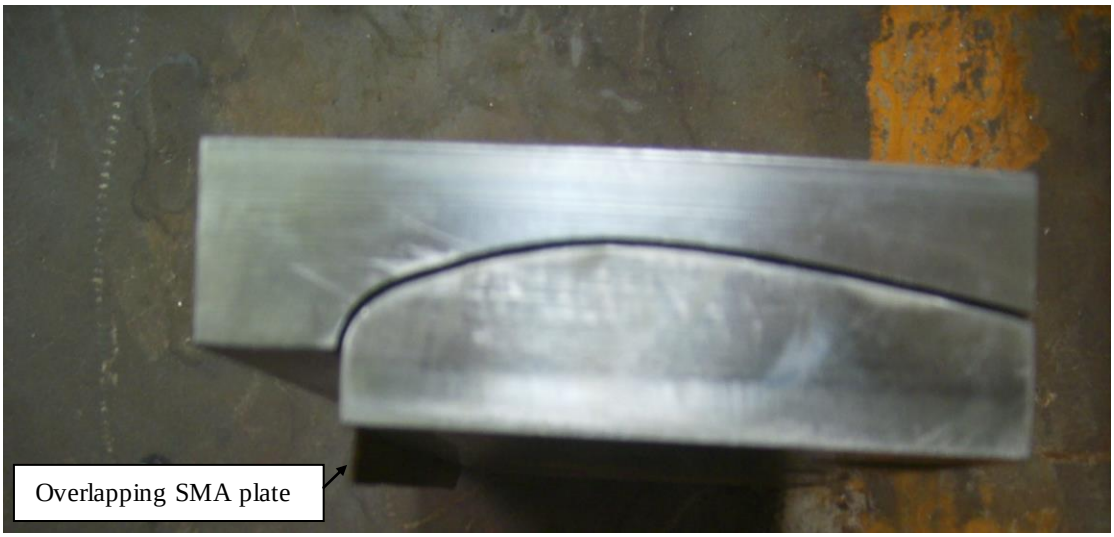


**Figure 3.10: A NiTi plate closed inside an actuated shape die.**

The NiTi plates were trained using the following procedure:

The furnace was allowed to heat up until it reached the training temperature of 500$^{o}$C. The die with NiTi plate was placed inside the furnace. The plate was kept at that temperature for 20 minutes. The plate was quickly removed from the furnace and quenched using tap water.

### 3.9 DATA ACQUISITION SETUP

Figure 3.11 shows the picture of a data acquisition setup. The DC power supply was used to supply voltage to the heater mat kit and deflection transducer (Type: D2/200A). The heater mat kits were installed so as to supply heat to the smart aileron when required for actuation. The temperature data was logged using the Xplorer GLX data logger. The deflection transducer was used to measure the deflection at the tip of the smart aileron (both upward and downward).

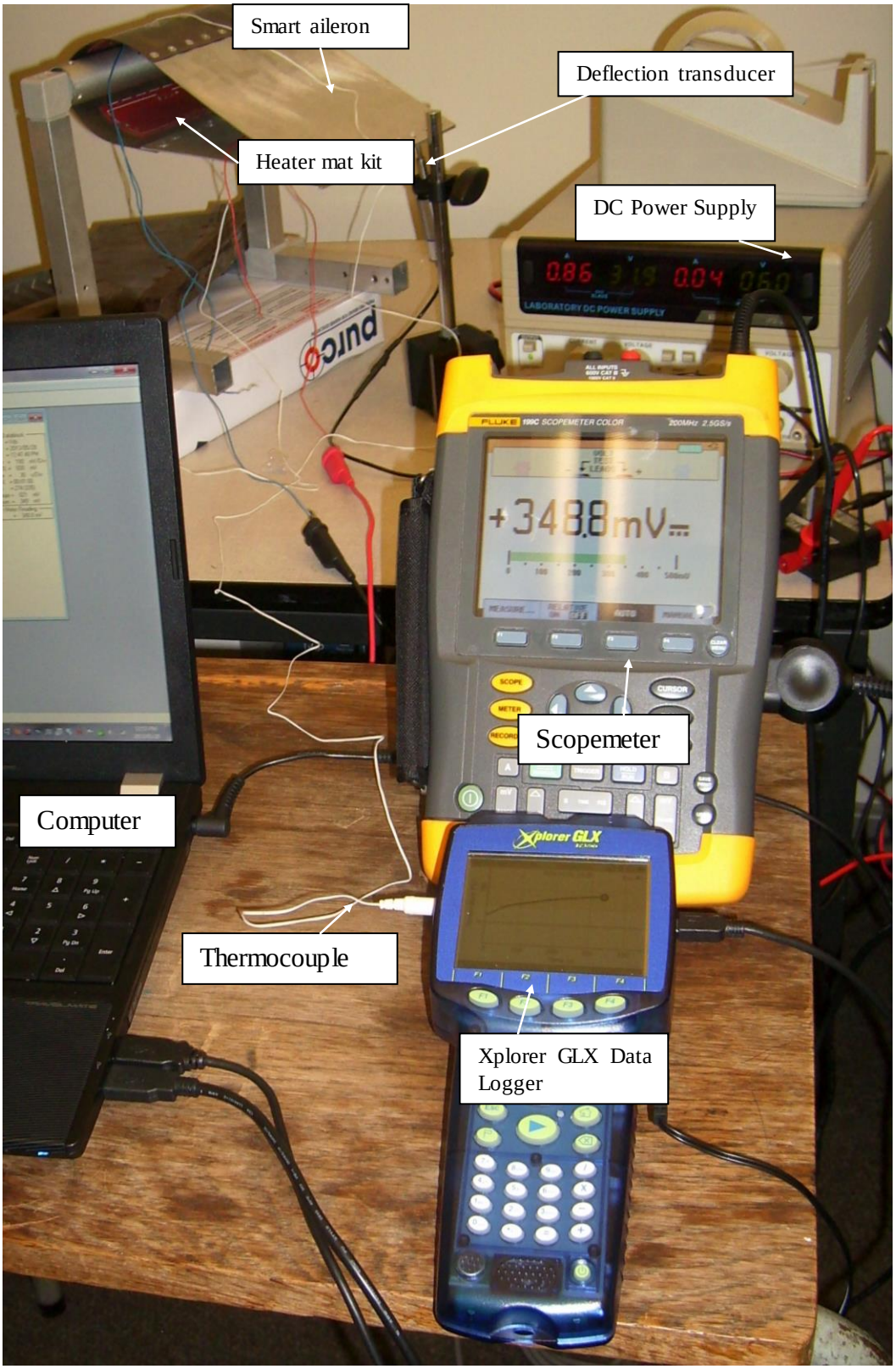


**Figure 3.11: Experimental apparatus and Data acquisition equipment**

The deflection transducer was connected to the Fluke 190C Scope meter. The Scope meter was connected to the computer so as to capture the deflection data. The output from the transducer was displayed into the Scope meter in the form of voltage. A setup mentioned previously was used to translate voltage into millimetres.

### 3.10 SMART AILERON DEFLECTION RESULTS

The temperature – deflection curves for the vertical (upward) deflection (positive y-direction) are shown in figures 3.12 and 3.13 and the vertical (downward) deflection (negative y-direction) are shown in figures 3.14 and 3.15 respectively. The upward deflection was achieved upon the activation of the top leading edge trained NiTi plate, whereas the downward deflection was achieved upon the activation of the bottom leading edge trained NiTi plate. The smart aileron was deflected to the maximum and back to initial position through the activation and deactivation of the trained NiTi plates and this process is referred to as a full cycle. Twenty cycles were recorded for upward and downward deflections but only six cycles are presented here as typical results.

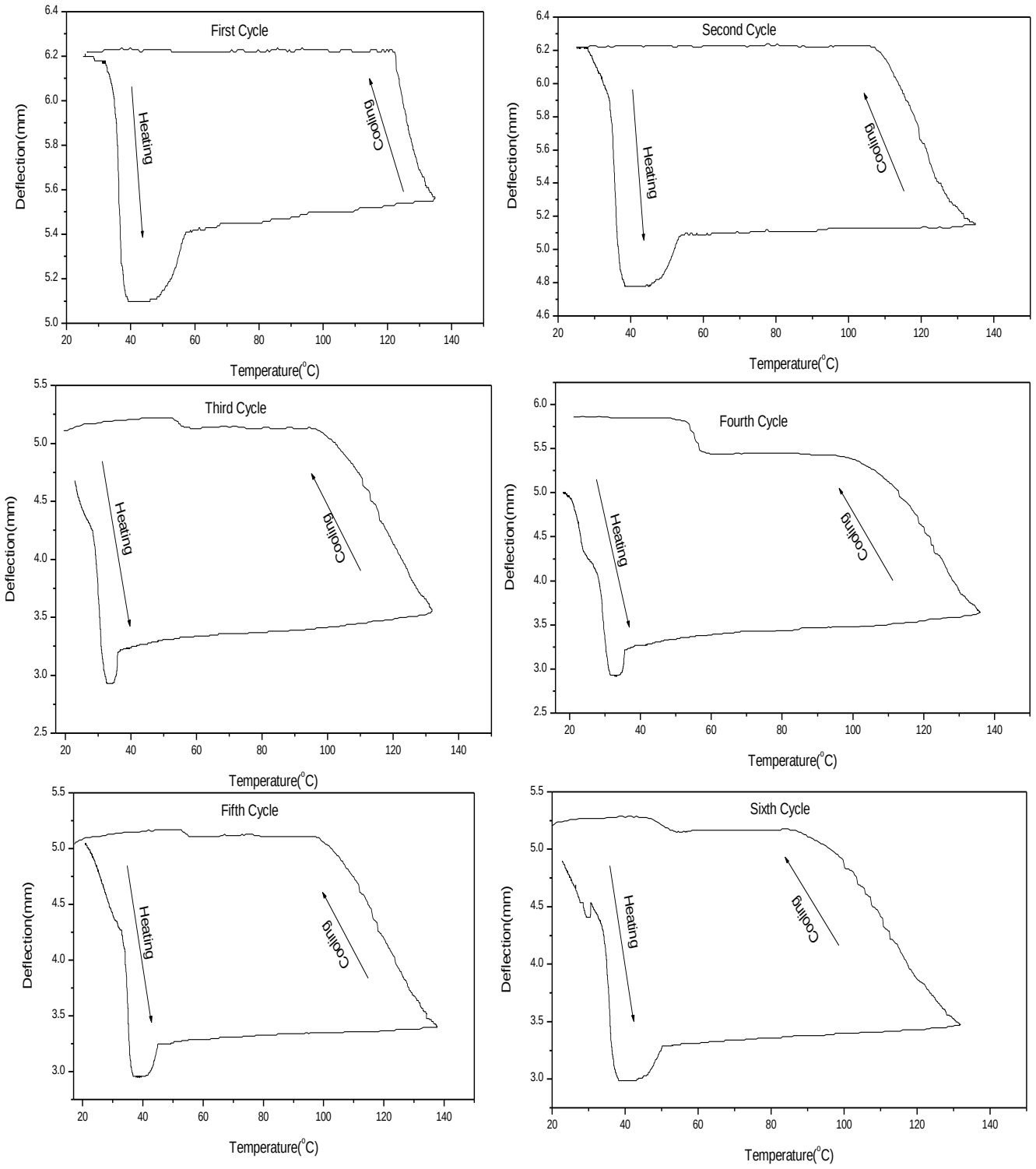


**Figure 3.12: Temperature – Deflection curves for upward deflection of the smart aileron**

The maximum upward deflection was measured to be approximately 2mm as deduced from figure 3.13. The time it takes for a complete or full cycle was measured, and using the recorded data figure 3.14 was plotted. The maximum duration of the full cycle was found to be approximately twenty four minutes. It should be noted that there were no cooling systems installed but only natural cooling occurred, hence the long time to complete a deflection cycle. The deflection cycle could be sped up by installing cooling systems.

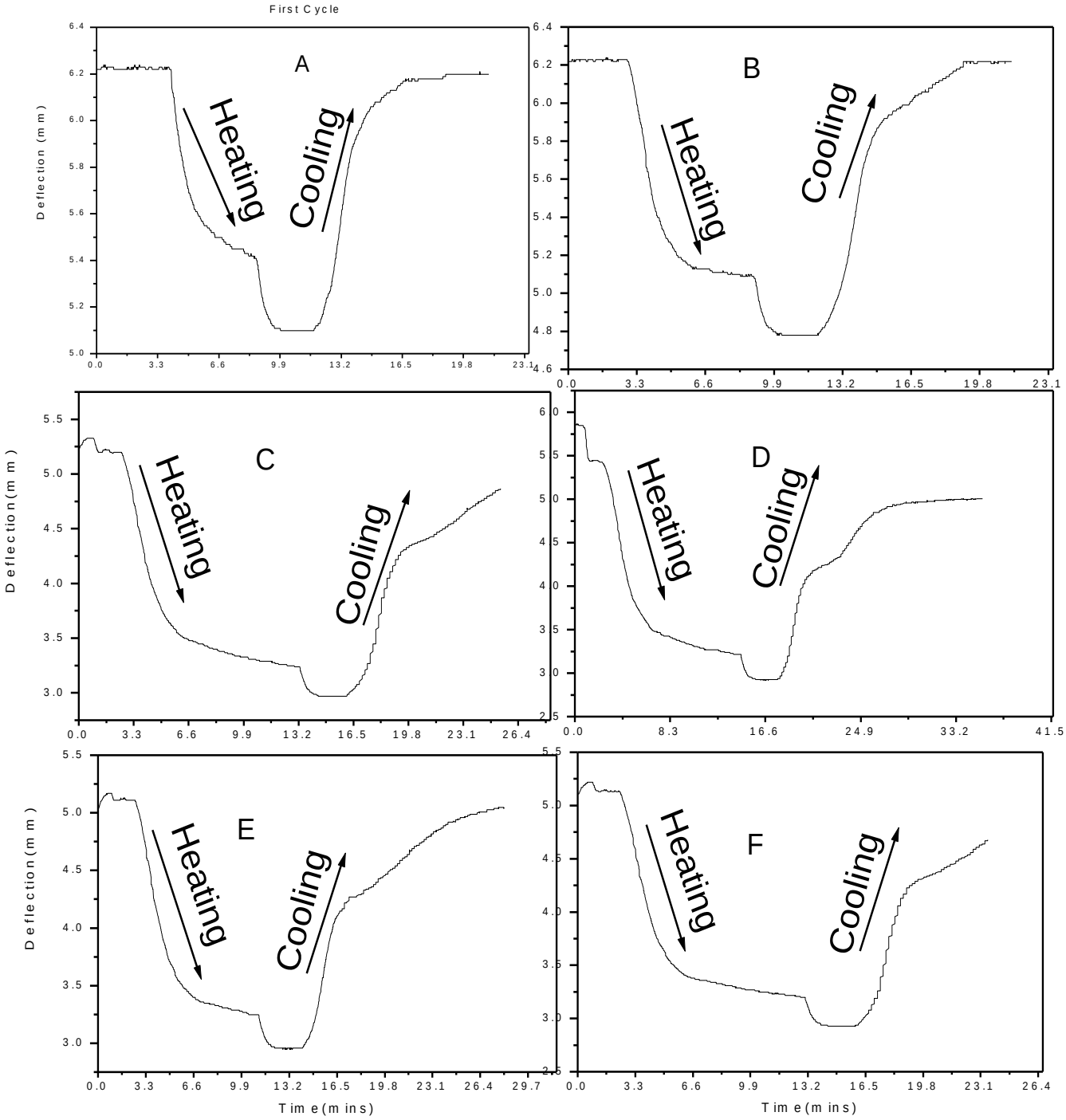


**Figure 3.13: Time – Deflection curves for upward deflection of the smart aileron**

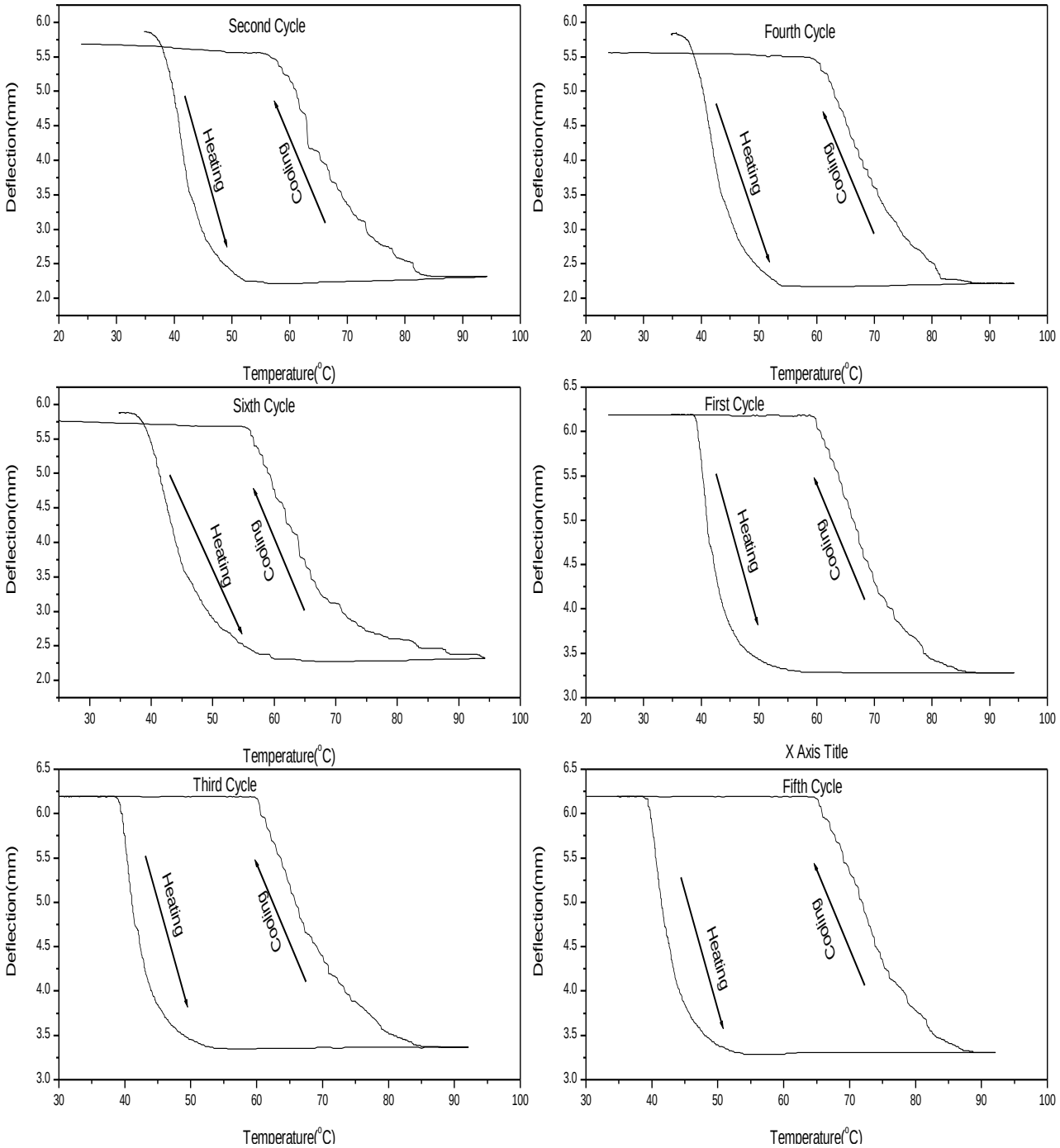


**Figure 3.14: Temperature - Deflection curves for downward deflection of the smart aileron**

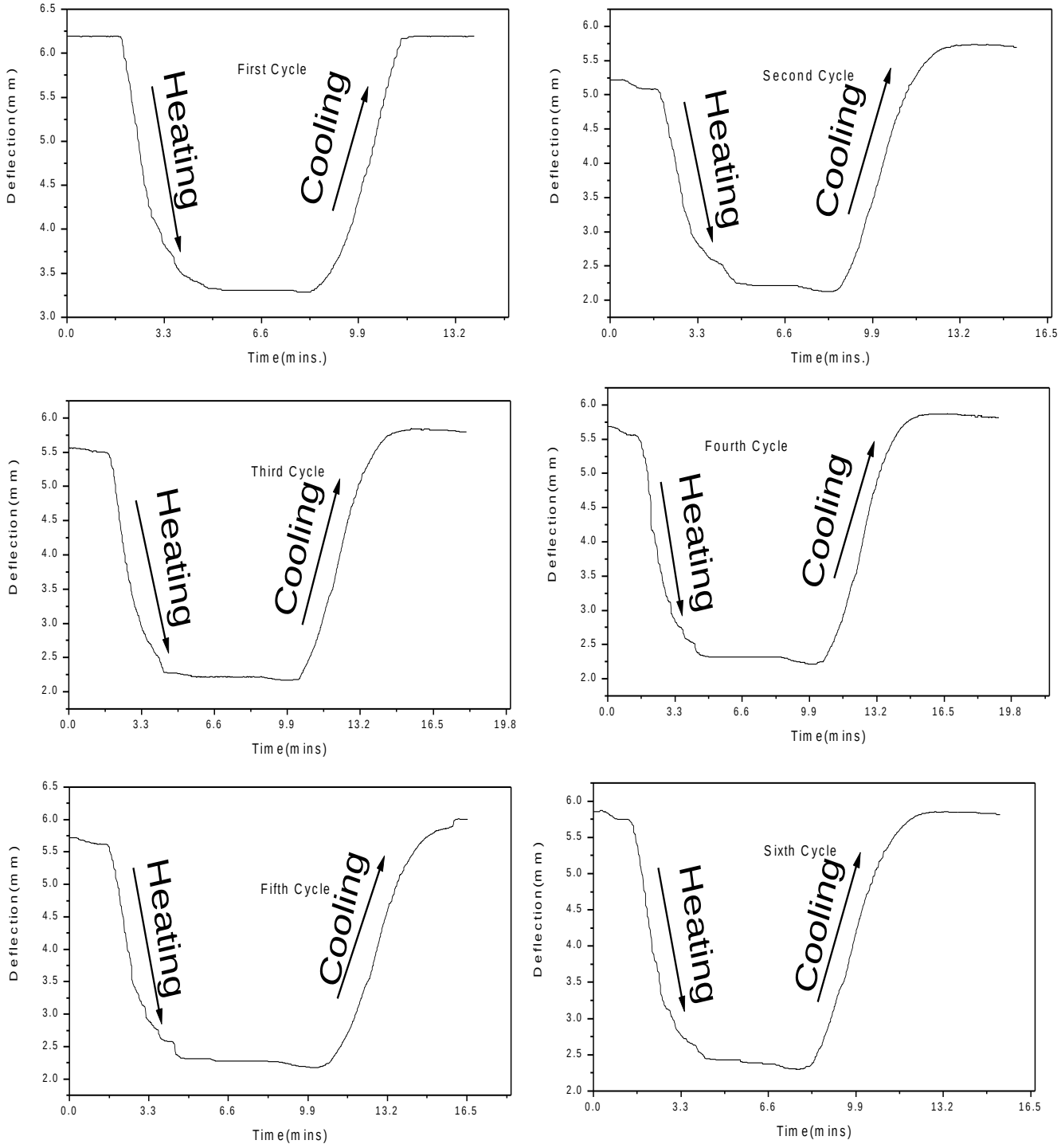


**Figure 3.15: Time – Deflection curves for downward of the smart aileron**

The downward deflection was also tested in a similar manner to the upward deflection. The maximum downward deflection was found to be approximately 3mm. There is also a notable difference in full cycle deflection time between the upward and downward deflections. The downward deflection takes about ten minutes to complete the full cycle (natural cooling). The other notable difference is the deflection start and deflection finish temperatures during heating and cooling. The temperatures during heating for the upward deflection (half cycle from rest position to maximum deflection) started at 117$^{o}$C and finished at 137$^{o}$C. The temperatures during cooling for the upward deflection (returning to the initial/ rest position) started at 52$^{o}$C and finished at 28$^{o}$C. Of course this means that time lapses in heating up to 117$^{o}$C before upward actuation begins and actuation stops at 137$^{o}$C then cooling begins and the return to the neutral position only begins when the plate has cooled down to 52$^{o}$C and stops at neutral when it has cooled down to 28$^{o}$C.

The deflection temperature during heating for the downward movement of the aileron (from rest position to maximum deflection) started approximately at 65$^{o}$C and finished at 85$^{o}$C (plate's temperature) respectively. The deflection temperature during cooling for the downward movement of the aileron (returning to the initial/ rest position) started at approximately 55$^{o}$C and finished at 38$^{o}$C (plate's temperature) respectively. These temperatures indicate the austenitic

start and finish during heating, and martensitic start and finish during cooling if one looks at the microstructural level of the NiTi plate.

The experimental results obtained during this study show that the manufactured model of a smart aileron was successfully operated by actuating it from neutral to either positive or negative vertical positions. The results are used in the next section to validate the simulation results obtained from ABAQUS numerical analysis software for the SMA user material implemented into ABAQUS as a FORTRAN subroutine.

# CHAPTER 4

## 4.1 SOLUTION ALGORITHMS FOR THE IMPLEMENTATION OF SMA MATERIAL INTO FE PROGRAMS

We look here at the algorithms needed for the inclusion of SMA material into finite element analysis (FEA) programs. Two implementations are looked at: implementation into a program using one dimensional combined beam bar elements in a two dimensional orientation written in C++, and a three dimensional implementation into a commercial finite element package ABAQUS using its UMAT subroutine interface. The FEA program using 1-D elements was written to both adjust SMA material parameters and check the model against physical experiments to see how good an approximation could be made by the model of the real behaviour of actuators.

### 4.1.1 SMA MATERIAL MODEL DESCRIPTION

An additive strain rate decomposition composition is assumed for the SMA material [Ronda and Oliver 2000]. Since we are working in only on a Cartesian basis it is sufficient to consider only the components of the second rank tensors. The decomposition of the total strain rate is then given by

$$\dot{\mathbf{L}}_{ij} = \dot{\mathbf{L}}^{e}_{ij} + \dot{\mathbf{L}}^{p}_{ij} + \dot{\mathbf{L}}^{th}_{ij} + \dot{\mathbf{L}}^{tr}_{ij} \tag{4.1}$$

Where $\dot{L}_{ij}$ is the total strain rate, $\dot{L}^{e}_{ij}$ is the elastic part of the strain rate, $\dot{L}^{p}_{ij}$ is the plastic part of the strain rate beyond the flow stress of the material, $\dot{L}^{th}_{ij}$ is

the part of the strain rate due to thermal changes and $\dot{L}_{ij}^{tr}$ is the part of the strain rate which is due to the phase transformation between the martensite phase and the austenite phase. There is also no transformation induced plasticity.

As the model is intended to only be used for designing structures in which the SMA material will operate in the elastic (includes pseudo-elastic) range we can neglect the plastic strain rate term so that

$$\dot{\mathbf{L}}_{ij} = \dot{\mathbf{L}}_{ij}^{e} + \dot{\mathbf{L}}_{ij}^{th} + \dot{\mathbf{L}}_{ij}^{tr} \tag{4.2}$$

The thermal and transformation parts of the strain rate have no deviatory parts, as they are caused by the volumetric expansion and contraction of the material due to thermal and phase changes respectively.

The material properties are calculated at a material point which in the isoparametric finite element formulation corresponds to the gauss integration points of the element as shown in figure 4.12 and to the nodal points in the direct finite element formulation. The direct formulation was used for the combined beam and bar element program written for SMA materials and the commercial package used in the three dimensional formulation, ABAQUS, uses the isoparametric finite element formulation. In both instances the properties at the material point will be considered to be a combination of the properties of the individual phases present.

Elastic properties, such as the Young's modulus, Poisson ratio and the thermal expansion coefficient of the individual phases, are combined in proportion to the volume fraction of the phase present which is known as a linear mixture rule

[Brinson, 1993], so that the Young's modulus at a material point, at any time instant, is given by:

$$\langle E \rangle = p^{aus} E^{aus} + p^{mart} E^{mart} \tag{4.3}$$

, where $\langle E \rangle$ is the averaged Young's modulus, $p^{aus}, E^{aus}, p^{mart}, E^{mart}$ austenitic phase fraction,austenitic Young's modulus, martensitic phase fraction and martensitic Young's modulus, respectively. The change in phase is also driven by temperature which provides an additional coupling between temperature and displacement. There is no additional time for phase kinetics considered, other than the time taken for the temperature to change for heating and cooling so that each temperature corresponds to a volume phase fraction in the heating or cooling regimes in the incremental solution for displacement.

The strain due to thermal change is

$$\dot{\mathbf{L}}_{ij}^{th} = \langle \alpha^{th} \rangle \Delta\theta \tag{4.4}$$

, where $\langle \alpha^{th} \rangle, \Delta\theta$ is the averaged thermal expansion coefficient and change in temperature, respectively. The strain due to phase transformation in the SMA material is determined from the austenite volume fraction and a material parameter determined from experiment

$$\dot{\mathbf{L}}_{ij}^{tr} = \alpha^{tr} p^{aus} \tag{4.5}$$

, where $\alpha^{tr}$ is the maximum recoverable strain. In order to use the material model in the commercial finite element package, ABAQUS, we need to define certain algorithmic tangent moduli for the non-linear solution which includes the

moduli for temperature displacement coupling in a transient temperature displacement problem.

The volume phase fraction is an internal state variable in this formulation so that we need to solve the following system of coupled temperature-displacement FE equations at any instant [Ronda and Oliver 2000]

$$\begin{bmatrix} K_{uu} & K_{u\theta} \\ K_{\theta u} & K_{\theta\theta} \end{bmatrix} \begin{bmatrix} \Delta u \\ \Delta\theta \end{bmatrix} = \begin{bmatrix} R_u \\ R_\theta \end{bmatrix} - \begin{bmatrix} F_u \\ F_\theta \end{bmatrix} \tag{4.6}$$

Where $K$ is the stiffness matrix with components which are due to either temperature and displacement, $\Delta u$ is the change in displacement, $\Delta\theta$ is the change in temperature. $F_u$ is the vector of applied mechanical loads and $F_\theta$ is the generalised loads due to temperature with $R_u$ and $R_\theta$ being the generalised residual forces in the non-linear solution using the Newton Raphson method [Ronda and Oliver 2000].

Because we are dealing with large deformation, the finite element sub-matrix is given by the following equation [Kai-ming et al., 2010]

$$\mathbf{K}_{uu} = \mathbf{K}_M^e + \mathbf{K}_G^e + \mathbf{K}_\Omega^e \tag{4.7}$$

where

$$\mathbf{K}_M^e = \int_{V_{n+1}^e} B^T \mathbf{C} B dV \text{ (Material stiffness)} \tag{4.8}$$

$$\mathbf{K}_G^e = \int_{V_{n+1}^e} G^T \left(\boldsymbol{\sigma} \otimes \mathbf{1}\right) G dV \text{ (Geometric nonlinear part),} \tag{4.9}$$

$$\mathbf{K}_\Omega^e = \int_{V_{n+1}^e} \left(B_u^W\right)^T \boldsymbol{\sigma} \Omega^T dV + \int_{V_{n+1}^e} \left(B_u^W\right)^T \Omega \boldsymbol{\sigma} dV \text{ (Finite rotation part)} \tag{4.10}$$

$$G = \left[\nabla N_1 .... \nabla N_i ..... \nabla N_{ne}\right] \tag{4.11}$$

with $\boldsymbol{B}$ being the strain-displacement matrix, $\boldsymbol{\Omega}$ denoting the rotation of spin tensor and $\boldsymbol{C}$ being the algorithmic tangent modulus which is a fourth order tensor that linearizes the relationship between the incremental change in stress, $\Delta T_{ij}$, and the incremental change in strain $\Delta L_{ij}$ [Ronda and Oliver, 2000]

$$C_{ijkl} = \frac{\partial \Delta T_{ij}}{\partial \Delta L_{kl}} \tag{4.12}$$

which is simply the elastic tangent modulus for an isotropic material with material properties defined using the mixture rule

$$\frac{\partial \Delta T_{ij}}{\partial \Delta L_{kl}} = \langle \kappa \rangle \delta_{ij}\delta_{ij} + \langle \mu \rangle \left[ \delta_{ik}\delta_{jl} + \delta_{il}\delta_{jk} - \frac{2}{3}\delta_{ij}\delta_{kl} \right] \tag{4.13}$$

Where $\langle \kappa \rangle$ is the bulk modulus formed from the mixture of the two phases and $\langle \mu \rangle$ is the shear modulus formed from the mixtures of the two phases.

The finite element sub-matrix, which is written as a vector,

$$K_{u\theta} = \int_{V_0} \mathbf{B}^T \frac{\partial \Delta T_{ij}}{\partial \Delta \theta} dV_0 \tag{4.14}$$

, where $\frac{\partial \Delta T_{ij}}{\partial \Delta \theta}$ is given by

$$\begin{aligned} \frac{\partial \Delta T_{ij}}{\partial \Delta \theta} &= 3\langle \kappa \rangle \delta_{ij} \left[ \alpha^{th} + \alpha^{tr} \frac{\partial p^{aus}}{\partial \theta} \right] \\ \frac{\partial p^{aus}}{\partial \theta} &= \frac{\partial}{\partial \theta}\left( \xi_m \left\{ 1 - \tanh\left[ t_A \left( \theta - A_s \right) + \vartheta_A \right] \right\} \right) \end{aligned} \tag{4.15}$$

The final form of equation (4.15) is

$$\frac{\partial \Delta T_{ij}}{\partial \Delta \theta} = 3\langle \kappa \rangle \delta_{ij} \left\{ \alpha^{th} + \alpha^{tr} \left[ -\xi t_A \sec h^2 t_A \left( \theta - A_S \right) \right] \right\} \tag{4.16}$$

There is no inelastic heat dissipation considered, so that the contribution to the stiffness matrix is identically zero, $\mathbf{K}_{\theta u} = 0$.

Transient heat transfer is given by

$$\langle \rho \rangle \langle c \rangle \frac{\partial \theta}{\partial t} - \nabla \left( \langle k \rangle \nabla \theta \right) = Q \tag{4.17}$$

where $\langle \rho \rangle$ is the volume averaged density, $\langle c \rangle$ is the volume averaged specific heat capacity and $\langle k \rangle$ is the volume averaged conductivity. These parameters are averaged for volume functions at a material point.

The stiffness contribution $\mathbf{K}_{\theta\theta}$, is the standard stiffness matrix for a transient thermal calculation which has contributions for heat capacity and conductivity, and the only modification to it that would arise from the inclusion of the shape-memory alloy material in the solution is the volume averaged definitions of the density, thermal heat capacity and conductivity and is given by the following equation

$$\mathbf{K}_{\theta\theta} = \frac{1}{\Delta t}\mathbf{C} + \mathbf{K}_c + \mathbf{K}_h + \mathbf{K}_r \tag{4.18}$$

where

$$\mathbf{C} = \int_V \langle \rho \rangle \langle c \rangle \mathbf{N}^T \mathbf{N} dV$$
$$\mathbf{K}_c = \int_V \langle k \rangle \mathbf{B}^T \mathbf{B} dV$$
$$\mathbf{K}_h = \int_{S_3} \langle h \rangle \mathbf{N}^T \mathbf{N} dS \qquad (4.19)$$
$$\mathbf{K}_r = \int_{S_4} \sigma \varepsilon \theta^4 \mathbf{N}^T dS$$

Latent heat effects from phase change might also be approximated by temperature dependence of the specific heat capacity.

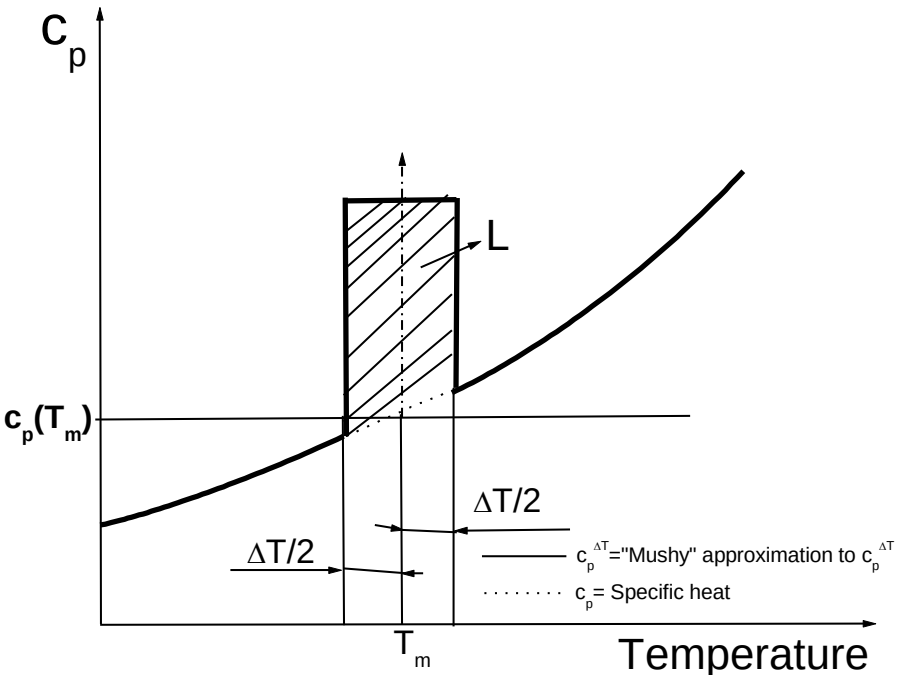


**Figure 4. 1: Temperature dependence of the specific heat [Storti et al., 1988]**

The above figure shows the temperature dependence of the specific heat. Before the latent heat effect we have a predominantly martensitic structure and after the latent affected part of the curve we have a predominantly austenitic

structure. Our mixture rule for the specific heat can thus be changed into a temperature function of specific heat as in our simplified formulation, where there is a direct correspondence between a temperature and a volume phase fraction (no time lag effect). Thus it is possible in this formulation to account for the latent heat if such data is available. In this case we were dependent on the available material data in literature, as we do not possess experimental equipment to accurately measure the specific heat ourselves [Zhou et al., 2009]

This was done to avoid the additional numerical problems with the non-linear solution, as the effect of these additions could cause inaccuracy which would negate the potential enhancement of the model by their inclusion.

The rest of the chapter will be demonstrating the use of the previous outlined mathematical equation into the finite element analysis. Figure 4.2 shows the general circulation of information in the FEM analysis.

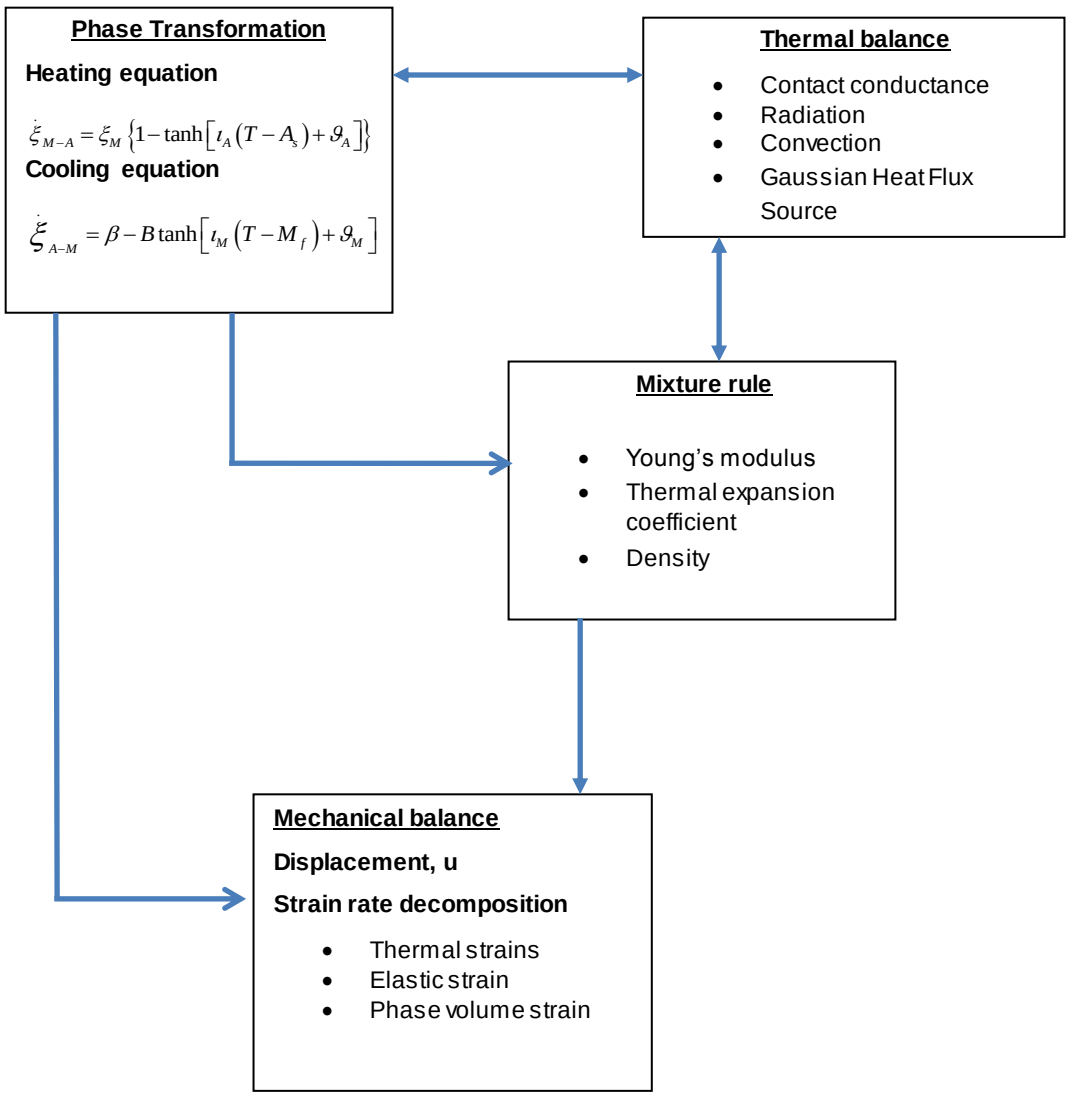


**Figure 4. 2: Thermal, mechanical and phase transformation couplings**

## 4.2 FINITE ELEMENT ANALYSIS ON 2-D BEAM SETUP

This section reflects the application of the proposed NiTi SMA model in predicting the response of the steel beam subjected to mechanical loading from NiTi SMA wire. Prior to the performance of the finite element analysis, an experiment was performed so as to find the simulation parameters like transformation temperature, the beam effective length and breadth, SMA wire

effective length, etc. The details about the experimental performance are found under the experimental performance section. To perform finite element analysis, a 4-noded with three elements structure was constructed as shown in figure 4.3. Two elements were steel beam elements and one element was NiTi SMA wire.

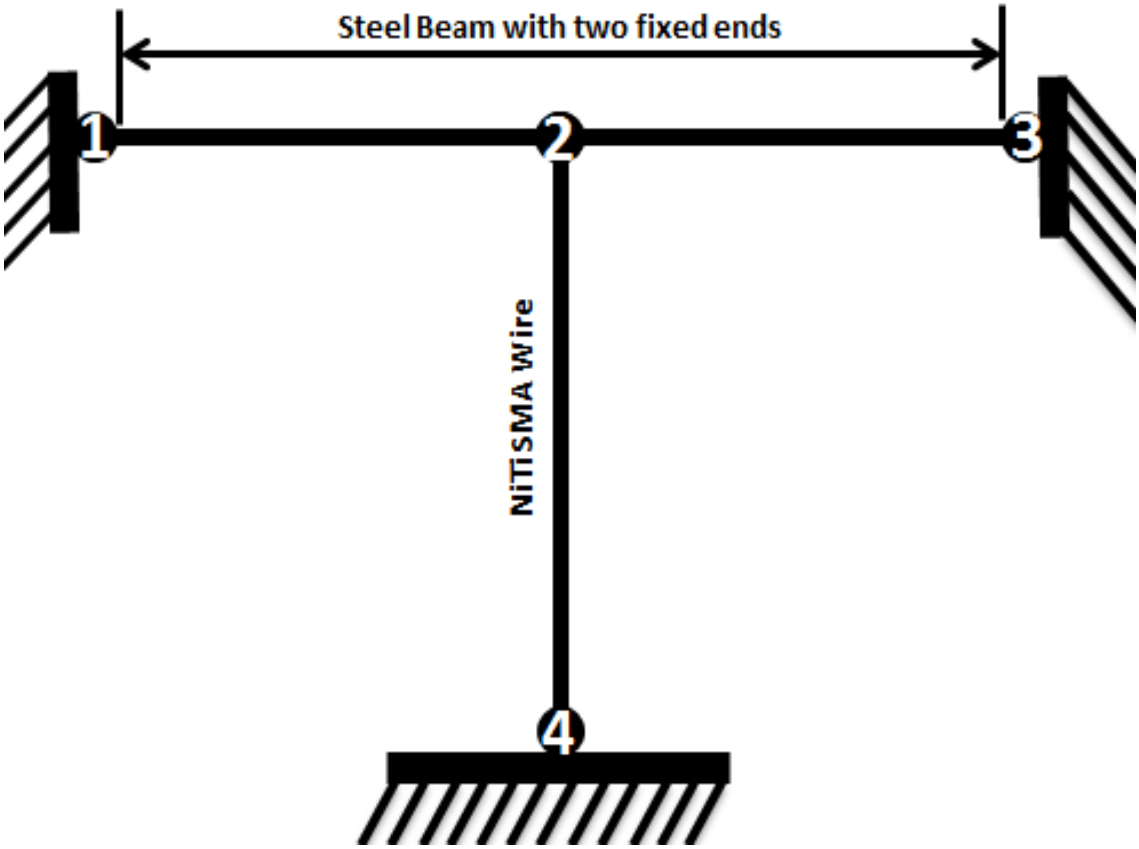


**Figure 4. 3: Steel beam bar – SMA setup**

## 4.3 IMPLEMENTATION OF SMA MATERIAL MODEL IN A 1-D BEAM-BAR FINITE ELEMENT WITH A TWO DIMENSIONAL ORIENTATION

This section deals with the computer implementation of the finite element analysis. The local and the global plane bar elements system is being

demonstrated schematically in figure 4.4. The system has got three elements where each element has six degrees of freedom (three degrees of freedom per node). The axial degrees of freedom are ignored due to the nature of loading hence the degrees of freedom per node is reduced from three to two and therefore the each element remains with four degrees of freedom (i.e. vertical displacement and rotation). The element node displacements and forces are given by equation (4.20).

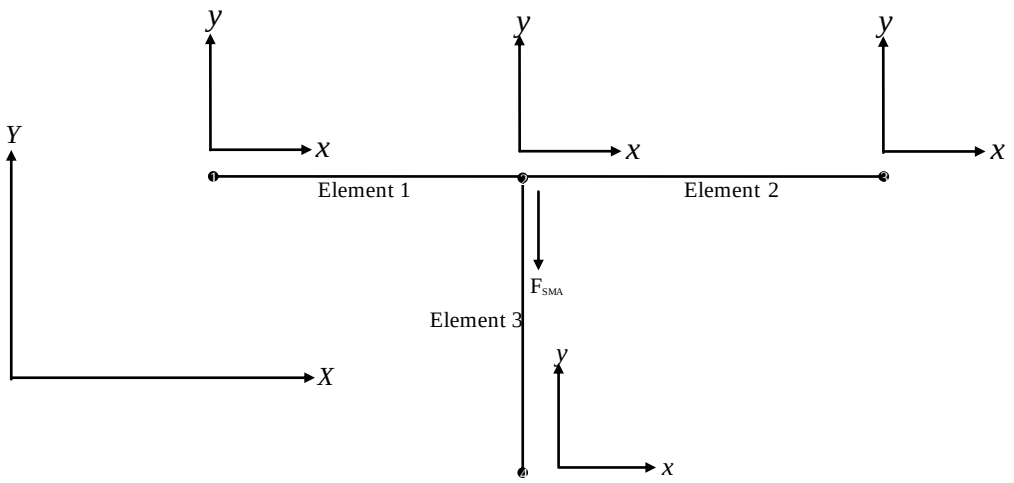


**Figure 4. 4: Plane bar elements in its local and global system.**

Element 1:

$$\underline{f^{(1)}} = \begin{bmatrix} f_{y1} \\ m_{\theta R1} \\ f_{y2} \\ m_{\theta R2} \end{bmatrix}$$
$$\underline{u^{(1)}} = \begin{bmatrix} u_{y1} \\ \theta_{R1} \\ u_{y2} \\ \theta_{R2} \end{bmatrix} \qquad (4.20)$$

Element 2:

$$\underline{f^{(2)}} = \begin{bmatrix} f_{y2} \\ m_{\theta R2} \\ f_{y3} \\ m_{\theta R3} \end{bmatrix}$$
$$\underline{u^{(2)}} = \begin{bmatrix} u_{y2} \\ \theta_{R2} \\ u_{y3} \\ \theta_{R3} \end{bmatrix} \qquad (4.21)$$

For stiffness calculations, the only material properties required are the modulus of elasticity E, cross section area A and the length $l$ of the beam, and these properties are taken to be constant throughout the beam. The solution procedure for our present problem is shown in appendix A.

The schematic diagram for solution flow is shown in figure 4.4. The solution diagram is a general solution flow to be used to solve one sided temperature and phase coupling of any given 2-D geometry. In our case, we assume that phases are only affected by temperature not by stress or pressure. The temperature affects the calculation of volume fraction through equation (2.6) and equation (2.10). The linear averaged property (Young's modulus,$E$ ) is then calculated together with other parameters mentioned in Chapter 2.

The stiffness matrix of beam is formed using material properties of the beam and then that affects the formation of forces due to shape-memory effect which is triggered by temperature variation. In our case, there are no external loads. This brings us to the calculation of the linear solution of equation A12 from appendix A. The process gets repeated until the maximum allowed temperature is reached.

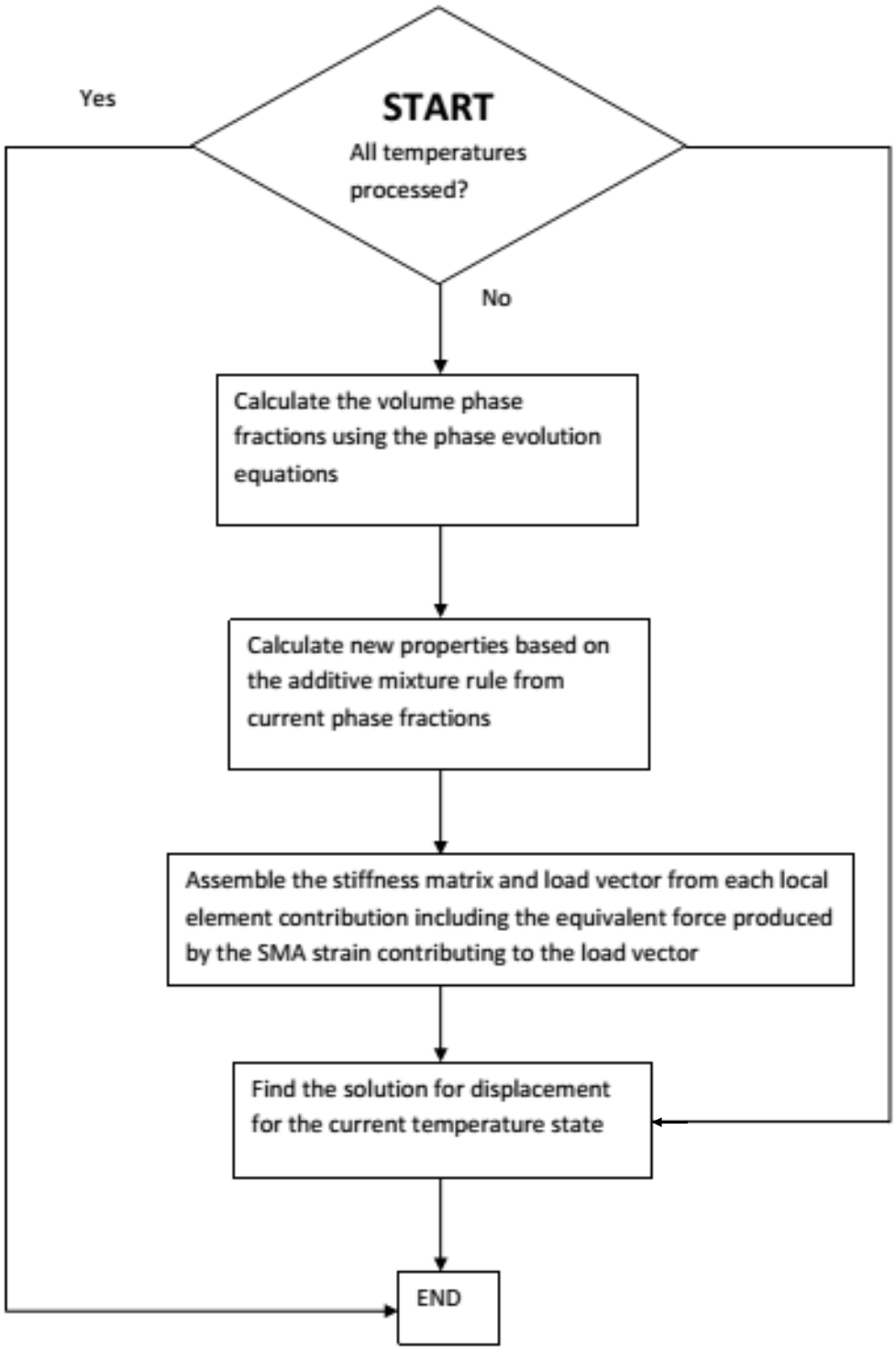


**Figure 4. 5: Schematic diagram for the solution process implemented in the beam-bar finite element program with one-sided thermo-mechanical coupling**

Figure 4.5 summarizes the solution flow process of the C++ program that is found in appendix B.

## 4.4 BEAM BAR SMA FEA RESULTS

This section reflects the numerical results obtained from 1-D finite element analysis. The material parameters used during FEA simulation are tabulated in table 4.1.

**Table 4.1: Material parameters for 0.5 mm diameter NiTi SMA wire used during simulation**

| Property | Value | Units |
|---|---|---|
| $E_M$ | 16.8 | GPa |
| $E_A$ | 31.8 | GPa |
| $Q_M$ | 0.6 | $^oC^{-1}$ |
| $Q_A$ | 0.06 | $^oC^{-1}$ |
| $\xi_M$ | 0.5 | - |
| $A_S$ | 43 | $^oC$ |
| $M_F$ | 18.3 | $^oC$ |
| $\varepsilon_L$ | 0.0485 | mm/mm |
| $A_{SMA}$ | 1.9635E-7 | $m^2$ |

Figure 4.6 shows the deflection – time graph where we wanted to see if the numerical results would match the experimental results.

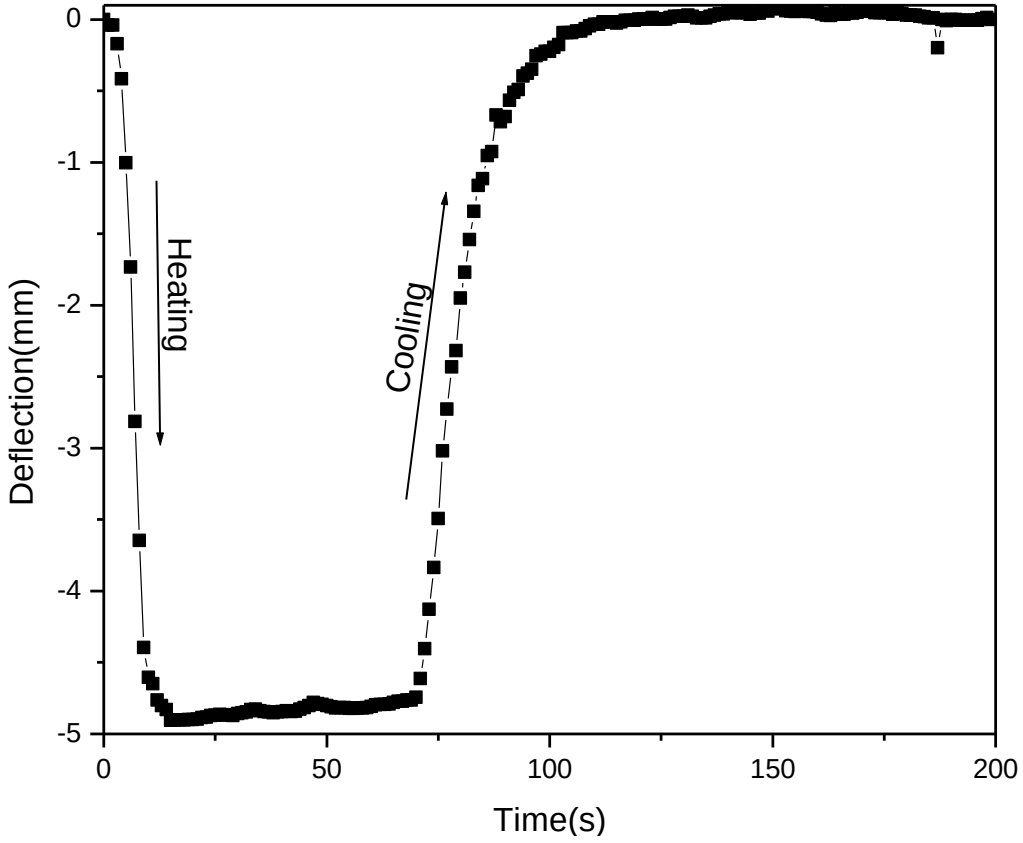


**Figure 4. 6: Beam bar numerical results for deflection – time curve**

So based on the results, it can be seen that the simulated numerical curve resembles the experimental curve. The maximum deflection of about 4.9mm is reached in less than ten seconds, like it was observed experimentally. The comparison for the deflection – time curves is shown in figure 4.6. The two curves follow the same trend and they both don't exceed the maximum deflection of 5mm.

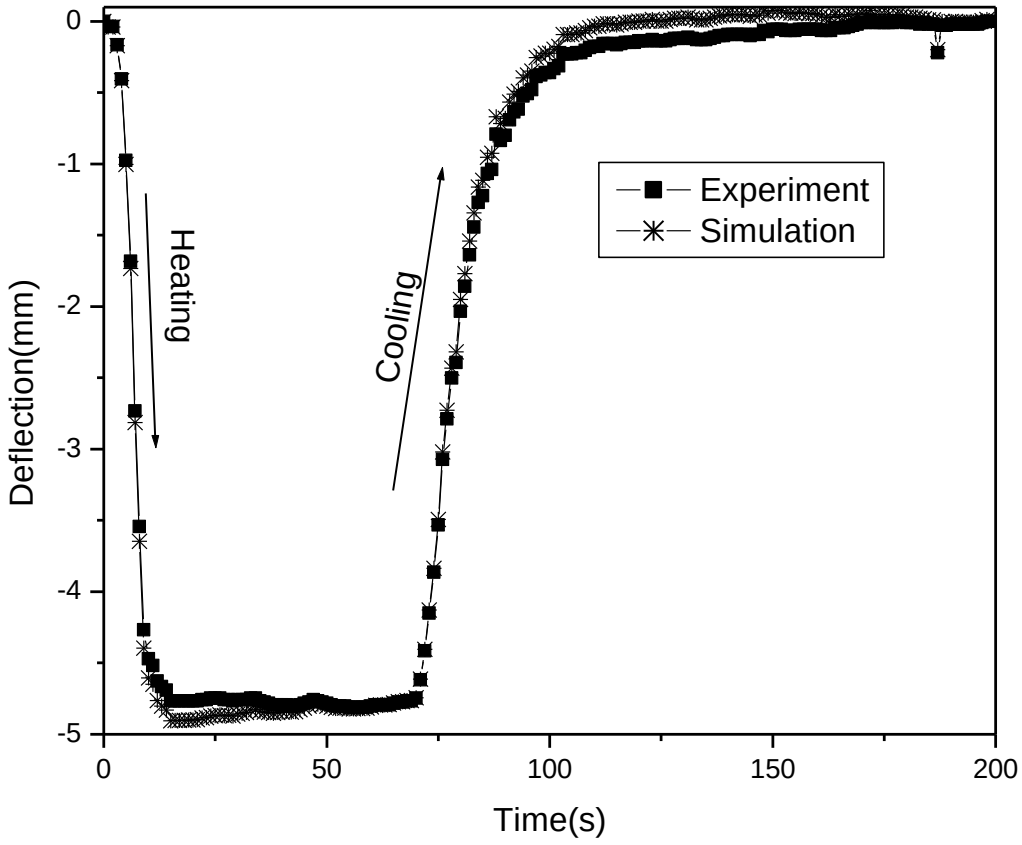


**Figure 4. 7: Numerical and experimental results for deflection – time curve**

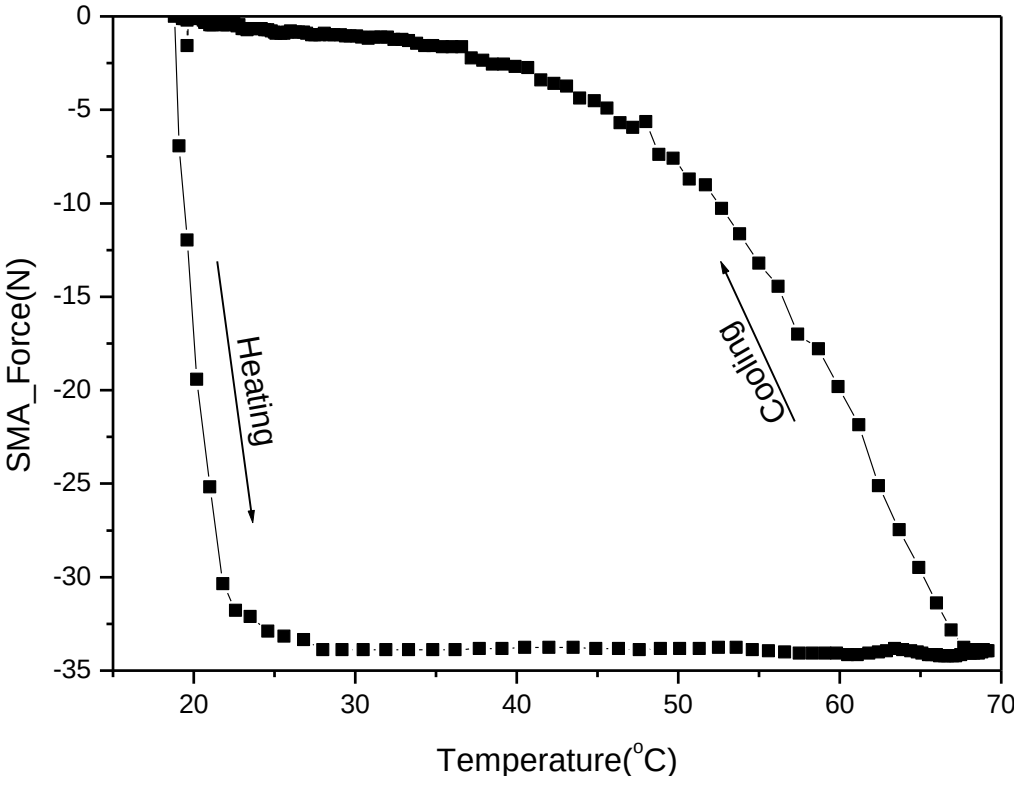


**Figure 4. 8: Beam bar numerical results for SMA force – temperature curve**

Figure 4.8 shows the numerical results for SMA force against temperature. The maximum deflection (in figure 4.6) was produced by a force of approximately 35.0N. The numerical results are in agreement with the experimental results reported in the previous chapter. The numerical results are combined with the experimental results in figure 4.9. It can be seen from the figure that the numerical prediction follows a similar trend with experiment.

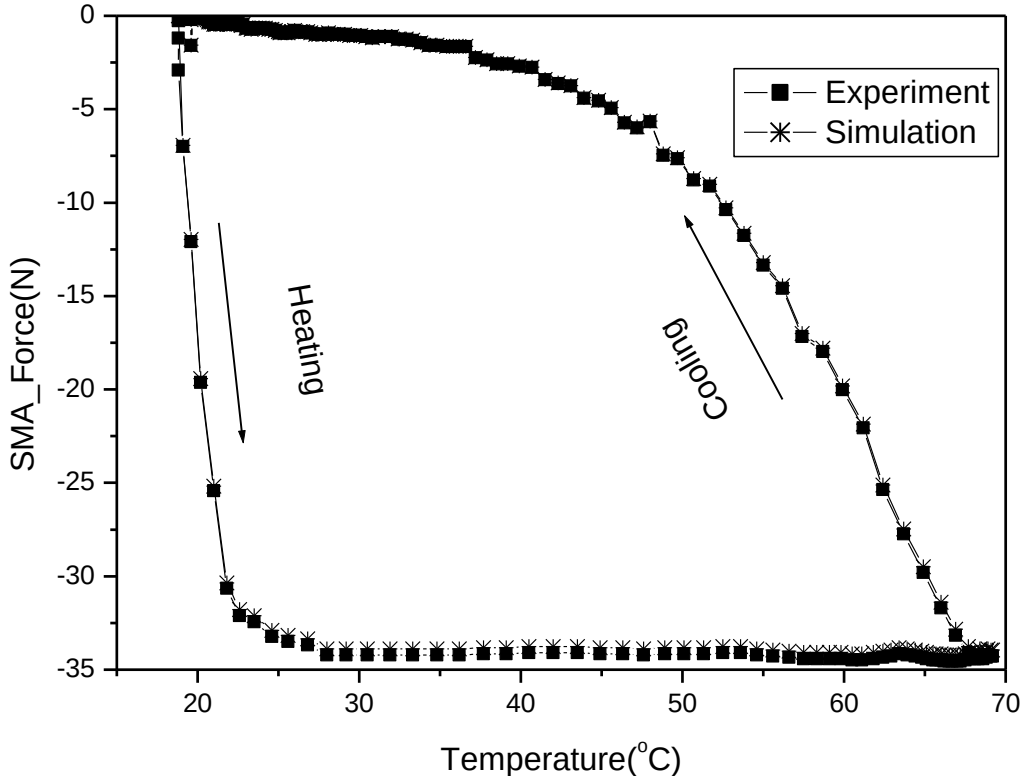


**Figure 4. 9: Numerical and experimental results for SMA force – temperature curves**

The maximum deflection for a steel beam as a function of temperature is shown in figure 4.10. The maximum deflection calculated through the code was less than 5mm, and this value agrees with the one observed experimentally. The comparison between the numerical results and experiment is shown in figure 4.11. All the graphs that were obtained numerically are in agreement with those obtained experimentally.

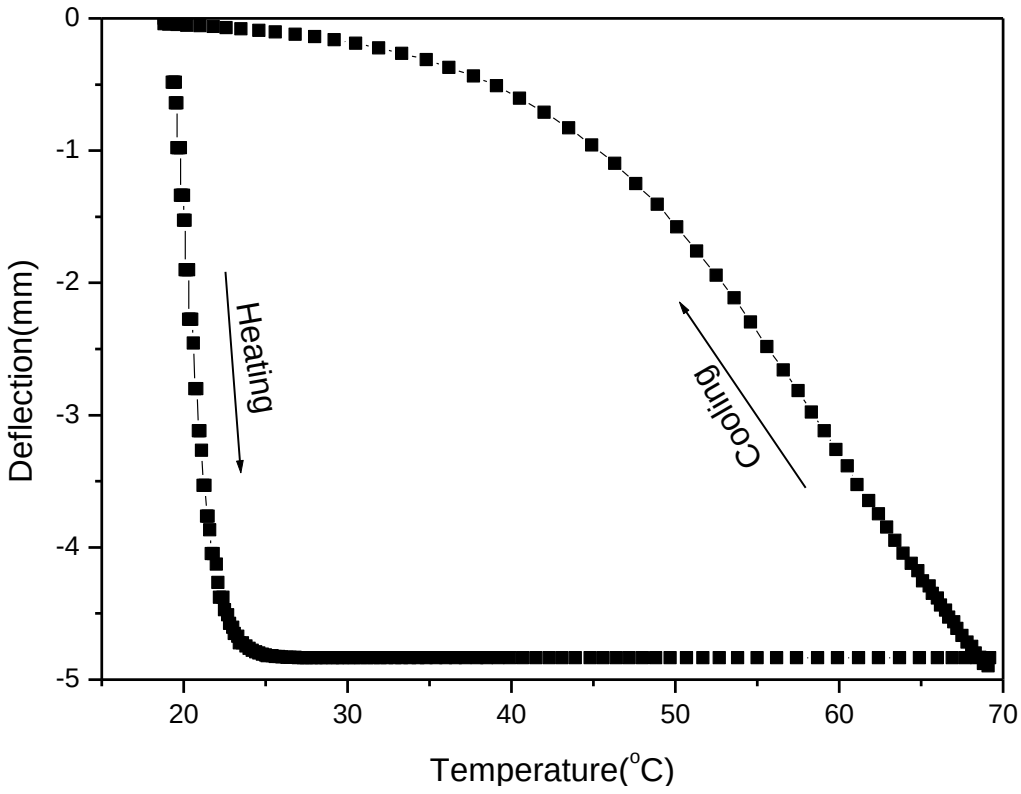


**Figure 4. 10: Beam bar numerical results for Deflection – temperature curve**

It can be concluded that the developed mathematical equations can be used to predict the behaviour of smart simple structures.

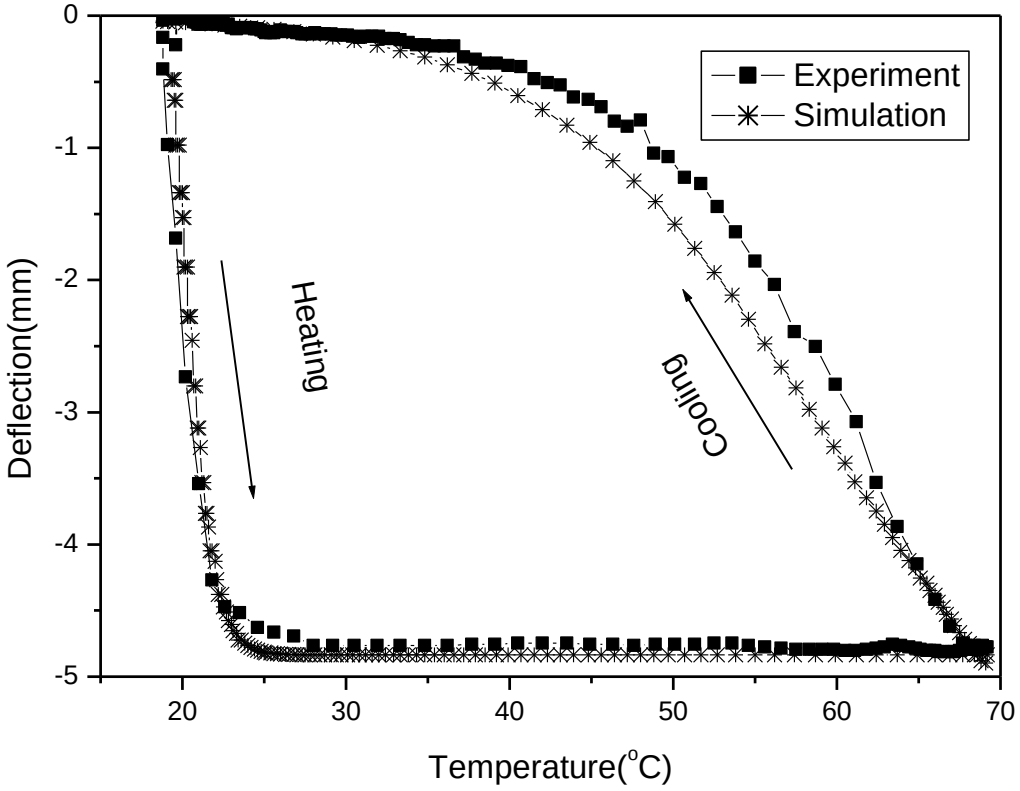


**Figure 4. 11: Experimental and numerical results for deflection – temperature curve**

## 4.5 THREE DIMENSIONAL IMPLEMENTATION INTO A COMMERCIAL FINITE ELEMENT PROGRAM (ABAQUS)

This section describes the implementation method of the previously introduced SMA model in a numerical environment. The end goal is the analysis of a smart aileron's deflection. The first section discusses the implementation of the model into the FEA framework (ABAQUS) that accounts for the vertical deflection of a smart aileron. It is arranged as follows: firstly, the description of the mathematical algorithm from the overall FEA framework to the local constitutive considerations. Secondly, the demonstration of the application of the developed simulation tool to the analysis of a complex smart aileron.

### 4.5.1 NUMERICAL IMPLEMENTATION OF THE SMA CONSTITUTIVE MODEL

Several individual topics are addressed in this first section: i) the FEA framework in the context of non-linear materials; ii) the possible methods of numerically integrating the local constrained evolution equations; iii) the particular form of the algorithm used to mathematically solve for an increment in stress at a material point, given an increment in strain and temperature.

### 4.5.2 FINITE ELEMENT ANALYSIS FOR NON-LINEAR MATERIALS

To provide the greatest capability for analysing active structural problems of varying complexity (including multi-step loading, large deflections, contact, etc.), the constitutive model of Chapter 2 was implemented in ABAQUS as a user material subroutine (UMAT). The method by which such an analysis tool calculates the mechanical response of a structure composed of a custom non-linear material is schematically illustrated in figure 4.12. Here we consider displacement-based (or strain-based) FEA, by far the most popular method of computational mechanics. Given a thermomechanical loading path, the process begins by applying the appropriate thermal and boundary conditions incrementally. Based on these boundary conditions, the global solver guesses an initial deformation for all nodes by solving the linear problem (i.e. the stiffness matrix is constructed considering only the elastic behaviour of the material) [Reddy, 1999]. In each element, at each material point (hence the superscript “mp”), these deformations are used to calculate local total strains, which are then passed into the UMAT. In the UMAT, updated local stresses are computed using the local total strains in addition to any internal variables

from the last loading increment. The local tangent stiffness, $C_j^{mp}$, at each material point is also calculated. The stresses are used to integrate the forces on the element, which are assumed to act at its nodes. The forces from all adjacent elements (acting at coincident nodes) are added, where the sum of forces at any given node should equal zero for static equilibrium.

The vector of sums is known as the force residual; if its magnitude is sufficiently small, the global solution is considered to be correct and the next loading path increment is applied. If the magnitude is too large, Newton's method (also known as the "Newton-Raphson" method) is used to compute a new guess for the global deformations, where the global tangent stiffness matrix (computed from the many local stiffness matrices) relates the deformation increments to the force residual. The process then repeats until convergence, at which point the boundary conditions are updated.

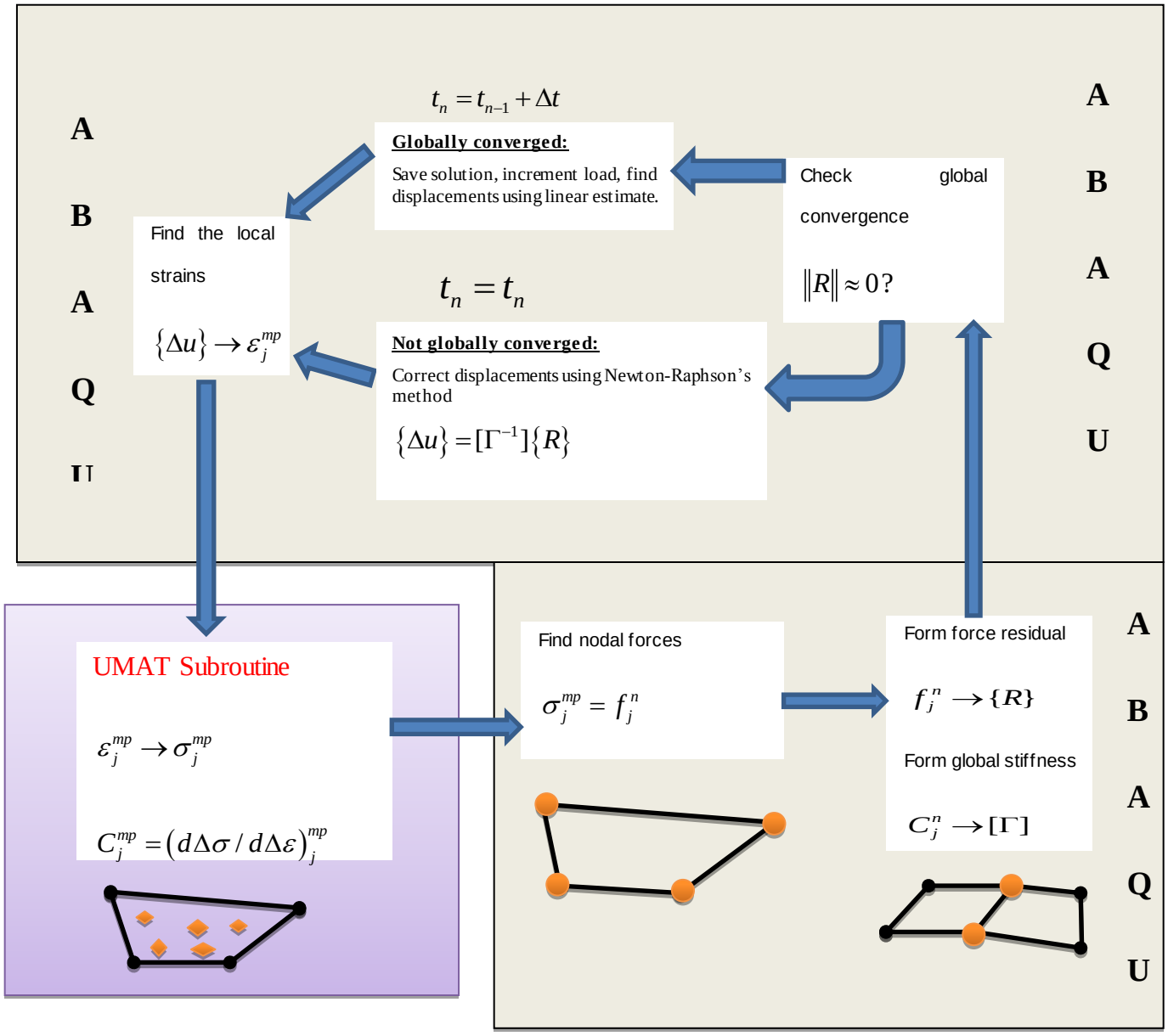


**Figure 4. 12: Schematic illustration of the global FEA solution process considering non-linear history-dependent materials [Hartl,2009]**

### 4.5.3 COMPACT SOLUTION ALGORITHM IMPLEMENTATION

Table 4.2 shows the summary of the solution algorithm needed to integrate the constitutive relation in ABAQUS framework.

**Table 4.2: Solution algorithm for modelling phase transformation phenomenon in SMAs**

**1. Initialize**

a. Give all the material properties

$\xi_m, E_m, E_A, \nu$, etc.

b. Set the "flag" using state variable: statev(1); statev(2); statev(3)

c. Set the training temperature (constant at 550$^{o}$C)

**2. Training Step**

a. Set the condition for starting the training using the flag in 1b.

b. IF $TEMP \geq 500^{o}C.AND.FLAG \leq 0$ THEN setup elastic stiffness tensor and then calculate the stress, ELSE EXIT

**3. Transformation step**

a. Check if the trained SMA plate is cooled down i.e.

IF $TEMP < A_S$ THEN set the SMA plate to fully martensite phase, ELSE EXIT.

b. Check if SMA plate is trained

IF $FLAG > 0$ AND $TEMP > A_S$ THEN $\xi(T)$

Set the transformation stiffness tensor/matrix

Calculate the transformation stress iteratively

c. If condition 3b is not met, the program stops and exit. If the condition is met the calculation continues until the SMA plate is fully austenite i.e. $\xi(T) = 0$

### 4.5.4 THREE DIMENSIONAL FINITE ELEMENT ANALYSIS RESULTS

This section presents predicted results for the 'smart' aileron which were obtained from the ABAQUS simulation package. The smart aileron solid model was developed through Solidworks, a CAD software. The developed simulation tool has two capabilities i.e. simulate NiTi SMA training and structural actuation. The results presented here are solely from the calculation of the mechanical response of the smart aileron in its vertical deflection

Figure 4.13 shows the developed 3-D solid model for smart aileron. The shape-memory alloy plates are shown in purple (leading edge) and the aluminium plates are shown in yellow (trailing edge) on the solid model. The dimensions used in developing the solid model are similar to those used for experiments.

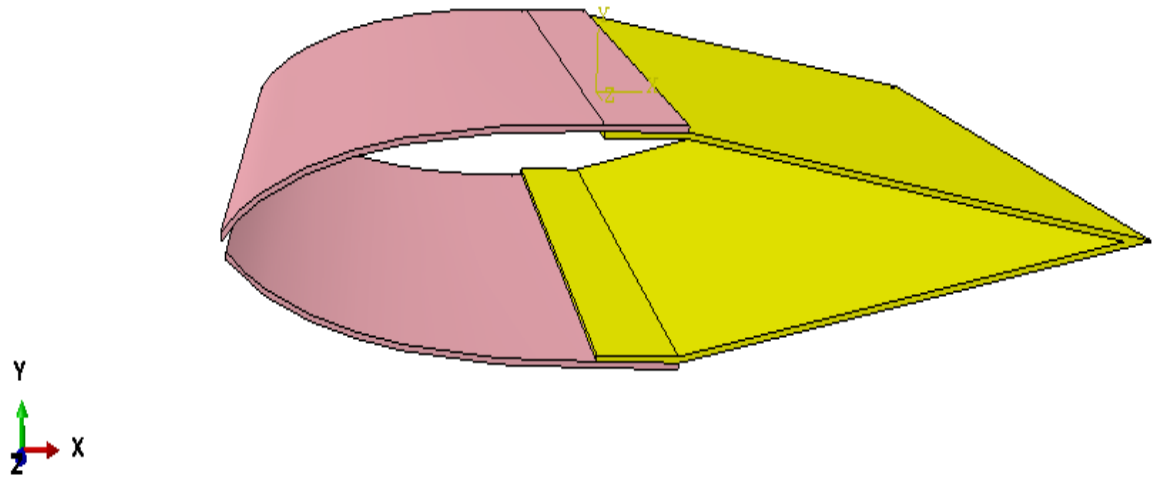


**Figure 4. 13: A solid model for Smart aileron on ABAQUS environment.**

When the material properties were specified and assigned to the model, the model was then meshed using hexagonal tetragonal methods with C3D8 elements and figure 4.14 was generated. The leading edge of a smart aileron

is fixed in all directions. Figures 4.15 – 4.22 show the simulation results for the top part of the smart aileron. The results presented are based on two steps i.e. training step and displacement step. During the training step, a vertical load of 2.5kN is applied to a NiTi SMA plate under a constant temperature of 550$^{o}$C. There is another step that was included during simulation called the actuation step. This step is aimed at cooling down the trained NiTi SMA before actuation application at displacement step, hence the mechanical load is zero and start temperature is 115$^{o}$C (See definition of values in the figures on appendix C). This temperature was chosen to be the start temperature for the simulation so as to reduce the number of iteration. Also, it is close to the austenitic start temperature (see **Table 4.3**). The displacement and strain results from the training and displacement steps are being compared.

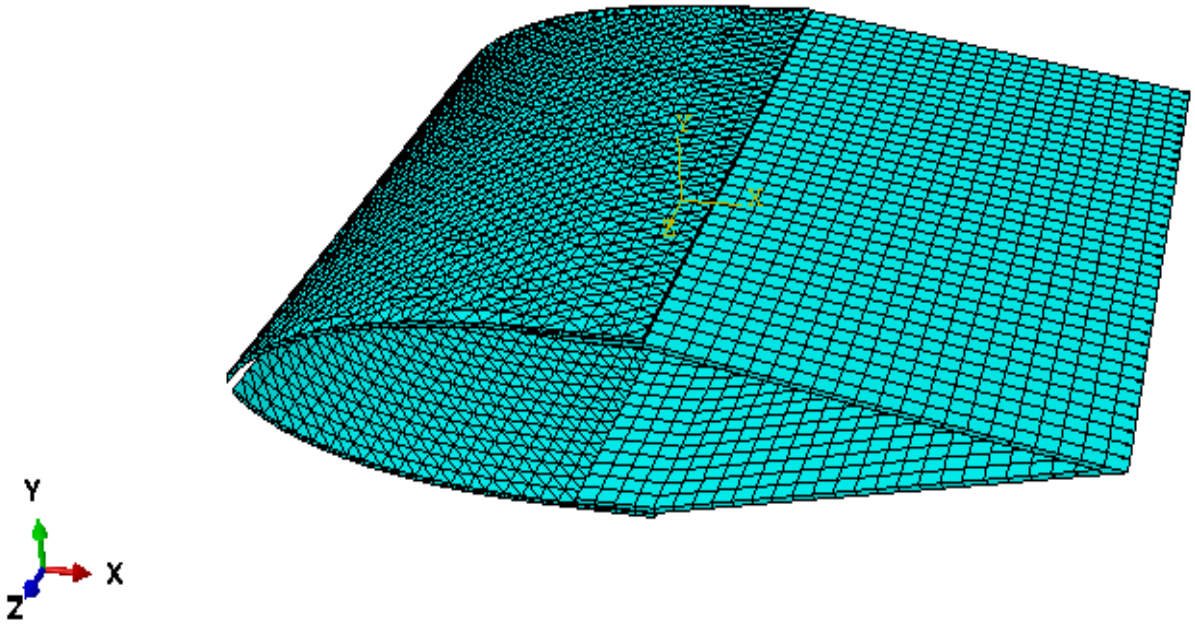


**Figure 4. 14: A 3-D mesh for Smart aileron on ABAQUS**

When a vertical load of -2.5kN (negative y-direction) is applied to a NiTi SMA plate (in the joint where the SMA plate joins the aluminium plate), the maximum vertical deflection (to the positive y-direction) of 39.34mm is

observed at the tip of the trailing edge. The distribution of deflection among various points of the smart aileron model are being coloured and their corresponding values are being displayed in figure 4.15. The red colour shows the points that experienced maximum deflection whereas the dark blue shows the points with no deflection.

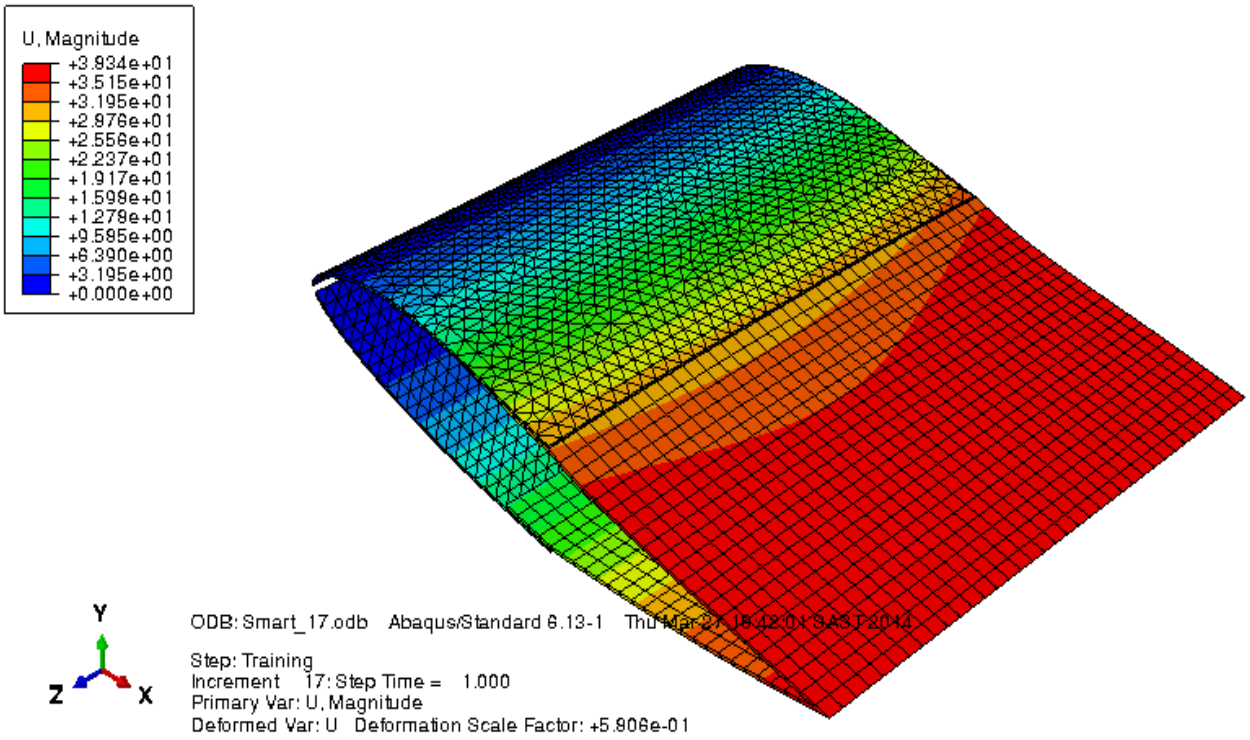


**Figure 4. 15: Displacement resulting from the applied load during the training step**

Figure 4.16 shows the distribution of strain in the entire body of the model. The regions close to the fixed points seem to have high values of strain which means the stress is also high in those regions. The maximum strain is observed at the bonding region (where the NiTi SMA plate bonds with the aluminium plate) whereas the minimum strain occurs at the tip of the trailing edge (free end). Figure 4.17 shows that the tip of the trailing edge experienced major deflection when compared to other parts of the body.

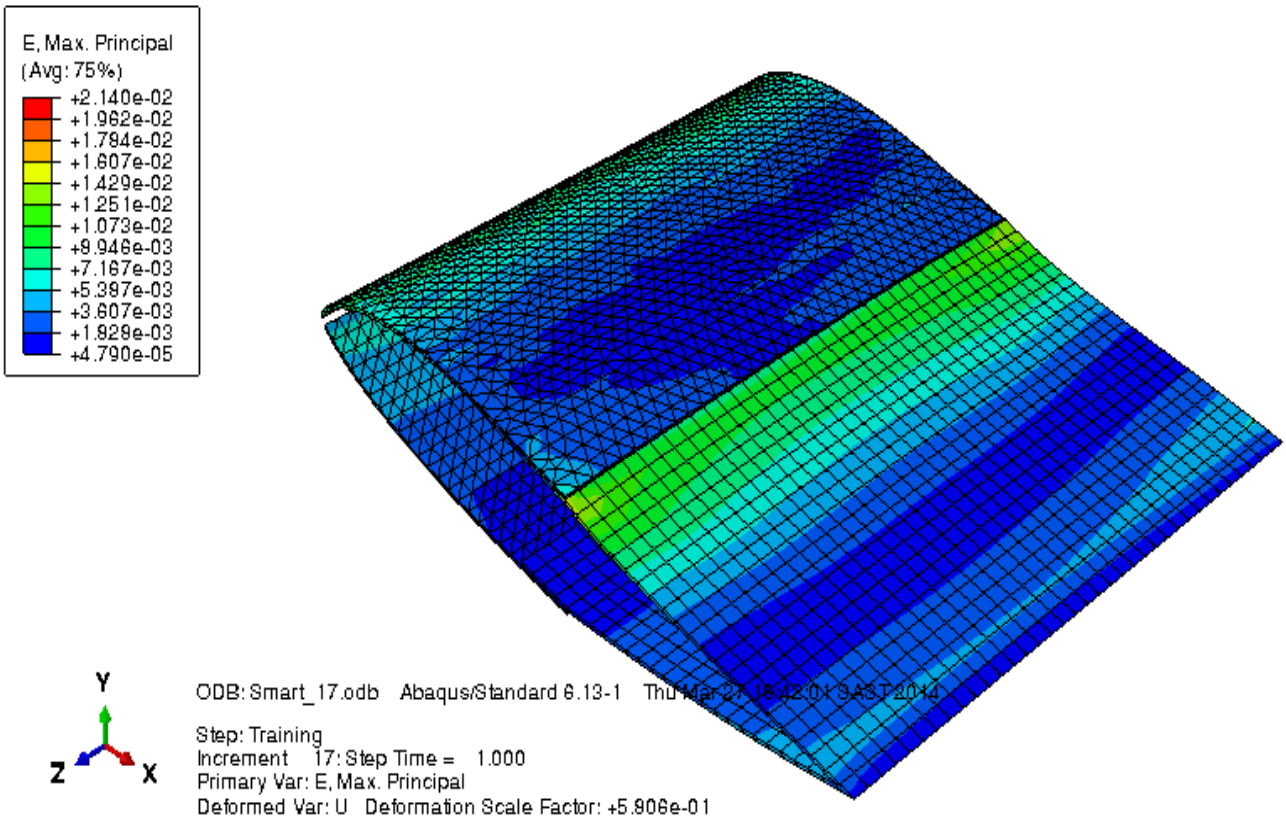


**Figure 4. 16: Strain resulting from applied load during training step**

Figure 4.18 shows the resulting deflection due to the shape-memory effect. The maximum upward deflection occurs at the tip of the trailing edge of the body and the minimum occurs in the regions close to the bond. The maximum deflection is 1.953mm which is approximately 5% of the deflection observed during the training step.

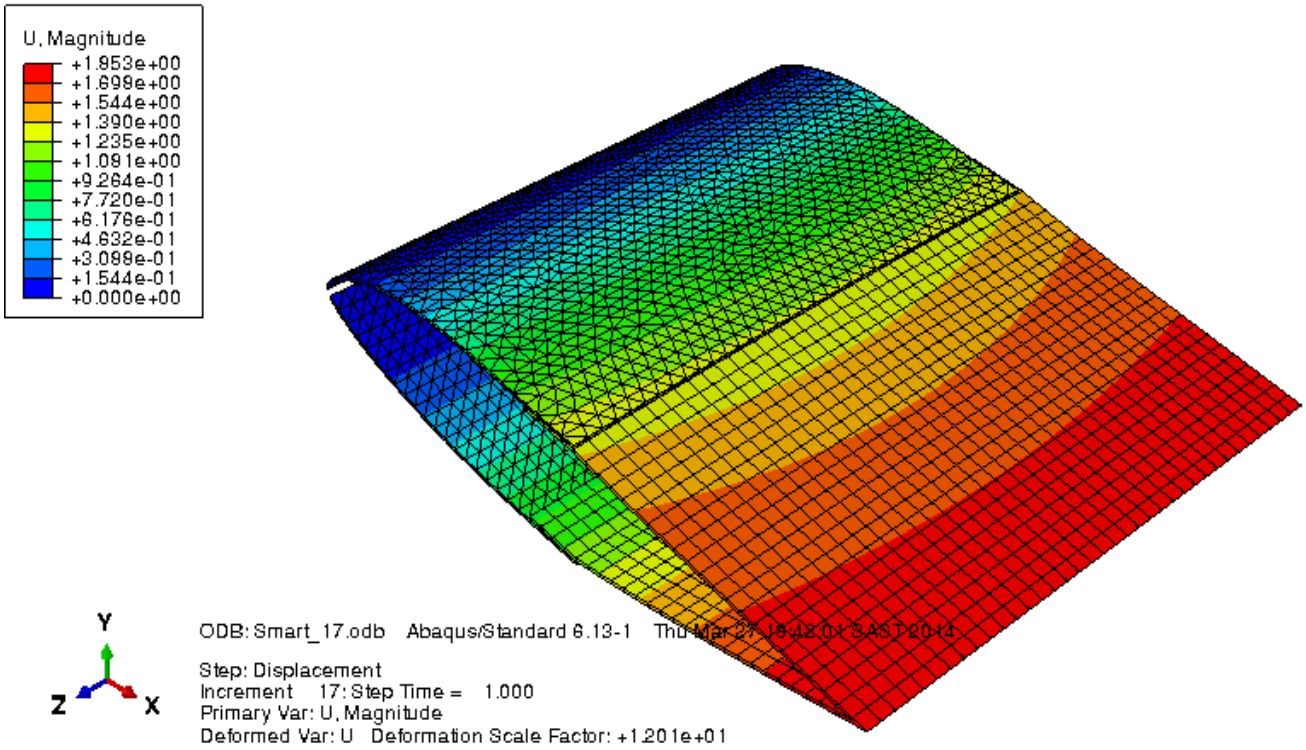


**Figure 4. 17: Displacement resulting from the transformation load during the displacement step**

The strain resulting from the shape-memory effect during the displacement step is shown in figure 4.19. The behaviour observed here is similar to the one shown in figure 4.15. The maximum recovered strain during transformation is approximately 5% which agrees with the percentage of deflection. The calculated recovered strain falls within the maximum recoverable strain for the NiTi SMA material reported in the literature [Zhou et al., 2009]. The values of deflection and strain agree with the values measured experimentally in the preceding Chapter 3.

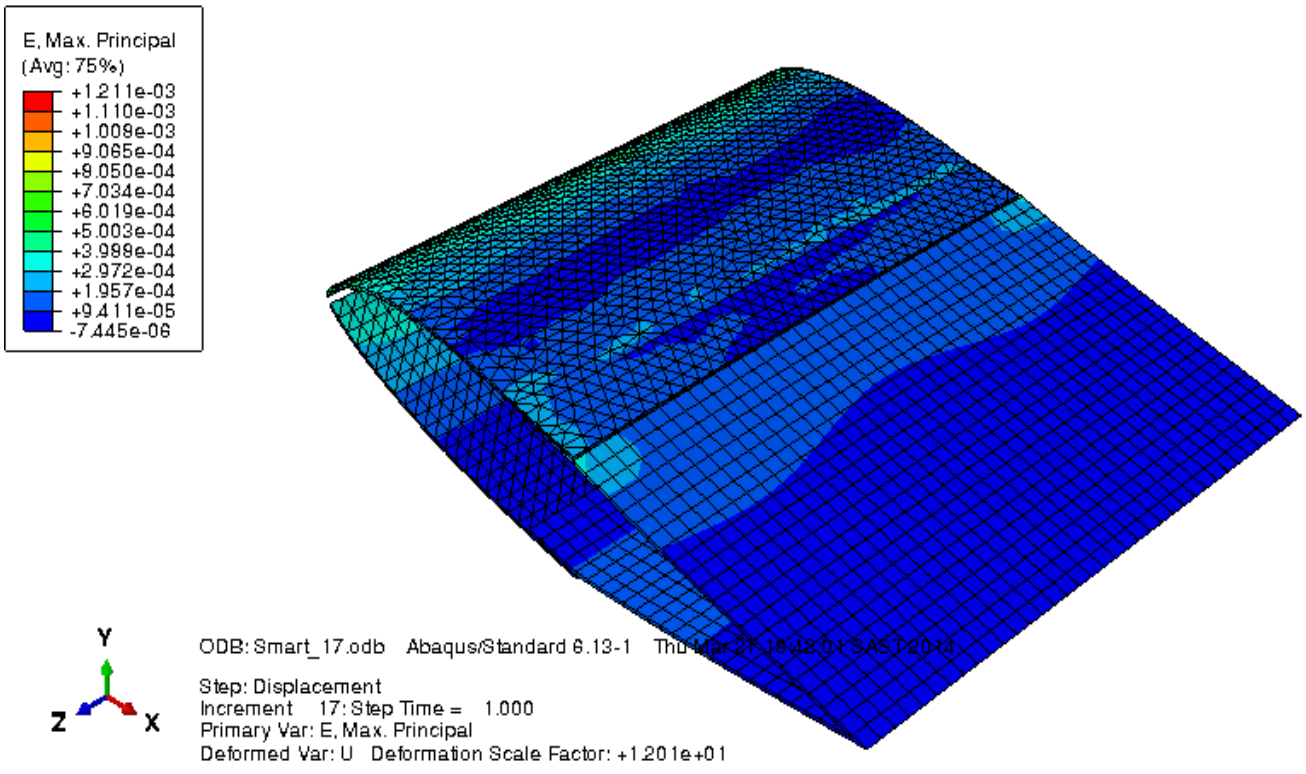


**Figure 4. 18: Strain resulting from the transformation load during the displacement step**

The Displacement – Time graph shown in figure 4.19 was plotted using ABAQUS when executing the training step. The graph was plotted from different nodes of the trailing edge of the smart aileron. The graph clearly shows different values of maximum deflection ranging between 29-39mm. The maximum deflection is associated with the tip of the trailing edge of the smart aileron, whereas the minimum is associated with the region close the bonding. The strain plot shown in figure 4.20 has a similar behaviour to the deflection plot. The nodes selected or used to generate the deflection plot are the same nodes used to generate the strain – time plot.

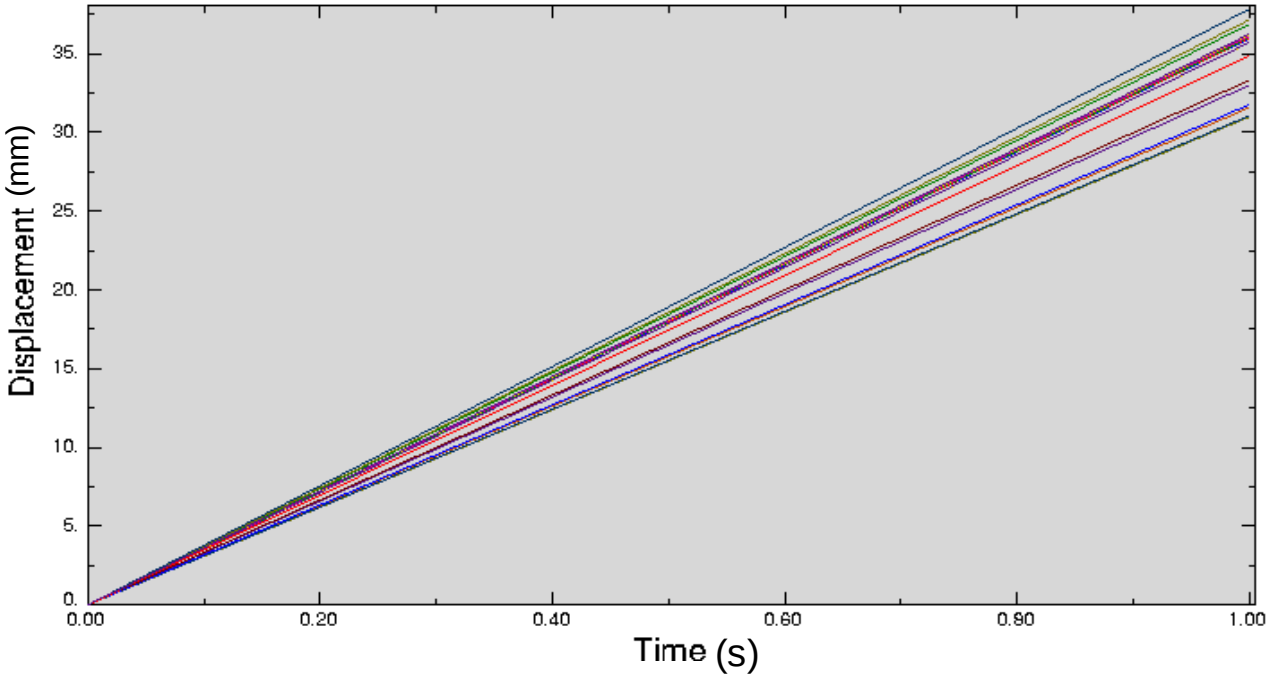


**Figure 4. 19: Displacement-time graph resulting from the applied load during the training step**

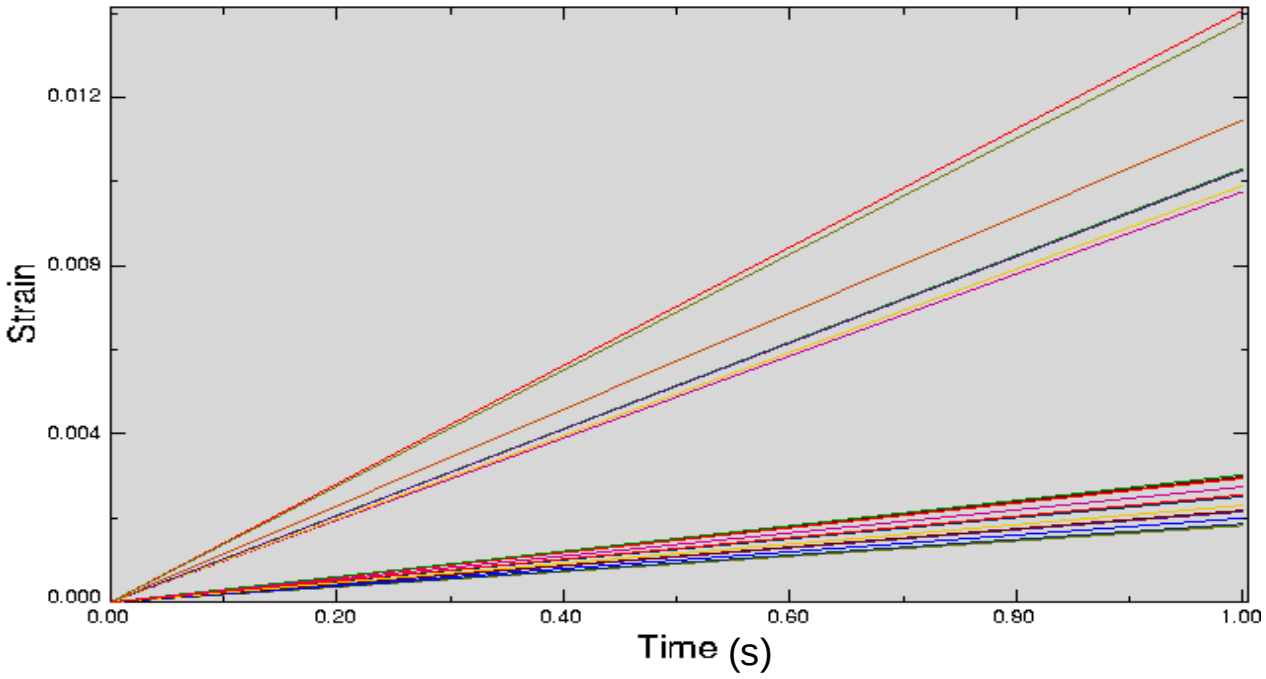


**Figure 4. 20: Strain-time graph resulting from the applied load during the training step**

The very same nodes were used to generate the curves for figures 4.21 and 4.22. The figures show the maximum deflections and maximum strains

respectively due to the shape-memory effect at various points of the trailing edge of the smart aileron. It can be seen that figures 4.21 and 4.22 exhibit similar behaviour but are different from figures 4.19 and 4.20. Figures 4.19 & 4.20 exhibit linear behaviour whereas figures 4.21 & 4.22 exhibit hyperbolic behaviour. This is due to the fact that the model describing SMA behaviour involves a hyperbolic function. It is also noted from figure 4.21 and 4.22 that the graphs exhibit flatness towards the end of the iteration. This symbolizes the end of phase transformation. Figure 4.22 also shows experimental plot and simulation plot which both have similar behaviour. Both curves attain similar maximum strain indicated on the graph. It was not possible to do the same with experimental and simulation deflection curves because the simulation data came out as a magnitude but both curves can show similar maximum deflection.

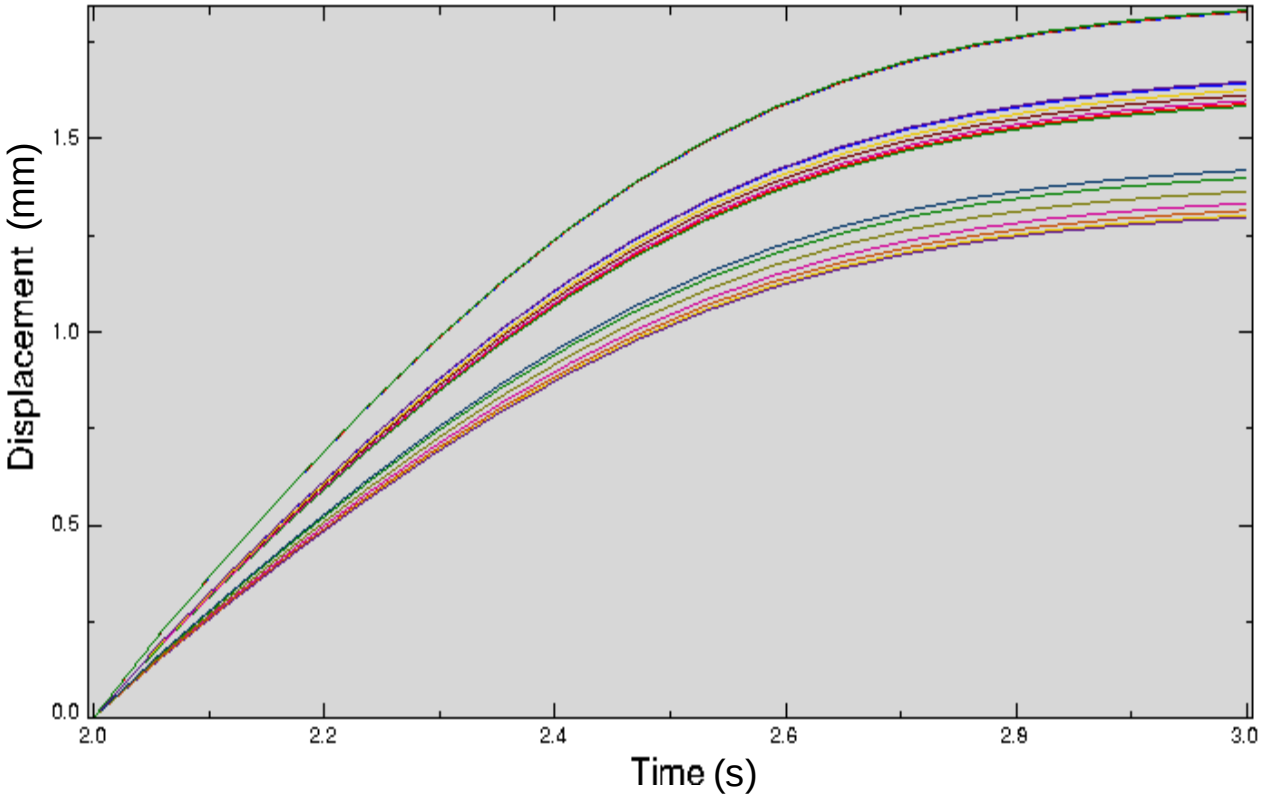


**Figure 4. 21: Displacement-time graph during the displacement step**

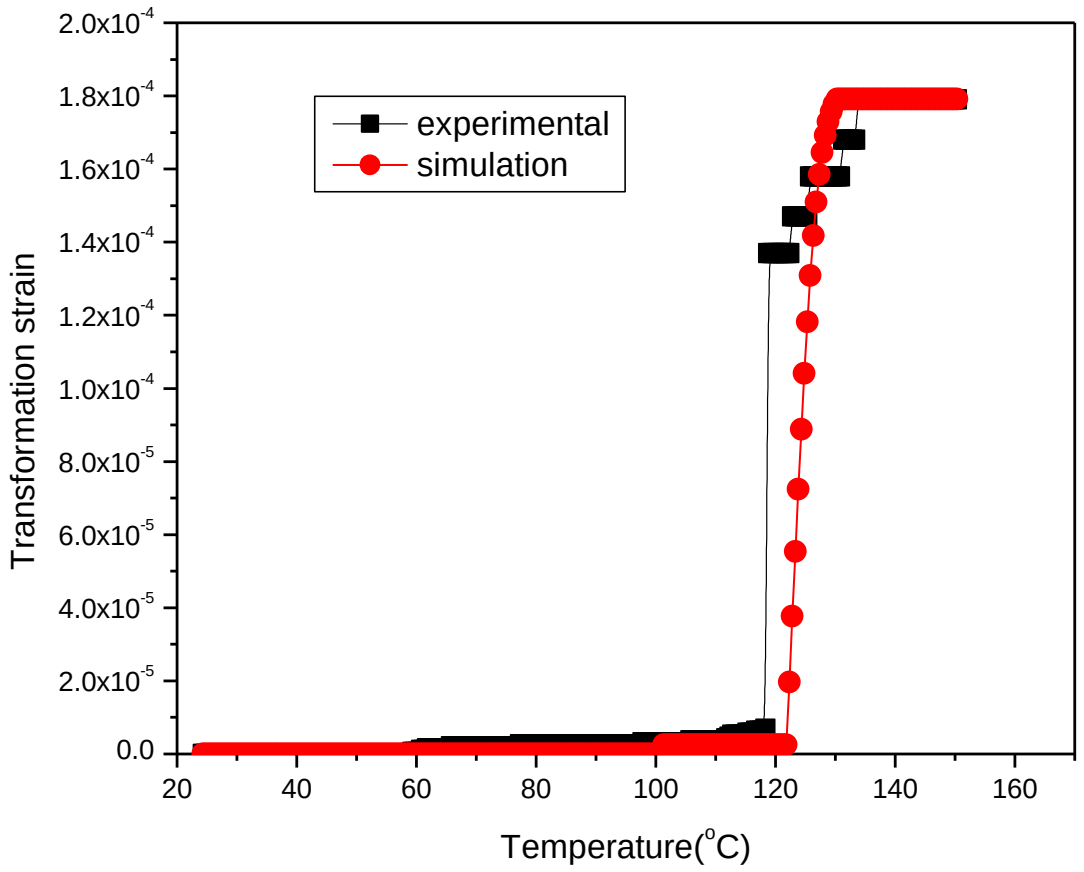


**Figure 4. 22: Strain-temperature graph during the displacement step (simulation and experiment)**

The results for the bottom part of the smart aileron are shown in figures 4.23 through 4.31. The discussion of these results is similar to the previous observed in figures 4.15 through 4.21. The vertical 5.0kN (positive y-direction) force was also applied to the NiTi plate under a constant temperature of 550$^{o}$C during the training step. The maximum deflection and strain were observed to be 46.44mm and 1.149E-2 % respectively. The maximum downward deflection was seen to be at the tip of the trailing edge of the smart aileron whereas the maximum strain was at the regions close to the joint (see figure 4.23 and 4.24).

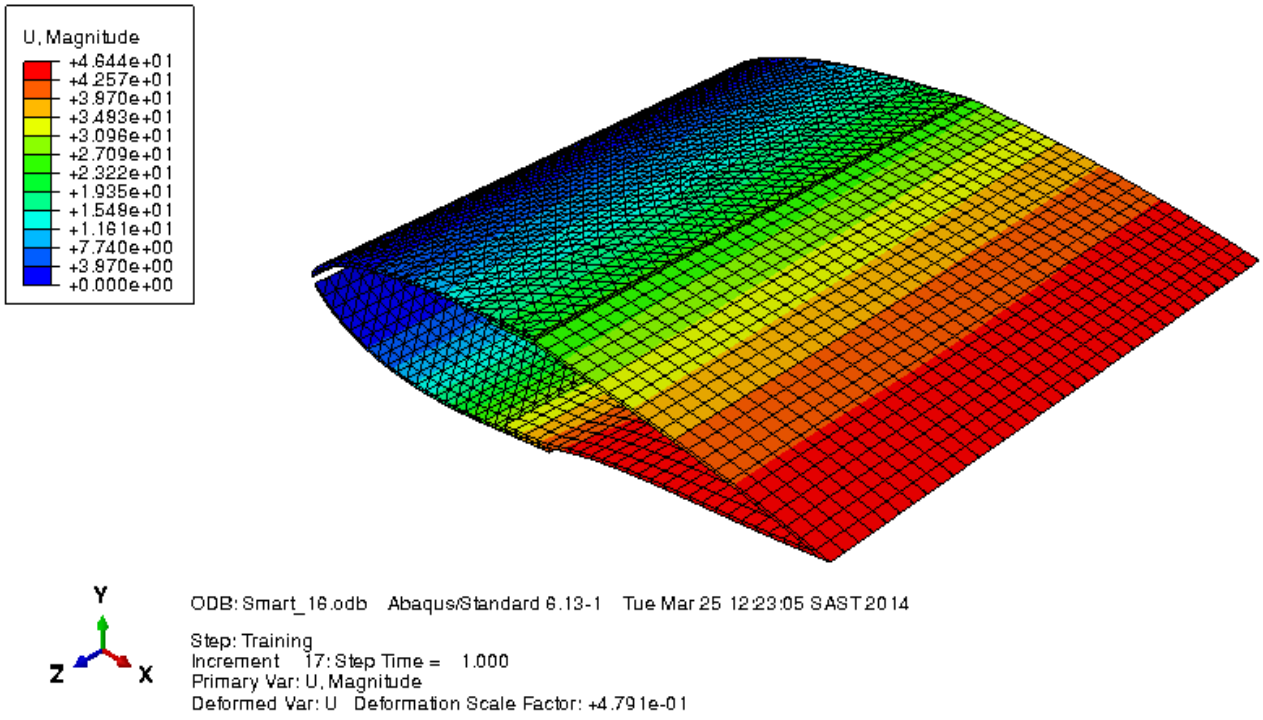


**Figure 4. 23: Downward deflection upon mechanical loading**

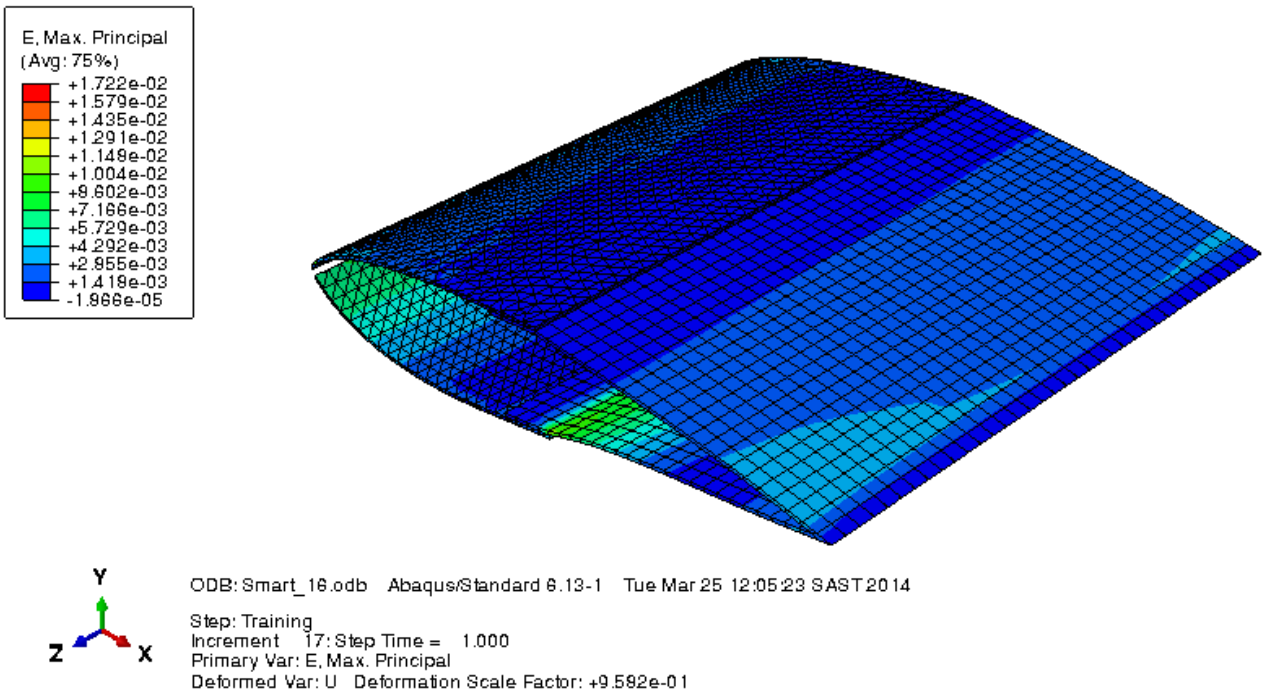


**Figure 4. 24: Downward deflection: mechanical strain during the training step**

Figures 4.25 and 4.26 show the recovered strain and the resulting downward deflection respectively due to the shape-memory effect. The maximum downward deflection was found to be 2.97mm whereas the maximum recovered strain was 9.0E-5. The strain graph on figure 4.29 shows both experimental and simulation curves for comparison purposes. The plots for different nodes on the bottom part of the smart aileron were generated and their behaviour is similar to those from the top part of the smart aileron.

The only difference between the top part and the bottom part is the temperature range at which the transformation is occurring. The transformation for the top part occurs at the temperature range above 100$^{o}$C whereas the bottom part occurs at temperature range below 100$^{o}$C (martensite transforms to austenite i.e. heating). This was caused by the quenching process which is discussed in the following chapters. Figure 4.31

reveals a linear variation between time and temperature. Some figures show a number of lines with different colours. They show the variation of either deflection or strain at various points of the structure.

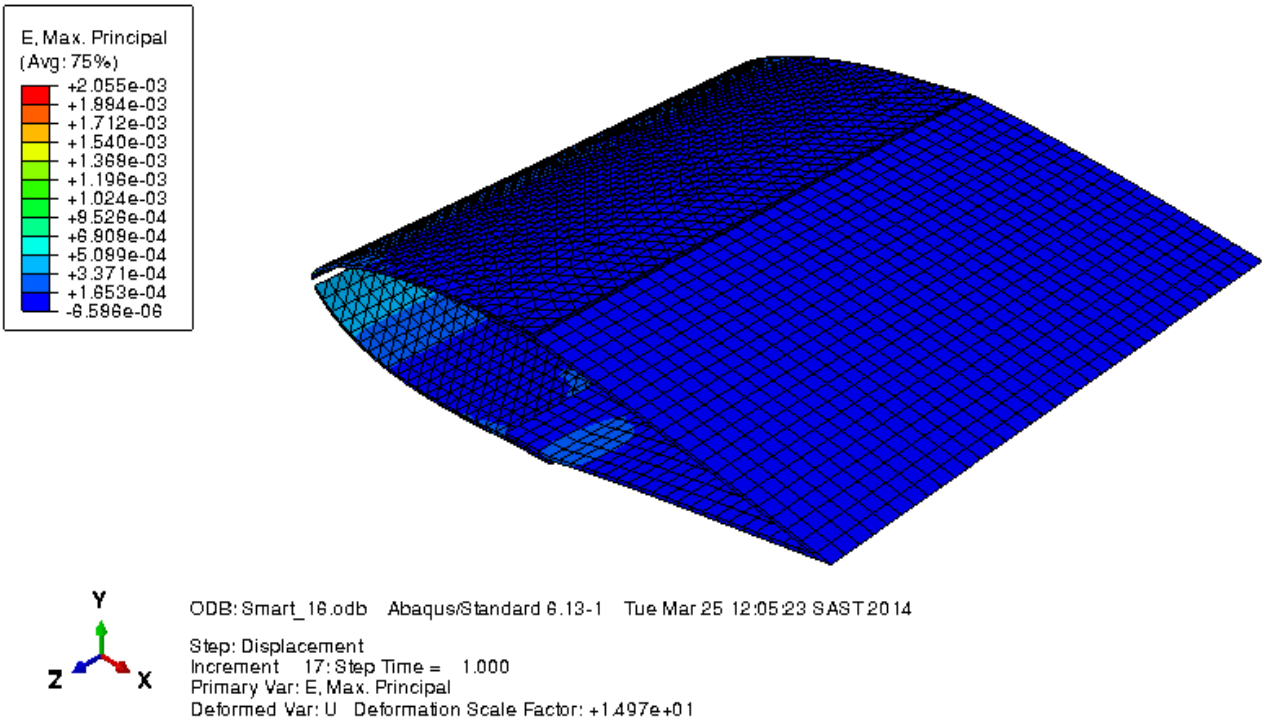


**Figure 4. 25: Downward deflection: transformation strain during the actuation step**

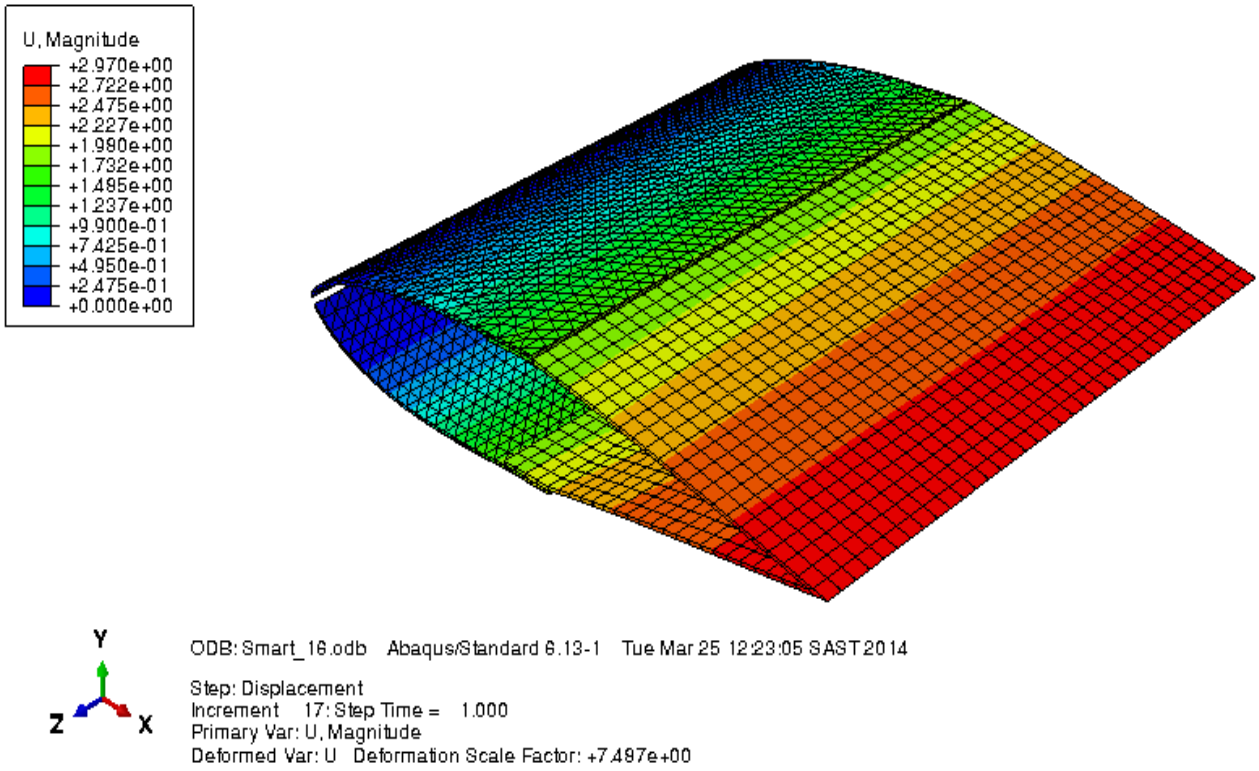


**Figure 4. 26: Downward deflection due to the phase transformation**

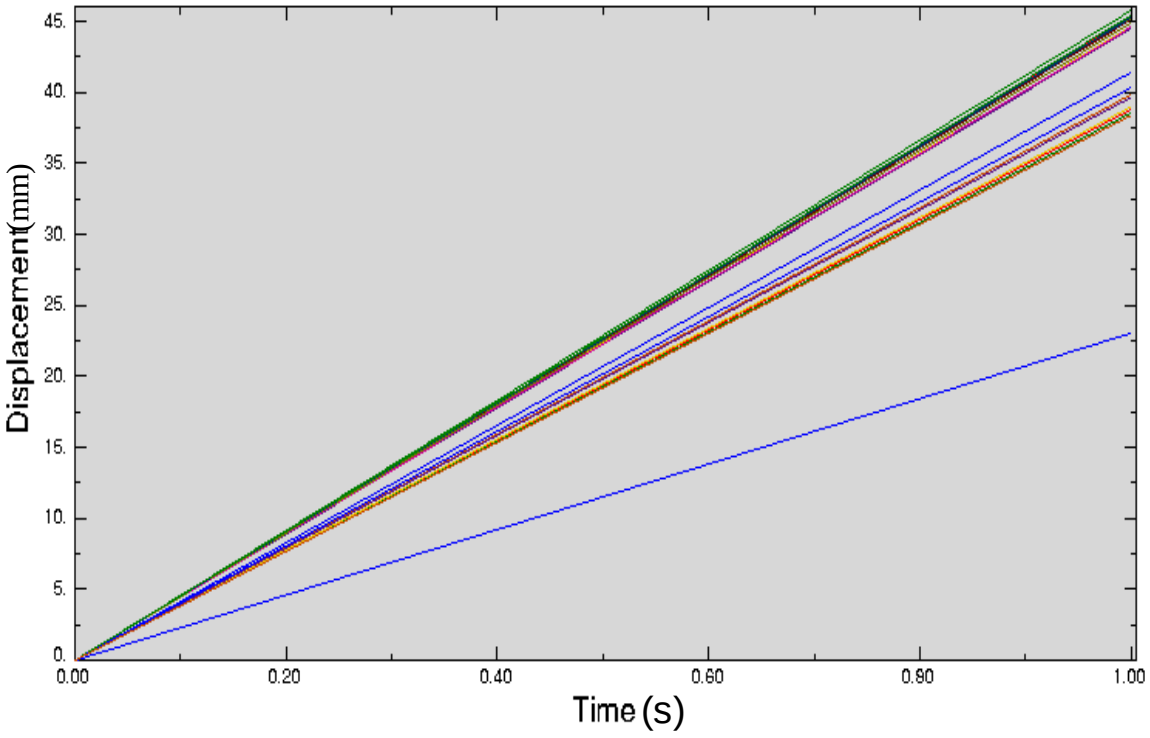


**Figure 4. 27: Vertical deflection-time graph during the training step**

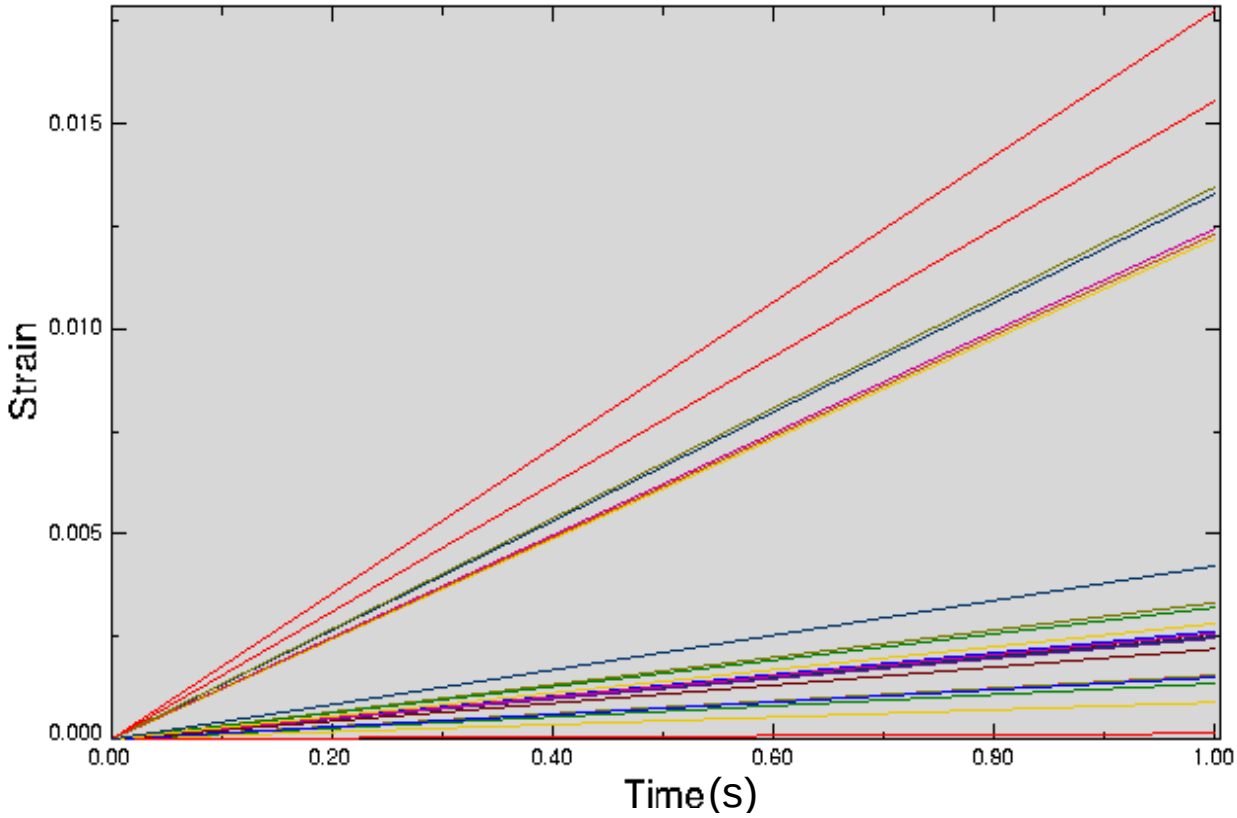


**Figure 4. 28: Mechanical strain-time curves during the training step**

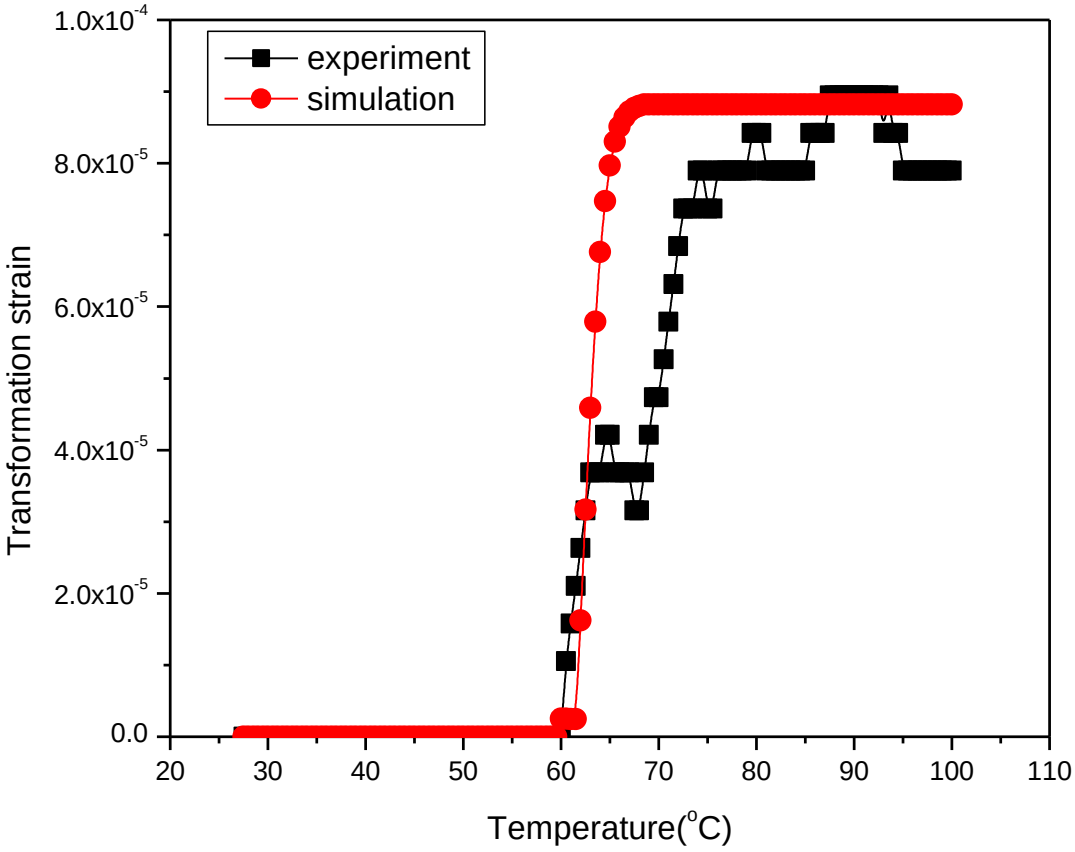


**Figure 4. 29: Transformation strain-temperature curves during the Displacement step (simulation and experiment)**

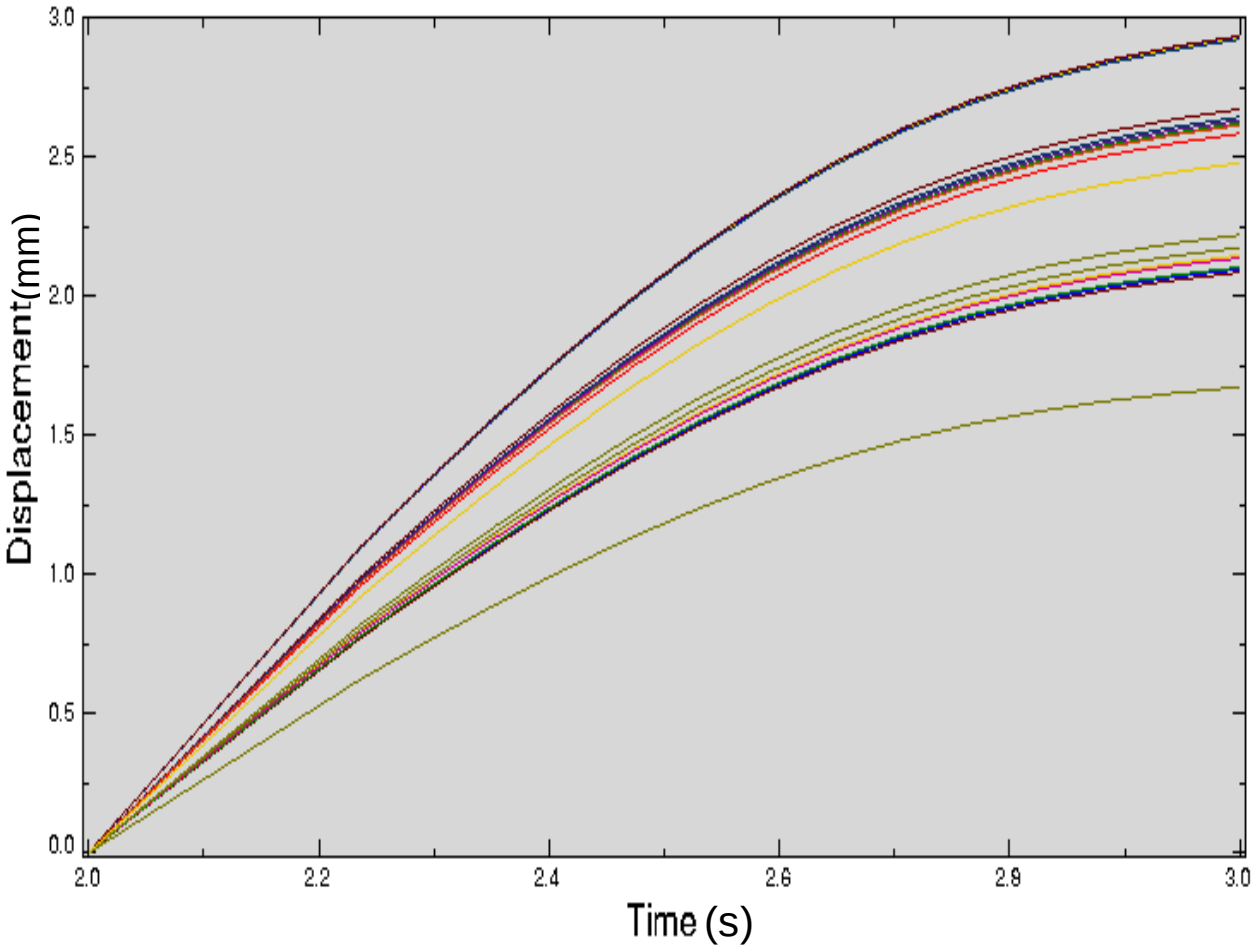


**Figure 4. 30: Deflection-time resulting from transformation during the Displacement step**

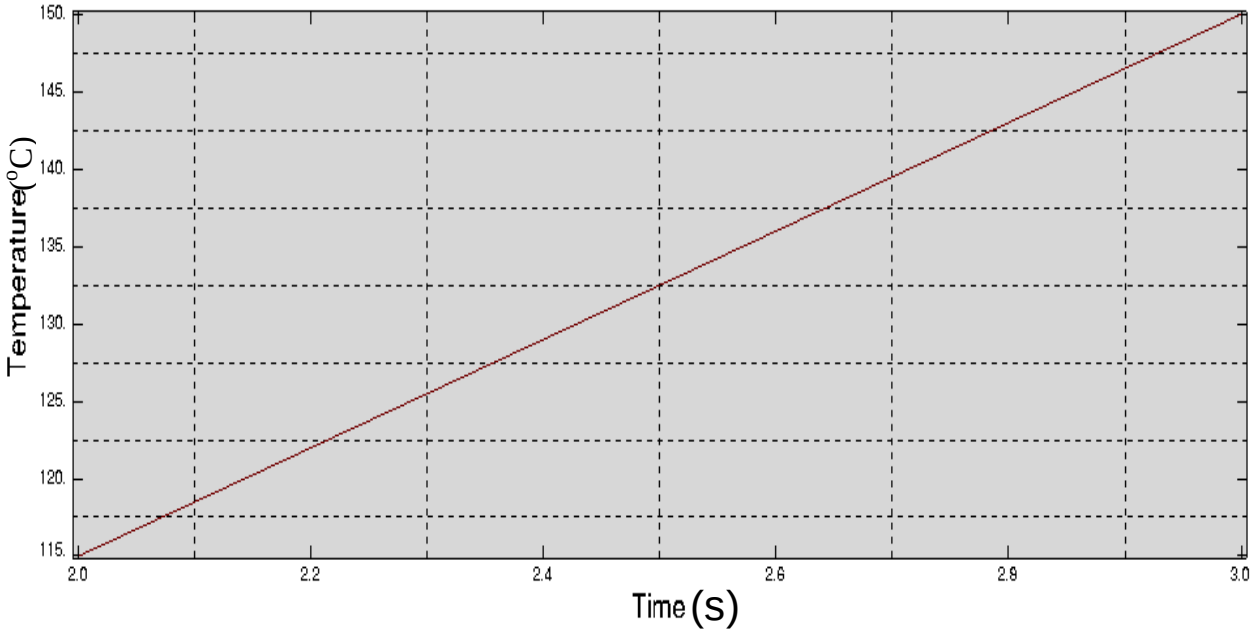


**Figure 4. 31: Temperature – Time graph relationship**

**Table 4.3: Material properties for NiTi SMA plate used during simulation**

| Property | Value | Units |
|---|---|---|
| **Thermoelastic properties** | | |
| $E_A$ | 70 | GPa |
| $E_M$ | 28.3 | GPa |
| $\nu_M = \nu_A$ | 0.33 | - |
| $\alpha_M = \alpha_A$* | $10^{-6}$ | /°C |
| **Phase Diagram Properties** | | |
| $M^T_s$ | 52.7 | °C |
| $M^T_f$ | 26.1 | °C |
| $A^T_s$ | 117.3 | °C |
| $A^T_f$ | 133.7 | °C |
| $M^B_s$ | 54.6 | °C |
| $M^B_f$ | 38.8 | °C |
| $A^B_s$ | 66 | °C |
| $A^B_f$ | 86.7 | °C |
| $C_M$* | 8.0 | MPa/ °C |
| $C_A$* | 13.8 | MPa/ °C |
| $\varepsilon_L$* | 6.7 | % |

* Values obtained from Zhou et al. (2009)

## COMPARISON OF RESULTS

This section compares the simulated deflection results to the experimental deflection results with the purpose of validating the developed tool. The strain-temperature curves shown in figure 4.22 and 4.29 are the curves for experimental and numerical results. They are plotted on the same graph so as to validate our developed model.

Figure 4.22 shows the strain-temperature plot for the top surface while figure 4.29 shows the strain-temperature plot for the bottom surface. The maximum transformation strain for the top surface was approximately 1.8e-4 mm/mm while the bottom surface shows the maximum of 1.0e-4 mm/mm. Although there is a slight difference between the maximum transformation strain on the top and bottom surface but the numerical and experimental curves show similar behaviour.

The activation temperatures for the upward and downward deflection are similar in both experimental and simulated results. The maximum upward deflection was approximately 2mm whereas the maximum simulated upward deflection was approximately 1.953mm.

The maximum downward deflection was approximately 3mm whereas the maximum simulated upward deflection was approximately 2.970 mm. The correlation between the simulation deflection values and experimental deflection values show the capability of the developed simulation tool in predicting the behaviour of a smart structure. It can be seen that there is a difference in values between the maximum downward and maximum upward deflection. This was due to the difference in training conditions.

The deflection start temperature for the upward deflection during heating is above factory activation temperature i.e. $89^{o}C$ yet the downward deflection start temperature are below the factory activation temperature. This is an indication that the training conditions for the top and bottom SMA plate were

not the same. An immediate quenching of SMA material results in low activation (austenitic start and finish) and high for the opposite.

The experimental results show that one full deflection cycle takes a maximum of about twenty minutes of which it is practical unhealthy. This high delay time shows that the constructed smart aileron needs some optimization before it can be implemented. The optimization would be to reduce the response time and to maximize the deflection in both directions.

# CHAPTER 5

## CONCLUSIONS

The aim of this work was to develop the ability to efficiently simulate the behaviour of SMA material to be used for the design of compact actuation mechanisms. The possible application was in aircraft to assist the actuation of flight surfaces such as for actuating a servo-tab to assist the movement of an aileron or for aeromorphing that would have a similar effect. Both SMA wire and SMA plate were therefore looked at in terms of the requirements for modelling an SMA actuator. The task was to capture enough of the SMA behaviour to predict the movement of the actuator and, where appropriate the structure attached to it, which would include determining the force produced by the actuator.

The aim was not to create a model that described all aspects of SMA behaviour, only the aspects critical to the design so that the solution process was efficient with sufficient accuracy in terms of predicting the experimentally measured behaviour. The model for the actuator was restricted to the shape memory effect which was taken to be a thermally activated phase change from the martensite phase to the austenite phase for actuation and the unloading was similarly the result of cooling below the critical temperature which produced the change from austenite to martensite.

A new form of the thermally activated phase change function was developed in the form of a hyperbolic tangent function not the cosine function described

in literature. This had the advantage of using a monotonically increasing function asymptotically approaching one in the positive quadrant, not a cyclic function so that there was a unique function value. This was a useful attribute for finding material parameters or for searching for a non-linear solution. The proposed model was then coded as an algorithm using C++ and FORTRAN.

The developed modelling procedure was validated against experimental tests and modelling parameters were identified so that the numerical simulations closely followed the experimental measured deflections of the structures tested.

Two main experiments were performed so as to obtain the material constants tabulated in Table 4.1 and in Table 4.3. Those material constants were used for simulation. Along with the determination of heating times the critical temperature for the transformation between martensite and austenite was determined experimentally for all the SMA material used. The heating and cooling times for the different experimental setups was also measured to determine the actuation and deactivation cycle time as another design constraint.

In addition tensile tests were performed on NiTi SMA plate so as to analyse its behavior to find limits on the loading and in the case of the plate the maximum bending. The maximum actuated load that a volume of SMA wire could produce was also determined ($0.993N/mm^3$ ) to as to provide a force limit for

the actuator which is important in accurately predicting the real behavior of any structure designed using the model.

Two implementations of the developed model were produced. The main implementation was a FORTRAN user material subroutine in the commercial package ABAQUS for three-dimensional coupled thermo-mechanical problems. The implementation in ABAQUS included an algorithm to determine the stress from ,the strain for a given temperature change or applied load along with the algorithmic tangent moduli used for the non-linear solution in ABAQUS.

Also a two dimensional truss-beam element code was written in C++ to implement the SMA actuator model. This was used to accurately simulate the bending of a bar by an SMA wire so as to determine material parameters for the wire actuator. This was not fully coupled but had the advantage of being able to record the temperature and response and to prescribe the temperature history in the simulation to be the same as the measured temperature and to thus identify the material parameters that would produce the same mechanical response.

In conclusion the goals for facilitating the simulation of SMA material in compact designs for actuators that could possibly be used in aerospace applications as originally set out in the Airbus sponsored student project, have been met.

# REFERENCES

Kutz, M. 1990, “Mechanical Engineering Handbook.”, Material and Mechanical Design, page 382.

Duerig, T.W., Melton, K.N., Stockel, D. & Wayman, C.M. 1990, “Engineering Aspects of Shape Memory Alloys.” Betterworth-Heinemann Company, London.

Savi,M.A, Paiva, A., Baeta-Neves ,A.P. & Pacheco,P.M. C. L. 2002,” Phenomenological Modeling and Numerical Simulation of Shape Memory Alloys: A Thermo-plastic-phase Transformation Coupled Model” , Journal of Intelligent Material Systems and Structures, Vol. 13, pp 261-273

James,R.D. 2000,”New materials from theory: trend in the development of active materials”, International Journal of Solids and structures, Vol. 37, pp. 239-250

Brinson, L.C. & Huang, M.S. 1996, "Simplifications and comparisons of shape memory alloy models", Journal of Intelligent Material Systems and Structures, vol. 7, no. 1, pp. 108-114.

Seelecke, S. & Müller, I. 2004, "Shape memory alloy actuators in smart structures: Modeling and simulation", Applied Mechanics Reviews, vol. 57, no. 1-6, pp. 23-46.

Petersen K.E. 1982, “Silicon as a mechanical material”, Proceedings IEEE, vol.70, no. 5.

Seelecke, S. 1997, “Control of Beam Structures by Shape Memory Wires.”, Proceedings of the 2nd Science Conference of Smart Mechanical Systems – Adaptronics, Otto-von-Guericke Univ. Magdeburg.

Bathe, K. J. 1982, “Finite Element Procedures in Engineering Analysis”, Prentice-Hall, Englewood Cliffs.

Funakubo, H. (ed.) 1984, “Shape Memory Alloys”, Gordon and Breach Science Publishers.

ANSYS User's Manual for Revision 6.1, Swanson Analysis Systems, Inc.

Seelecke,S. & Papenfuss, N. 2000, “A Finite Element Formulation for SMA Actuators.”, Journal of Applied Mechanics and Engineering, vol. 5, no.1, pp 160-178.

Auricchio, F. & Taylor, R.L. 1997, "Shape-memory alloys: Modelling and numerical simulations of the finite-strain superelastic behavior", Computer Methods in Applied Mechanics and Engineering, vol. 143, no. 1-2, pp. 175-194.

Auricchio, F. 2001, "A robust integration-algorithm for a finite-strain shape-memory-alloy superelastic model", International Journal of Plasticity, vol. 17, no. 7, pp. 971-990

Auricchio, F., Marfia, S. & Sacco, E. 2003, "Modelling of SMA materials: Training and two way memory effects", Computers and Structures, vol. 81, pp. 2301-2317

Thamburaja, P. & Anand, L. 2001, "Polycrystalline shape-memory materials: Effect of crystallographic texture", Journal of the Mechanics and Physics of Solids, vol. 49, no. 4, pp. 709-737.

Christ, D. & Reese, S. 2009, "A finite element model for shape memory alloys considering thermomechanical couplings at large strains", International Journal of Solids and Structures, vol. 46, no. 20, pp. 3694-3709.

Fremond, M. 1996, “Shape memory alloy: a thermomechanical macroscopic theory”, CISM Courses and Lectures, no. 351, Springer, New York, pp. 3–68.

Dong, Y., Boming, Z. & Jun, L. 2008, "A changeable aerofoil actuated by shape memory alloy springs", Materials Science and Engineering A, vol. 485, no. 1-2, pp. 243-250.

Mani, R., Lagoudas, D.C. & Rediniotis, O.K. 2008, "Active skin for turbulent drag reduction", Smart Materials and Structures, vol. 17, no. 3.

Good, M.G. 2003, “Development of a Variable Camber Compliant Aircraft Tail using Structural Optimization.”, Master of Science in Mechanical Engineering at Virginia Polytechnic Institute and State University.

Brinson, L.C. & Lammering, R. 1993, "Finite element analysis of the behavior of shape memory alloys and their applications", International Journal of Solids and Structures, vol. 30, no. 23, pp. 3261-3280.

Trochu, F. & Qian, Y. 1997, "Nonlinear finite element simulation of superelastic shape memory alloy parts", Computers and Structures, vol. 62, no. 5, pp. 799-810.

Msomi, V. & Oliver, G.J, 2015, “Smart morphing based on shape memory alloy plate”, Journal of Engineering, Design and Technology (Accepted for publication).

Panahandeh, M. & Kasper, E.P. 1997, "Coupled thermomechanical simulation of shape memory alloys", Proceedings of SPIE - The International Society for Optical Engineering, pp. 468.

Govindjee, S. & Kasper, E.P. 1997, "A shape memory alloy model for uranium-niobium accounting for plasticity", Journal of Intelligent Material Systems and Structures, vol. 8, no. 10, pp. 815-823.

Reisner, G., Werner, E.A. & Fischer, F.D. 1998, "Micromechanical modeling of martensitic transformation in random microstructures", International Journal of Solids and Structures, vol. 35, no. 19, pp. 2457-2473.

Lagoudas, D.C., Boyd, J.G. & Bo, Z. 1994, "Micromechanics of active composites with SMA fibers", Journal of Engineering Materials and Technology, Transactions of the ASME, vol. 116, no. 3, pp. 337-347.

Boyd, J.G. & Lagoudas, D.C. 1996, "A thermodynamical model for shape memory materials. Part I. The monolithic shape memory alloy", International Journal of Plasticity, vol. 12, no. 6, pp. 805-842.

Hartl,D., 2009, “Modelling of shape memory alloys considering rate-dependent and rate –independent irrecoverable strains”, Doctor of Philosophy thesis, Texas A&M University.

Simo, J.C. & Ortiz, M. 1985, "A unified approach to finite deformation elastoplastic analysis based on the use of hyperelastic equations", Computer Methods in Applied Mechanics and Engineering, vol. 49, no. 2, pp. 221-245.

Sottos, N.R., Kline, G.E., Qidwai, M.A. & Lagoudas, D.C. 1996, "Analysis of phase transformation fronts in SMA composites", Proceedings of SPIE - The International Society for Optical Engineering, pp. 427.

Jonnalagadda, K.D., Sottos, N.R., Qidwai, M.A. & Lagoudas, D.C. 1998, "Transformation of embedded shape memory alloy ribbons", Journal of Intelligent Material Systems and Structures, vol. 9, no. 5, pp. 379-390.

Jonnalagadda, K.D., Sottos, N.R., Qidwai, M.A. & Lagoudas, D.C. 1997, "Transformation of embedded shape memory alloy ribbons", Proceedings of SPIE - The International Society for Optical Engineering, pp. 242.

Bo, Z. & Lagoudas, D.C. 1999, "Thermomechanical modeling of polycrystalline SMAs under cyclic loading, Part I: Theoretical derivations", International Journal of Engineering Science, vol. 37, no. 9, pp. 1089-1140.

Moss, W.C. 1984, "On the computational significance of the strain space formulation of plasticity theory.", International Journal for Numerical Methods in Engineering, vol. 20, no. 9, pp. 1703-1709.

Ortiz, M. & Popov, E.P. 1985, "Accuracy and stability of integration algorithms for elastoplastic relations.", International Journal for Numerical Methods in Engineering, vol. 21, no. 9, pp. 1561-1576.

Li Q. 2006, “Modeling and Finite Element Analysis of Smart Materials.” Doctor of Philosophy dissertation, Graduate Faculty of North Carolina State University.

Tanaka K. 1986, “A thermomechanical sketch of shape memory effect: one-dimensional tensile behaviour.” Research of Mechanics, vol. 18, pp. 251-263.

Tanaka, K., Kobayashi, S. & Sato, Y. 1986, "Thermomechanics of transformation pseudoelasticity and shape memory effect in alloys", International Journal of Plasticity, vol. 2, no. 1, pp. 59-72.

Liang, C. & Rogers, C.A. 1990, "One-dimensional thermomechanical relations for shape memory materials", Collection of Technical Papers - AIAA/ASME/ASCE/AHS/ASC Structures, Structural Dynamics and Materials Conference, pp. 16.

Brinson, L.C. 1993, "One-dimensional behavior of shape memory alloys: Thermomechanical derivation with non-constant material functions and redefined martensite internal variable", Journal of Intelligent Material Systems and Structures, vol. 4, no. 2, pp. 229-242.

Bekker, A. & Brinson, L.C. 1997, "Temperature-induced phase transformation in a shape memory alloy : Phase diagram based kinetics approach", Journal of the Mechanics and Physics of Solids, vol. 45, no. 6, pp. 949-988.

Bekker, A. & Brinson, L.C. 1998, "Phase diagram based description of the hysteresis behavior of shape memory alloys", Acta Materialia, vol. 46, no. 10, pp. 3649-3665.

Boyd, J.G. & Lagoudas, D.C. 1994, "Thermomechanical response of shape memory composites", Journal of Intelligent Material Systems and Structures, vol. 5, no. 3, pp. 333-346.

Auricchio, F., Taylor, R.L. & Lubliner, J. 1997, "Shape-memory alloys: Macromodelling and numerical simulations of the superelastic behavior",

Computer Methods in Applied Mechanics and Engineering, vol. 146, no. 3-4, pp. 281-312.

Lu, Z.K. & Weng, G.J. 1998, "A self-consistent model for the stress-strain behavior of shape-memory alloy polycrystals", Acta Materialia, vol. 46, no. 15, pp. 5423-5433.

Patoor, E., Eberhardt, A. & Berveiller, M. 1996, "Micromechanical modelling of superelasticity in shape memory alloys", Journal De Physique.IV : JP, vol. 6, no. 1, pp. C1-277-C1-292

Gao, X. & Brinson, L.C. 2002, "A simplified multivariant SMA model based on invariant plane nature of martensitic transformation", Journal of Intelligent Material Systems and Structures, vol. 13, no. 12, pp. 795-810

Brocca, M., Brinson, L.C. & Bažant, Z.P. 2002, "Three-dimensional model for shape memory alloys based on microplane model", Journal of the Mechanics and Physics of Solids, vol. 50, no. 5, pp. 1051-1077.

Ivshin, Y. & Pence, T.J. 1994, "A model for hysteretic phase transition behavior", International Journal of Engineering Science, vol. 32, no. 4, pp. 681-704.

Wu, X. & Pence, T.J. 1998, "Two variant modeling of shape memory materials: Unfolding a phase diagram triple point", Journal of Intelligent Material Systems and Structures, vol. 9, no. 5, pp. 335-354.

Shaw, J.A. 2002, "A thermochemical model for a 1-D shape memory alloy wire with propagating instabilities", International Journal of Solids and Structures, vol. 39, no. 5, pp. 1275-1305.

Auricchio, F. & Sacco, E. 1999, "A temperature-dependent beam for shape-memory alloys: modelling, finite-element implementation and numerical simulations", Computer Methods in Applied Mechanics and Engineering, vol. 174, no. 1-2, pp. 171-190.

Auricchio, F. 2001, "A robust integration-algorithm for a finite-strain shape-memory-alloy superelastic model", International Journal of Plasticity, vol. 17, no. 7, pp. 971-990.

Trochu, F. & Qian, Y. 1997, "Nonlinear finite element simulation of superelastic shape memory alloy parts", Computers and Structures, vol. 62, no. 5, pp. 799-810.

Lagoudas, D.C., Ravi-Chandar, K., Sarh, K. & Popov, P. 2003, "Dynamic loading of polycrystalline shape memory alloy rods", Mechanics of Materials, vol. 35, no. 7, pp. 689-716.

Peultier, B., Ben Zineb, T. & Patoor, E. 2006, "Macroscopic law of shape memory alloy thermomechanical behaviour. Application to structure computation by FEM", Mechanics of Materials, vol. 38, no. 5-6, pp. 510-524.

Amalraj, J.J., Bhattacharyya, A. & Faulkner, M.G. 2000, "Finite-element modeling of phase transformation in shape memory alloy wires with variable material properties", Smart Materials and Structures, vol. 9, no. 5, pp. 622-631

Krevet, B. & Kohl, M. 2004, "Finite element simulation of SMA mlcroactuators with large deflection", Journal De Physique. IV: JP, pp. 365.

Achenbach, M. *and* I. Muller 1985 *"*Simulations of Material Behaviour of Alloys with Shape Memory*",* Arch Mech *,* 37*(6)* 573-585.

Achenbach, M. 1989, "A model for an alloy with shape memory", International Journal of Plasticity, vol. 5, no. 4, pp. 371-395.

Zhou, B., Yoon, S. & Leng, J. 2009, "A three-dimensional model for shape memory alloy", Smart Materials and Structures, vol. 18, no. 9.

Qidwai, M.A. & Lagoudas, D.C. 2000, "Numerical implementation of a shape memory alloy thermomechanical model using return mapping algorithms", International Journal for Numerical Methods in Engineering, vol. 47, no. 6, pp. 1123-1168.

Goo, B.C. & Lexcellent, C. 1997, "Micromechanics-based modeling of two-way memory effect of a single crystalline shape-memory alloy", Acta Materialia, vol. 45, no. 2, pp. 727-737.

Ikuta, K., Tsukamoto, M. & Hirose, S. 1991, "Mathematical model and experimental verification of shape memory alloy for designing micro actuator", Proceedings. IEEE Micro Electro Mechanical Systems, pp. 103.

Madill, D.R. & Wang, D. 1994, "Modelling and L2-stability of a shape memory alloy position control system", Proceedings - IEEE International Conference on Robotics and Automation, pp. 293.

Seelecke, S. & Bueskens, C. 1997, "Optimal control of beam structures by shape memory wires", International Conference on Computer Aided Optimum Design of Structures, OPTI, Proceedings, pp. 457.

Xia, K.-M., Pan, T.-Y., Liu, S.-H. 2010,”Three dimensional large deformation analysis of phase transformation in shape memory alloys”, Applied Mathematics and Mechanics, vol. 31, no.10, pp. 1261-1272.

Richter, F., Kastner, O. & Eggeler, G. 2009, "Implementation of the Müller-Achenbach-Seelecke model for shape memory alloys in ABAQUS", Journal of Materials Engineering and Performance, vol. 18, no. 5-6, pp. 626-630.

Goo, B.C. & Lexcellent, C. 1997,"Micromechanics-based modeling of two-waymemory effect of a singlecrystalline shape-memory alloy", ACTA Materialia, vol.45, no. 2, pp. 727–737.

Tanaka, K., Nishimura, F. & Tobushi, H.1994, "Phenomenological analysis on sub-loops in shape memory alloys due to incomplete transformations", Journal of Intelligent Material Systems and Structures, vol. 5, pp. 387–493.

Ikuta, K. 1990, "Micro/Miniature Shape Memory Alloy Actuator", Proceedings of IEEE Conference on Robotics and Automation, Vol. 3, pp. 2156-2161.

Brinson, L.C. & Lammering, R. 1993, "Finite Element Analysis of the behavior of shape memory alloys and their applications", International Journal of Solid Structures, Vol. 30, no 23, pp3261-3280.

Arghavani, J., Auricchio, E., Naghdabadi, R. & Reali, A. 2010, "A 3-D Finite strain phenomenological model for shape memory alloys considering martensite reorientation", Continuum Mech. Thermodynamics, Vol. 22, no. 5, pp 345-362.

Ronda, J., Oliver, G.J. 2000, "Consistent thermo-mechano-metallurgical model of welded steel with unified approach to derivation of phase evolution laws and transformation-induced plasticity", Computer Methods in Applied Mechanics and Engineering, 189 (2), pp. 361-417.

Zhou, B., Liu, Y., Leng, J., Zou, G.,2009, “A macro-mechanical constitutive model of shape memory alloys” Science in China, Series G: Physics, Mechanics and Astronomy, 52 (9), pp. 1382-1391.

Wayman, C. M. and Otsuka, K., 1999, “Shape Memory materials”, University of Cambridge Press. Pp. 267-279.

**APPENDICES**

# APPENDIX A

## Beam bar elements used to solve our system presented in the main text

The element stiffness matrix in global coordinates (*X,Y*) is explicitly given by:

Element 1:

$$\underline{\underline{K^{(1)}}} = \begin{bmatrix} kc^2 & ksc & -kc^2 & -ksc \\ ksc & ks^2 & -ksc & -ks^2 \\ -kc^2 & -ksc & kc^2 & ksc \\ -ksc & -ks^2 & ksc & ks^2 \end{bmatrix} = k \begin{bmatrix} X_{21}X_{21} & X_{21}Y_{21} & -X_{21}Y_{21} & -X_{21}Y_{21} \\ X_{21}Y_{21} & Y_{21}Y_{21} & -X_{21}Y_{21} & -Y_{21}Y_{21} \\ -X_{21}X_{21} & -X_{21}Y_{21} & X_{21}X_{21} & X_{21}Y_{21} \\ -X_{21}Y_{21} & -Y_{21}Y_{21} & X_{21}Y_{21} & Y_{21}Y_{21} \end{bmatrix} \quad \text{(A1)}$$

Element 2:

$$\underline{\underline{K^{(2)}}} = \begin{bmatrix} kc^2 & ksc & -kc^2 & -ksc \\ ksc & ks^2 & -ksc & -ks^2 \\ -kc^2 & -ksc & kc^2 & ksc \\ -ksc & -ks^2 & ksc & ks^2 \end{bmatrix} = k \begin{bmatrix} X_{32}X_{32} & X_{32}Y_{32} & -X_{32}Y_{32} & -X_{32}Y_{32} \\ X_{32}Y_{32} & Y_{32}Y_{32} & -X_{32}Y_{32} & -Y_{32}Y_{32} \\ -X_{321}X_{32} & -X_{32}Y_{32} & X_{32}X_{32} & X_{32}Y_{32} \\ -X_{32}Y_{32} & -Y_{32}Y_{32} & X_{32}Y_{32} & Y_{32}Y_{32} \end{bmatrix} \quad \text{(A2)}$$

Here

$$X_{21} = X_2 - X_1; Y_{21} = Y_2 - Y_1; c = \cos\theta = \frac{X_{21}}{r}; s = \sin\theta = \frac{Y_{21}}{r}; \mathrm{r} = \sqrt{X_{21}^2 + Y_{21}^2} \quad \text{(A3)}$$

And also

$$X_{32} = X_3 - X_2; Y_{32} = Y_3 - Y_2; c = \cos\theta = \frac{X_{32}}{r}; s = \sin\theta = \frac{Y_{32}}{r}; \mathrm{r} = \sqrt{X_{32}^2 + Y_{32}^2} \quad \text{(A4)}$$

It can be seen that the matrix elements numbering depends on the bar element to be solved. The coefficient *k* is calculated as follows

$$k = \frac{AE}{r^3} \qquad \text{(A5)}$$

The angle $\theta$ is formed by the local and global coordinates upon force application. It should be note that the axial degrees of freedom is being ignored due to the fact the beam is loaded vertically hence the stiffness matrix for each element is 4X4 matrix.

Writing element stiffness in terms of beam properties, the above stiffness matrices will be the same but different nodes:

$$\underline{\underline{K}}^{(1)} = \frac{EI}{r^3}\begin{bmatrix} 12 & 6r & -12 & 6r \\ 6r & 4r^2 & -6r & 2r^2 \\ -12 & -6r & 12 & -6r \\ 6r & 2r^2 & -6r & 4r^2 \end{bmatrix}$$
$$\underline{\underline{K}}^{(2)} = \frac{EI}{r^3}\begin{bmatrix} 12 & 6r & -12 & 6r \\ 6r & 4r^2 & -6r & 2r^2 \\ -12 & -6r & 12 & -6r \\ 6r & 2r^2 & -6r & 4r^2 \end{bmatrix} \qquad \text{(A6)}$$

The global stiffness matrix would be

$$\underline{\underline{K}}^{G} = \frac{EI}{r^3}\begin{bmatrix} 12 & 6r & -12 & 6r & 0 & 0 \\ 6r & 4r^2 & -6r & 2r^2 & 0 & 0 \\ -12 & -6r & 24 & 0 & -12 & 6r \\ 6r & 2r^2 & 0 & 8r^2 & -6r & 2r^2 \\ 0 & 0 & -12 & -6r & 12 & -6r \\ 0 & 0 & 6r & 2r^2 & -6r & 4r^2 \end{bmatrix} \qquad \text{(A7)}$$

The global FE equations would be

$$\begin{bmatrix} F_{Y1} \\ M_1 \\ F_{Y2} \\ M_2 \\ F_{Y3} \\ M_3 \end{bmatrix} = \frac{EI}{r^3}\begin{bmatrix} 12 & 6r & -12 & 6r & 0 & 0 \\ 6r & 4r^2 & -6r & 2r^2 & 0 & 0 \\ -12 & -6r & 24 & 0 & -12 & 6r \\ 6r & 2r^2 & 0 & 8r^2 & -6r & 2r^2 \\ 0 & 0 & -12 & -6r & 12 & -6r \\ 0 & 0 & 6r & 2r^2 & -6r & 4r^2 \end{bmatrix}\begin{bmatrix} u_{y1} \\ \theta_{R1} \\ u_{y2} \\ \theta_{R2} \\ u_{y3} \\ \theta_{R3} \end{bmatrix} \qquad \text{(A8)}$$

The boundary conditions for our system are as follows

$$F_{x1} = F_{y1} = F_{x3} = F_{y3} = F_{x2} = 0$$
$$u_{x1} = u_{y1} = u_{x3} = u_{y3} = 0 \quad \text{(A9)}$$
$$F_{y2} = F_{SMA}$$

The global FE equations would now look like the following

$$\begin{bmatrix} 0 \\ 0 \\ F_{y2} \\ 0 \\ 0 \\ 0 \end{bmatrix} = \frac{EI}{r^3} \begin{bmatrix} 12 & 6r & -12 & 6r & 0 & 0 \\ 6r & 4r^2 & -6r & 2r^2 & 0 & 0 \\ -12 & -6r & 24 & 0 & -12 & 6r \\ 6r & 2r^2 & 0 & 8r^2 & -6r & 2r^2 \\ 0 & 0 & -12 & -6r & 12 & -6r \\ 0 & 0 & 6r & 2r^2 & -6r & 4r^2 \end{bmatrix} \begin{bmatrix} 0 \\ 0 \\ u_{y2} \\ \theta_{R2} \\ 0 \\ 0 \end{bmatrix} \quad \text{(A10)}$$

The reduced FE equations would then be

$$F_{SMA} = \frac{EI}{r^3} 24 u_{y2} \quad \text{(A11)}$$

The deflection could then be calculated by the following equation

$$u_{y2} = \frac{F_{SMA} r}{24EI} \quad \text{(A12)}$$

This is the deflection that needs to be solved by the FEA.

# APPENDIX B

## This program implements the finite element for 2-D truss elements

```
// author G.J. Oliver & V. Msomi
#include <iostream>
#include <math.h>
#include "Matrix.h"
#include <fstream>
const double pi=3.14159265358979323846264338327 95;
void sma_phase(double &vol_phase_A, double &vol_phase_M, double temp,double dtemp);
void sma_force(double *F_sma, double E, double A, double vol_phase_A, double vol_phase_M);
void rotateM(double **K, double c, double s);
void rotateV(double *F,double c, double s);

using namespace std;
double temp,dtemp;

ofstream out_file;
ofstream out_file2;
ofstream fgout;
ofstream out2;
int main()
{
  // open the file for reading
       ifstream feinp("smabbexp.inp");
  if (feinp.is_open())
  {
  // okay
  }
  else
```

```
    {
       cout<<"COULD  NOT OPEN INPUT FILE!!!!!";
       return 0;
    }
    ifstream  dataf("beam_expf.inp");
    if (dataf.is_open())
    {
    // okay
    }
    else
    {
       cout<<"COULD  NOT OPEN EXPERIMENTAL  DATA FILE!!!!!";
       return 0;
    }
 /// output  files
out_file.open("plot.csv");
out_file2.open("plot2.csv");
fgout.open("output.txt");
int i,j;
          int  node,nodes;  // number  of nodes
          int  element,elements;  // number  of elements
          feinp>>nodes>>elements;  // reads in from file  the number  of nodes and elems.
          fgout<<nodes<<"  "<<elements<<"\n";  // writes  out to the screen
          // define  two vectors that contains  the nodal coordinates
          // the number  of rows corresponds to the number  of nodes and the vectors
          // contain  the x coordinates  and y coordinates  respectively

          double  *node_x,*node_y;
          node_x=dvector(1,nodes);
          node_y=dvector(1,nodes);
          // read in the coordinates  of the nodes
          for(i=1;i<=nodes;i++)
          {
                feinp>>node>>node_x[i]>>node_y[i];
          }
```

```
 for(i=1;i<=nodes;i++)
{
        fgout<<node_x[i]<<"  "<<node_y[i]<<"\n";

}
int *elem_node1,  *elem_node2;
elem_node1=ivector(1,elements);
elem_node2=ivector(1,elements);
// read in element  connectivity
// read in the elements  node 1 and node2
for(i=1;i<=elements;i++)
{
        feinp>>element>>elem_node1[i]>>elem_node2[i];
}
 for(i=1;i<=elements;i++)
{
        fgout<<elem_node1[i]<<"  "<<elem_node2[i]<<"\n";
}
// read in the constraints
int **constraint;
constraint=imatrix(1,nodes,1,3);
 for(i=1;i<=nodes;i++)
{
        feinp>>node>>constraint[i][1]>>constraint[i][2]>>constraint[i][3];
}
fgout<<"  Constraint   0 fixed  1 free \n";
fgout<<"  X         Y                 Rotation\n";
 for(i=1;i<=nodes;i++)
{
        fgout<<constraint[i][1]<<"  "<<constraint[i][2]<<"
"<<constraint[i][3]<<"\n";
}
// read in the loads
double *f_x,*f_y,  *M;
f_x=dvector(1,nodes);
```

```
        f_y=dvector(1,nodes);
        M=dvector(1,nodes);
        fgout<<"FX        FY              Moments\n";
         for(i=1;i<=nodes;i++)
        {
                feinp>>node>>f_x[i]>>f_y[i]>>M[i];
        }
          for(i=1;i<=nodes;i++)
        {
                fgout<<f_x[i]<<"  "<<f_y[i]<<"  "<<M[i]<<"\n";
        }


        // read in the properties
   // area, second moment of area, Young's modulus 1, Young's modulus 2 (moduli
the same if not SMA material)
        double *A,*I, *EA,*EM;
        A=dvector(1,elements);
        I=dvector(1,elements);
        EA=dvector(1,elements);
        EM=dvector(1,elements);
        int *etype;
        // etype is the type of element made of SMA or other material: 1 normal 2
SMA
        etype=ivector(1,elements);
        for(i=1;i<=elements;i++)
        {
                feinp>>etype[i]>>element>>A[i]>>I[i]>>EA[i]>>EM[i];
        }
        fgout<<" Element type: Properties A,I, EA, EM \n";
   for(i=1;i<=elements;i++)
        {
                fgout<<etype[i]<<"  "<<A[i]<<"  "<<I[i]<<"  "<<EA[i]<<"
"<<EM[i]<<"\n";
        }
//-------------------------------------------------------
// create the stiffness matrix for each element
```

```
        int e,n1,n2;
        double k,x,y,L,c,s;
        double **KL;
        KL=matrix(1,6,1,6);
        double E;
        double *F;
        F=dvector(1,nodes*3);
        double **K;
        K=matrix(1,nodes*3,1,nodes*3);
        double *F_sma;
        F_sma=dvector(1,6);
        // volume phase fraction variables
        double vol_phase_A, vol_phase_M;
        // node reference in assembly
int *n;
        n=ivector(1,2);

 int *bound;
         bound=ivector(1,nodes*3);
         for(i=1;i<=nodes;i++)
         {
                 bound[i*3-2]=constraint[i][1];
    bound[i*3-1]=constraint[i][2];
                 bound[i*3]=constraint[i][3];
         }
         // determine how many boundary conditions we have
        int num_free;  // the number of unconstrained degrees of freedom
        num_free=0;
        for(i=1;i<=nodes*3;i++)
        {
                num_free+=bound[i];
        }
        cout<<'The number of DOF to solve for is "<<num_free<<"\n";

        // stiffness and force system to solve
```

```
        double **KD,**FD;
        KD=matrix(1,num_free,1,num_free);
        FD=matrix(1,num_free,1,1);
        int id,jd;

//-------------------------------------------------
        int flag=1;
        temp=18;
        int t_i;
        int di,dj;
        double *tempi, *dispi;
        tempi=dvector(1,200);
        dispi=dvector(1,200);
        for(t_i=1;t_i<=200;t_i++)
        {
         dataf>>tempi[t_i]>>dispi[t_i];
         fgout<<tempi[t_i]<<" "<<dispi[t_i]<<"\n";
        }
        // initialize martensite and austenite
        vol_phase_A=0.0;
        vol_phase_M=1.0;

  for(t_i=2;t_i<=200;t_i++)
  {
     temp=tempi[t_i];
     dtemp=tempi[t_i]-tempi[t_i-1];
    cout<<"temperature: "<<temp<<" dtemp: "<<dtemp<<"\n";
    fgout<<"temperature: "<<temp<<" dtemp: "<<dtemp<<"\n";
  // make the stiffness matrix 0 at the start of each temperature driven calculation
  for(i=1;i<=nodes*3;i++)
        {
                for(j=1;j<=nodes*3;j++)
                {
                        K[i][j]=0.0;
                }
```

```
      }
      // define the applied load for the entire system for each temperature
       for(i=1;i<=nodes;i++)
       {
              F[i*3-2]=f_x[i];
              F[i*3-1]=f_y[i];
  F[i*3]=M[i];
}

      ////////////////////////////// for each element ////////////////////////////////
      for(e=1;e<=elements;e++)
      {
 // determine node 1 and node 2 for the current element
        n1=elem_node1[e];
        n2=elem_node2[e];
        n[1]=n1;
        n[2]=n2;
        // x length
        x=(node_x[n2]-node_x[n1]);
        // y length
        y=(node_y[n2]-node_y[n1]);
        // Length of element
        L=sqrt(pow(x,2)+pow(y,2));
        // the cos and sine for the element
        c=x/L;
        s=y/L;

        if(etype[e]==2)
 {
    // phase kinetic calculation
    sma_phase(vol_phase_A,vol_phase_M,temp,dtemp);
    // additive phase property rule for Young's modulus
    E=vol_phase_M*EM[e]+vol_phase_A*EA[e];
    out_file2<<vol_phase_A<<  ","<<E<<endl;
```

```
        fgout<<"phase martensite "<<vol_phase_M<<" phase austenite
"<<vol_phase_A<<endl;
       sma_force(F_sma,E, A[e],vol_phase_A, vol_phase_M);
        fgout<<"sma_force"<<endl;
       for(i=1;i<=6;i++)
        {
          fgout<<F_sma[i]<<endl;
        }
    }
    else
     {
        // normal material so either EA or EM is the Young's modulus for the element
        E=EA[e];
     }

         // beam bar element in local coordinates
    KL[1][1]=E*A[e]/L; KL[1][2]=0; KL[1][3]=0; KL[1][4]=-E*A[e]/L;
KL[1][5]=0;KL[1][6]=0;
    KL[2][1]=0;
KL[2][2]=12*E*I[e]/pow(L,3);KL[2][3]=6*E*I[e]/pow(L,2);KL[2][4]=0;KL[2][5]=-
12*E*I[e]/pow(L,3);KL[2][6]=6*E*I[e]/pow(L,2);
    KL[3][1]=0;
KL[3][2]=6*E*I[e]/pow(L,2);KL[3][3]=4*E*I[e]/L;KL[3][4]=0;KL[3][5]=-
6*E*I[e]/pow(L,2);KL[3][6]=2*E*I[e]/L;
    KL[4][1]=-E*A[e]/L; KL[4][2]=0; KL[4][3]=0; KL[4][4]=E*A[e]/L;
KL[4][5]=0;KL[4][6]=0;
    KL[5][1]=0; KL[5][2]=-12*E*I[e]/pow(L,3);KL[5][3]=-
6*E*I[e]/pow(L,2);KL[5][4]=0;KL[5][5]=12*E*I[e]/pow(L,3);KL[5][6]=-
6*E*I[e]/pow(L,2);
    KL[6][1]=0;
KL[6][2]=6*E*I[e]/pow(L,2);KL[6][3]=2*E*I[e]/L;KL[6][4]=0;KL[6][5]=-
6*E*I[e]/pow(L,2);KL[6][6]=4*E*I[e]/L;

   // rotate local stiffness matrix to global coordinates
   rotateM(KL,c,s);
    // add the contribution of each local K to the global K

         for(i=1;i<=2;i++)
```

```
    {
            for(j=1;j<=2;j++)
            {
              for(di=0;di<3;di++)
  {
     for(dj=0;dj<3;dj++)
     {
       K[n[i]*3-di][n[j]*3-dj]=K[n[i]*3-di][n[j]*3-dj]+KL[i*3-di][j*3-dj];
     }
  }
     }
     if(etype[e]==2)
{
  rotateV(F_sma,c,s);
  for(i=1;i<2;i++)
  {
    for(di=0;di<3;di++)
    {
     F[n[i]*3-di]=F_sma[i*3-di];
    }
  }
}// etype
    }
  }// element e
  // solution for displacement for current temperature
  //++++++++++++++++++++++++++++++++++++++++++++++++++++++++++

   id=0;
   for(i=1;i<=nodes*3;i++)
   {
            if(bound[i]==1)
            {
                     id++;
                     jd=0;
             for(j=1;j<=nodes*3;j++)
```

```
                {
                        if(bound[j]==1)
                        {
                                jd++;
                                KD[id][jd]=K[i][j];
                        }
                }
                FD[id][1]=F[i];
            }
          }
 // solve for the displacements using gauss elimination routine
          gaussj(KD,num_free, FD, 1);
          cout<<"displacements: \n";

    for(i=1;i<=num_free;i++)
    {
                        cout<<FD[i][1]<<"\n";

         out_file<<temp<<","<<FD[i][1]*1000.0<<","<<dispi[t_i]<<"\n";
          }
 } // for temperature
         //---------------------------------------------------------------------
   cout << "Program Finished!" << endl;
   return 0;
}
void sma_phase(double &vol_phase_A, double &vol_phase_M, double temp,double
dtemp)
{
   double MPO;
   double QA,QM,AS,MF;
   QA=0.06;
   QM=0.6;
   MPO=0.5;
  // AS=23;
   AS=43;
   MF=18.3;
```

```
   if(dtemp>0.1)
   {
     // heating
     vol_phase_M=MPO*(1.0-tanh(QA*(temp-AS)-1.0));
     vol_phase_A=1.0-vol_phase_M;
     fgout<<"phases heating "<<vol_phase_M<<" "<<vol_phase_A<<"\n";

   }
   // cooling
   else if(dtemp<(-0.1))
   {
     vol_phase_M=MPO*(1.50-tanh(QM*(temp-MF)-1.0));
     vol_phase_A=1.0-vol_phase_M;
     fgout<<"phases cooling "<<vol_phase_M<<" "<<vol_phase_A<<"\n";
   }
   else
   {
      // do nothing
       fgout<<"phases nothing "<<vol_phase_M<<" "<<vol_phase_A<<"\n";
   }
}
void sma_force(double *F_sma, double E, double A, double vol_phase_A, double
vol_phase_M)
{
   double sma_strain,strain_max;
   strain_max=0.0485;
   sma_strain=strain_max*vol_phase_A;
   //out_file2<<vol_phase_A<<" , "<<sma_strain<<endl;
 // local force for beam bar element has only x component no y or rotation (moment)
 F_sma[1]=-E*A*sma_strain;
 F_sma[2]=0;
 F_sma[3]=0;
 F_sma[4]=E*A*sma_strain;
 F_sma[5]=0;
 F_sma[6]=0;
```

```
}
void rotateM(double  **K,double c, double s)
{
 double **T,**T_trans; // rotation matrix  and transpose
 double **KT;
 int i,j,k;
 T=matrix(1,6,1,6);
 T_trans=matrix(1,6,1,6);
 KT=matrix(1,6,1,6);
 T[1][1]=c;T[1][2]=s;T[1][3]=0;T[1][4]=0;T[1][5]=0;T[1][6]=0;
 T[2][1]=-s;T[2][2]=c;T[2][3]=0;T[2][4]=0;T[2][5]=0;T[2][6]=0;
 T[3][1]=0;T[3][2]=0;T[3][3]=1;T[3][4]=0;T[3][5]=0;T[3][6]=0;
 T[4][1]=0;T[4][2]=0;T[4][3]=0;T[4][4]=c;T[4][5]=s;T[4][6]=0;
 T[5][1]=0;T[5][2]=0;T[5][3]=0;T[5][4]=-s;T[5][5]=c;T[5][6]=0;
 T[6][1]=0;T[6][2]=0;T[6][3]=0;T[6][4]=0;T[6][5]=0;T[6][6]=1;
 for(i=1;i<=6;i++)
 {
    for(j=1;j<=6;j++)
    {
       T_trans[i][j]=T[j][i];
    }
 }
 for(i=1;i<=6;i++)
 {
    for(j=1;j<=6;j++)
    {
       KT[i][j]=0.0;
       for(k=1;k<=6;k++)
       {
         KT[i][j]=KT[i][j]+K[i][k]*T[k][j];
       }

    }
 }
 for(i=1;i<=6;i++)
```

```
{
    for(j=1;j<=6;j++)
    {
        K[i][j]=0.0;
        for(k=1;k<=6;k++)
        {
          K[i][j]=K[i][j]+T_trans[i][k]*KT[k][j];
        }

    }
}
}
void rotateV(double  *F,double  c, double  s)
{
 double  **T; // rotation  matrix
  int  i,j;
 T=matrix(1,6,1,6);
  double  *F_temp;
  F_temp=dvector(1,6);
 T[1][1]=c;T[1][2]=s;T[1][3]=0;T[1][4]=0;T[1][5]=0;T[1][6]=0;
 T[2][1]=-s;T[2][2]=c;T[2][3]=0;T[2][4]=0;T[2][5]=0;T[2][6]=0;
 T[3][1]=0;T[3][2]=0;T[3][3]=1;T[3][4]=0;T[3][5]=0;T[3][6]=0;
 T[4][1]=0;T[4][2]=0;T[4][3]=0;T[4][4]=c;T[4][5]=s;T[4][6]=0;
 T[5][1]=0;T[5][2]=0;T[5][3]=0;T[5][4]=-s;T[5][5]=c;T[5][6]=0;
 T[6][1]=0;T[6][2]=0;T[6][3]=0;T[6][4]=0;T[6][5]=0;T[6][6]=1;
 for(i=1;i<=6;i++)
 {
     F_temp[i]=0.0;
    for(j=1;j<=6;j++)
    {
         F_temp[i]=F_temp[i]+T[i][j]*F[j];

    }
 }
    for(i=1;i<=6;i++)
```

```
            {
          F[i]=F_temp[i];
            }

}
//---------------------------------------------------------------------------
void gaussj(double **a, int n, double **b, int m)
{
 int *indxc,*indxr, *ipiv;
 int i,icol,irow,j,k,l,ll;
 double big,dum,pivinv;
 indxc=ivector(1,n);
 indxr=ivector(1,n);
 ipiv=ivector(1,n);
 for(j=1;j<=n;j++) ipiv[j]=0;
 for(i=1;i<=n;i++)
 {
  big=0.0;
  for(j=1;j<=n;j++)
   if(ipiv[j]!=1)
    for(k=1;k<=n;k++)
    {
     if(ipiv[k]==0)
     {
      if (fabs(a[j][k])>=big)
      {
       big=fabs(a[j][k]);
       irow=j;
       icol=k;
      }
     } else if (ipiv[k]>1) fgout<<"gaussj:Singular Matrix-1";
   }
   ++(ipiv[icol]);
   if(irow!=icol)
    {
```

```
      for(l=1;l<=n;l++) SWAP(a[irow][l],a[icol][l])
      for(l=1;l<=m;l++) SWAP(b[irow][l],b[icol][l])
     }
    indxr[i]=irow;
    indxc[i]=icol;
    if (a[icol][icol]==0.0) fgout<<"gaussj:Singular Matrix-2";
    pivinv=1.0/a[icol][icol];
    a[icol][icol]=1.0;
    for(l=1;l<=n;l++) a[icol][l]*=pivinv;
    for(l=1;l<=m;l++) b[icol][l]*=pivinv;
    for(ll=1;ll<=n;ll++)
      if(ll!=icol)
      {
        dum=a[ll][icol];
        a[ll][icol]=0.0;
        for(l=1;l<=n;l++) a[ll][l]-=a[icol][l]*dum;
        for(l=1;l<=m;l++) b[ll][l]-=b[icol][l]*dum;
      }
  }
  for(l=n;l>=1;l--)
  {
    if(indxr[l]!=indxc[l])
      for(k=1;k<=n;k++)
        SWAP(a[k][indxr[l]],a[k][indxc[l]]);
  }
  free_ivector(ipiv,1,n);
  free_ivector(indxr,1,n);
  free_ivector(indxc,1,n);
}
```

# APPENDIX C

Steps during the simulation

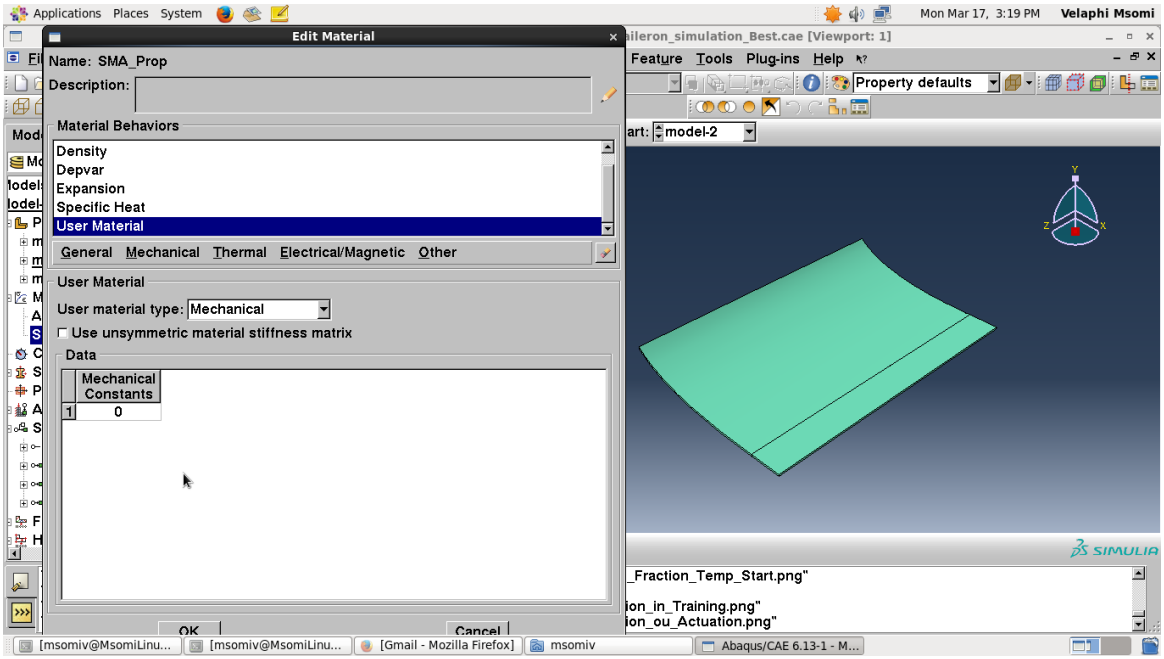


**Figure C 1: Definition of SMA material properties**

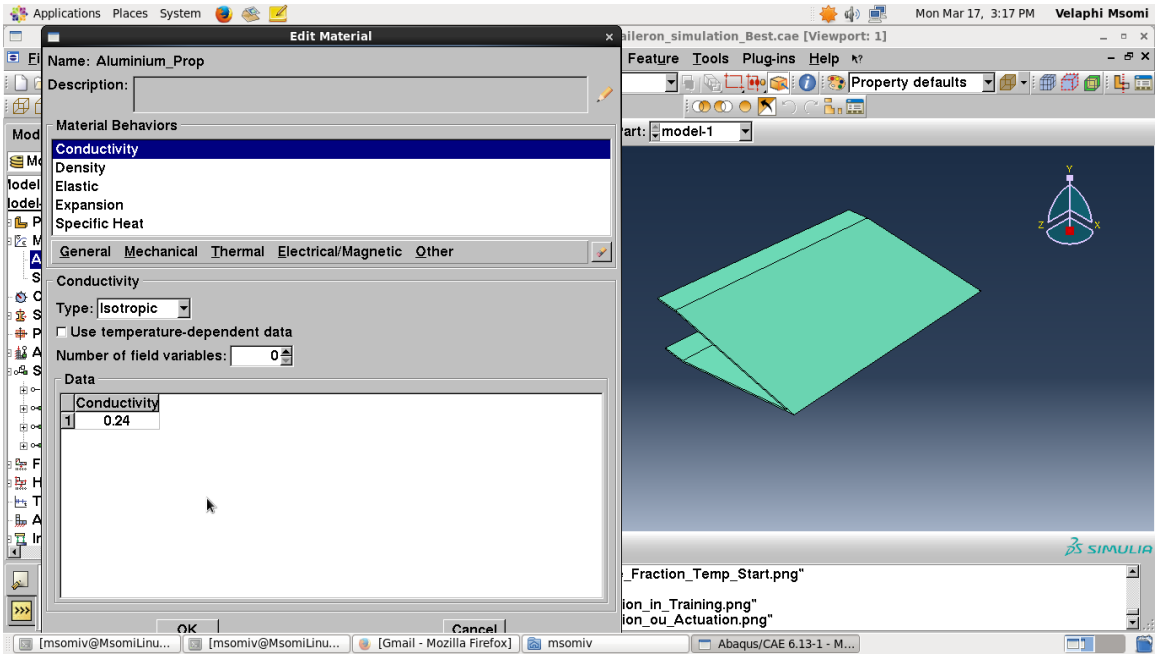


**Figure C 2: Definition of aluminium material properties**

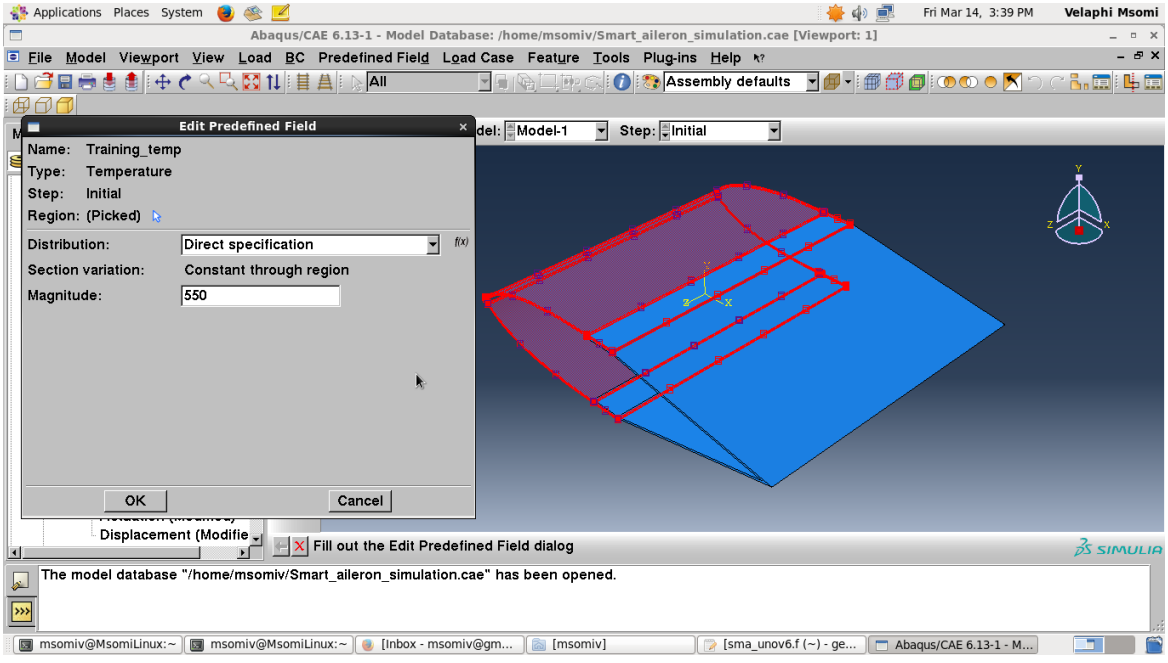


**Figure C 3: Definition of training temperature in the initial step**

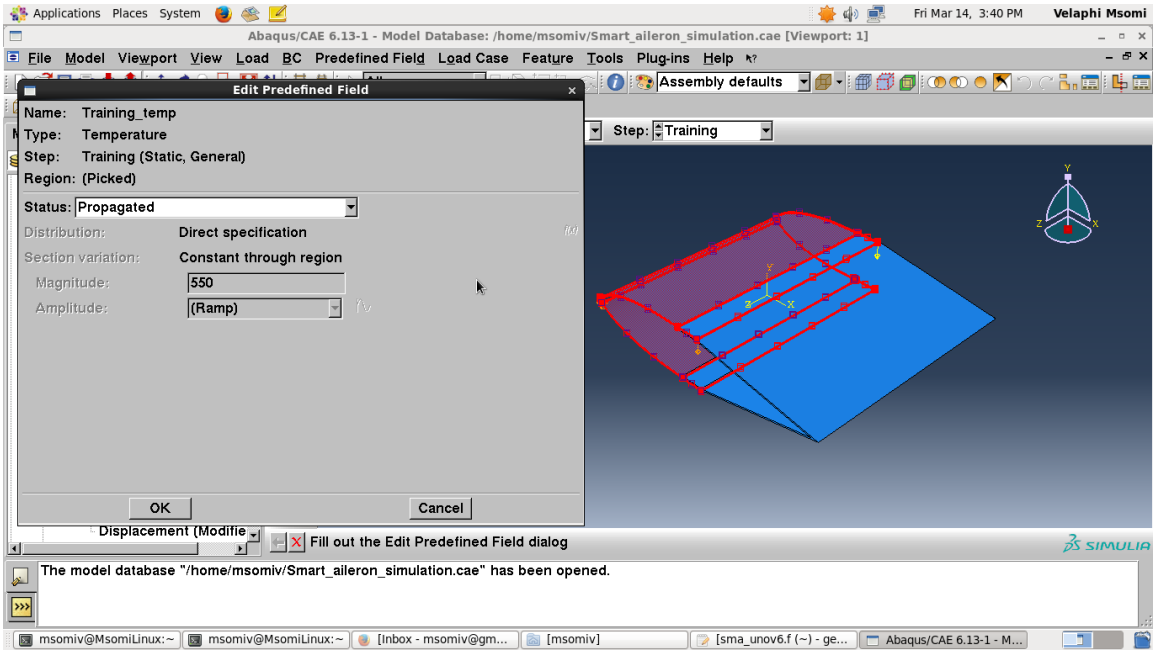


**Figure C 4: Propagation of training temperature to the training step**

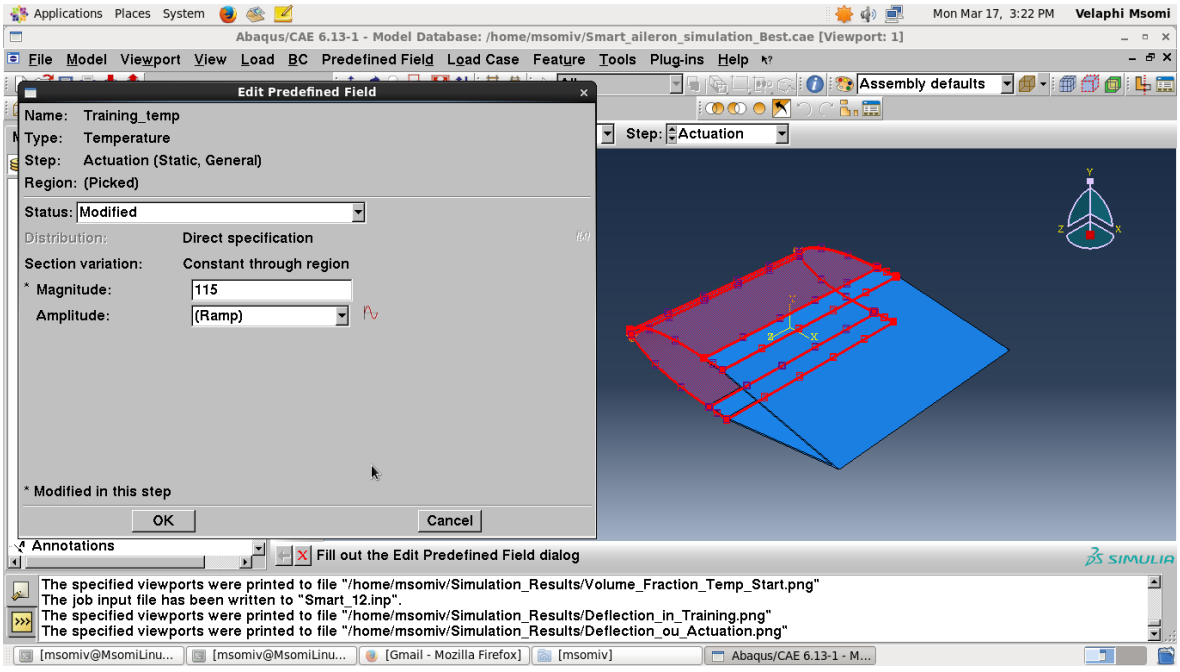


**Figure C 5: Definition of initial actuation temperature in the actuation step**

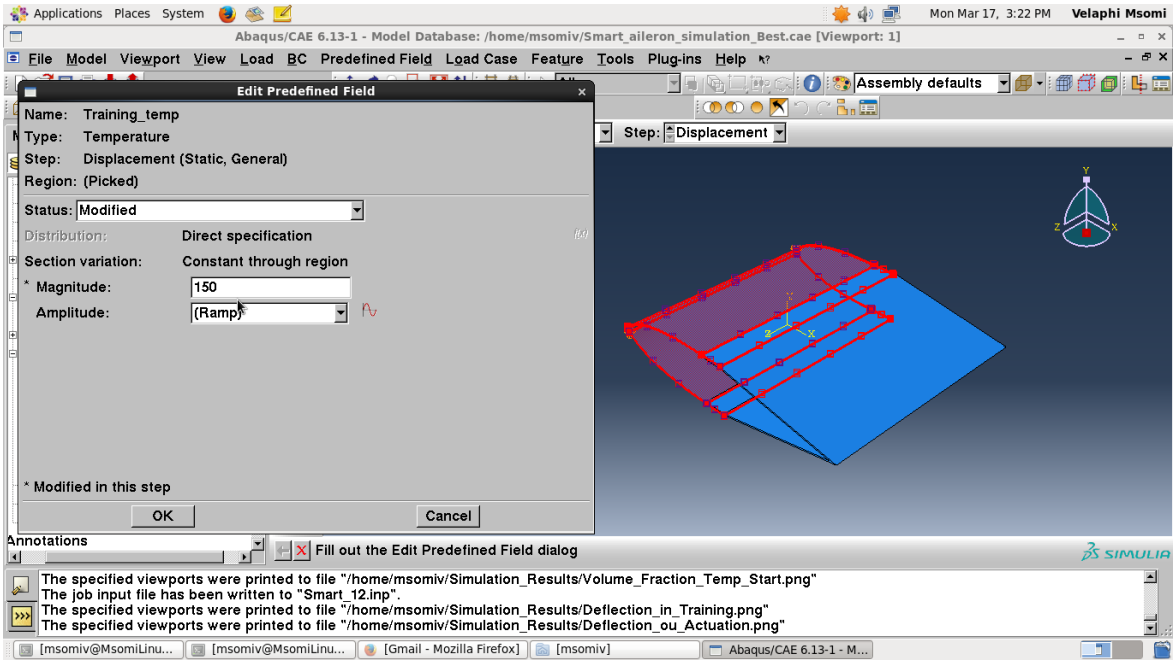


**Figure C 6: Definition of final actuation temperature in the actuation step**

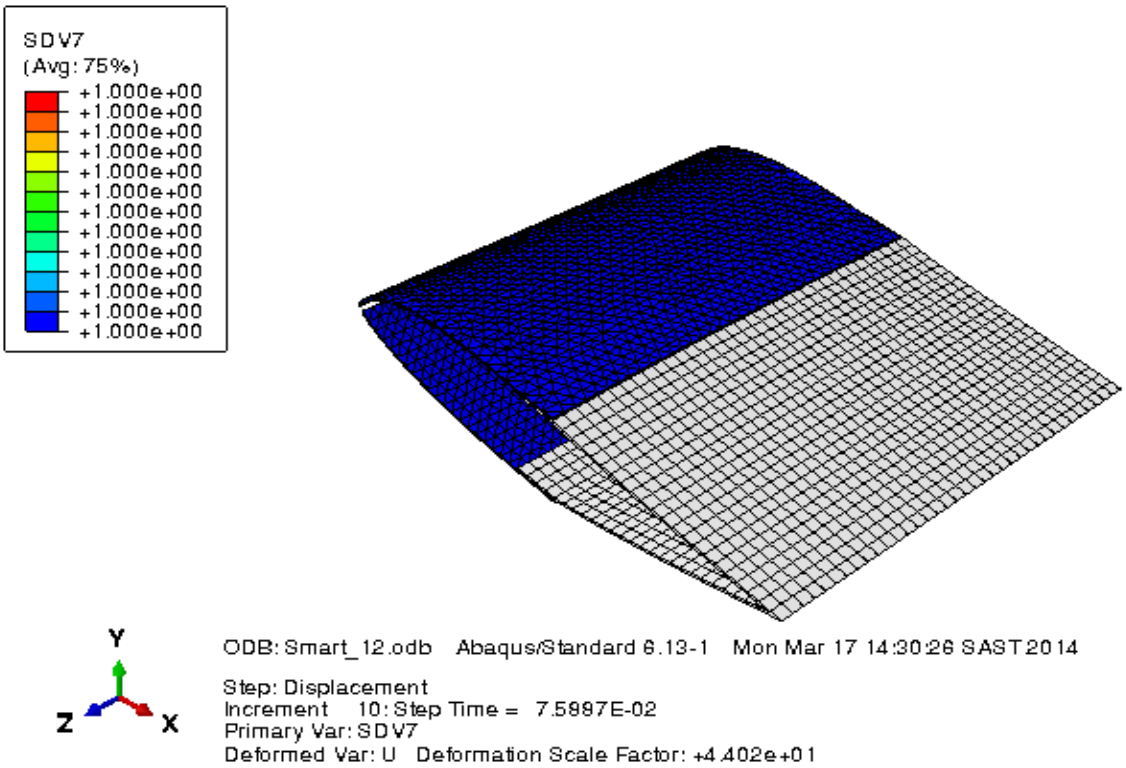


**Figure C 7: Martensite volume fraction (TEMP<As) in the actuation step**

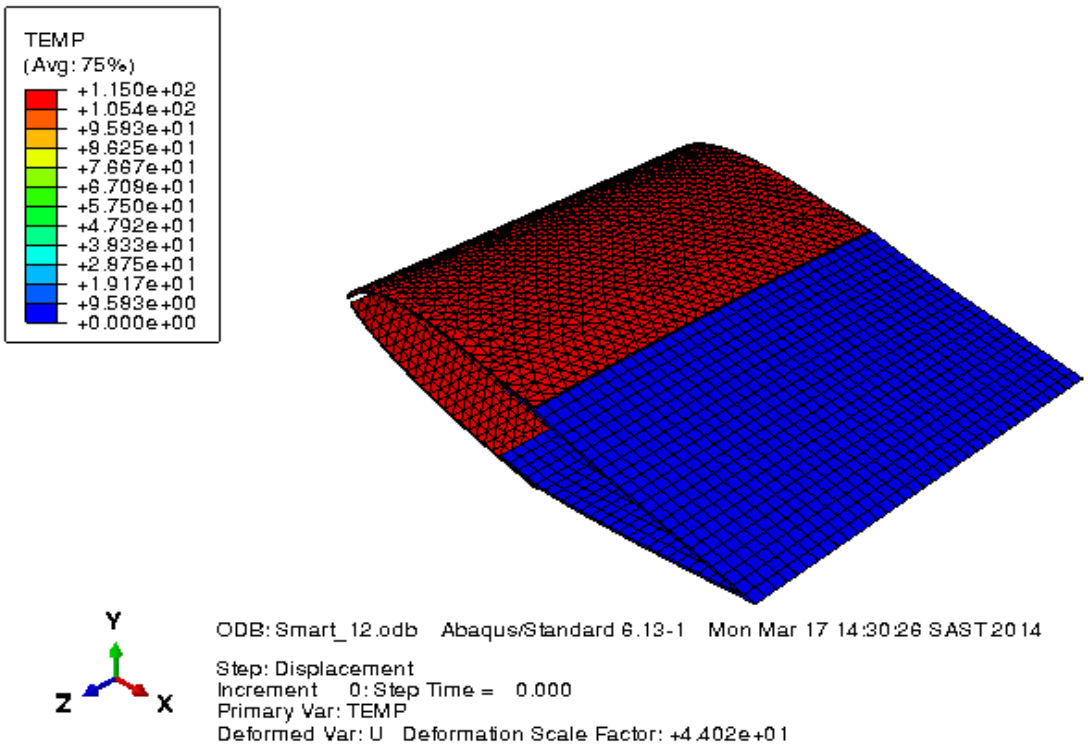


**Figure C 8: Definition of start actuation temperature in the actuation step**

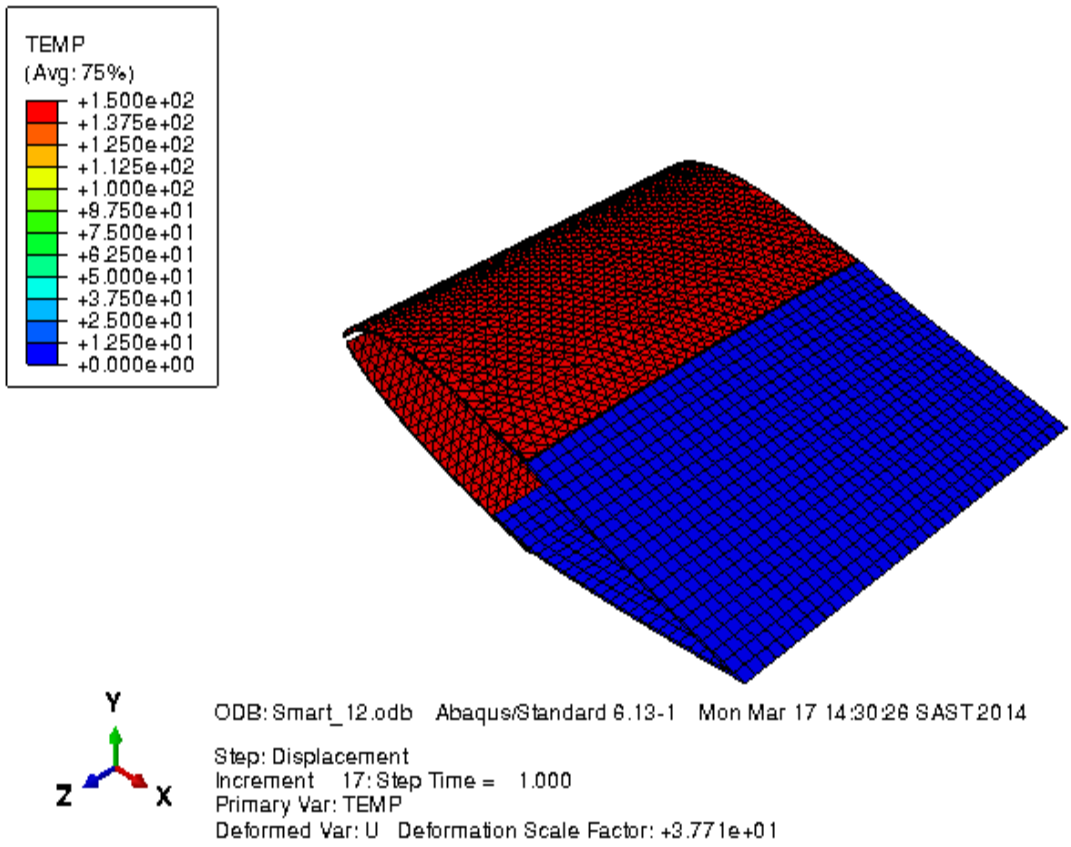


**Figure C 9: Definition of final actuation temperature in the actuation step**

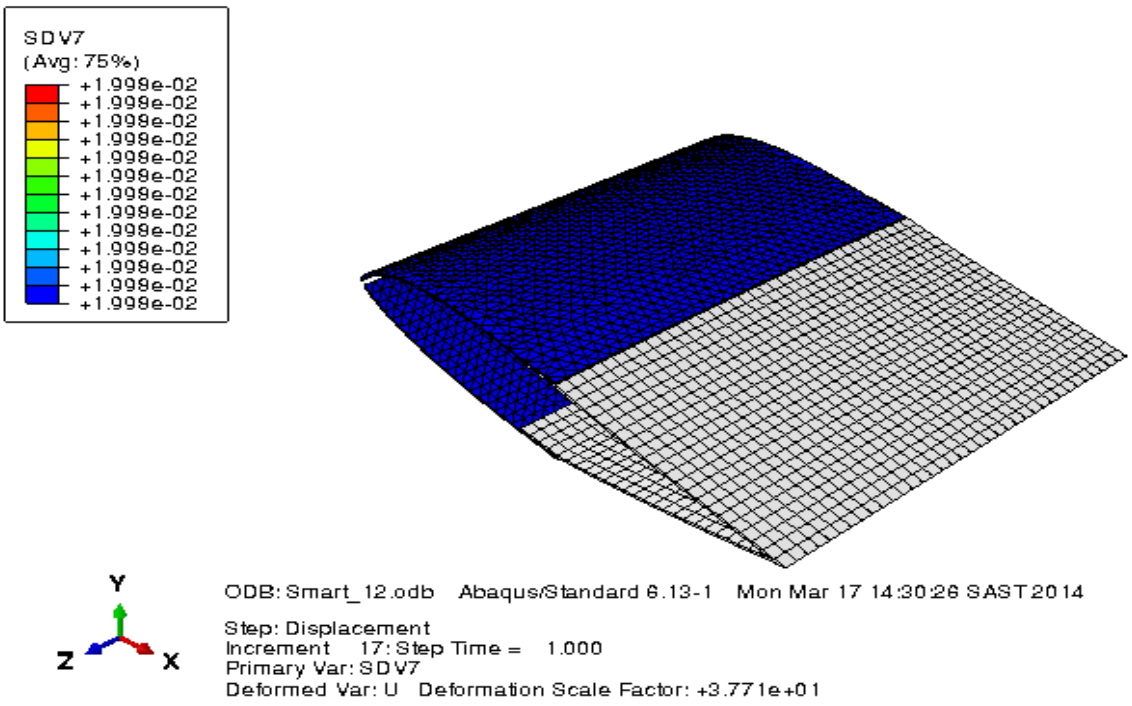


**Figure C 10: Martensite volume fraction at the end of the actuation step**

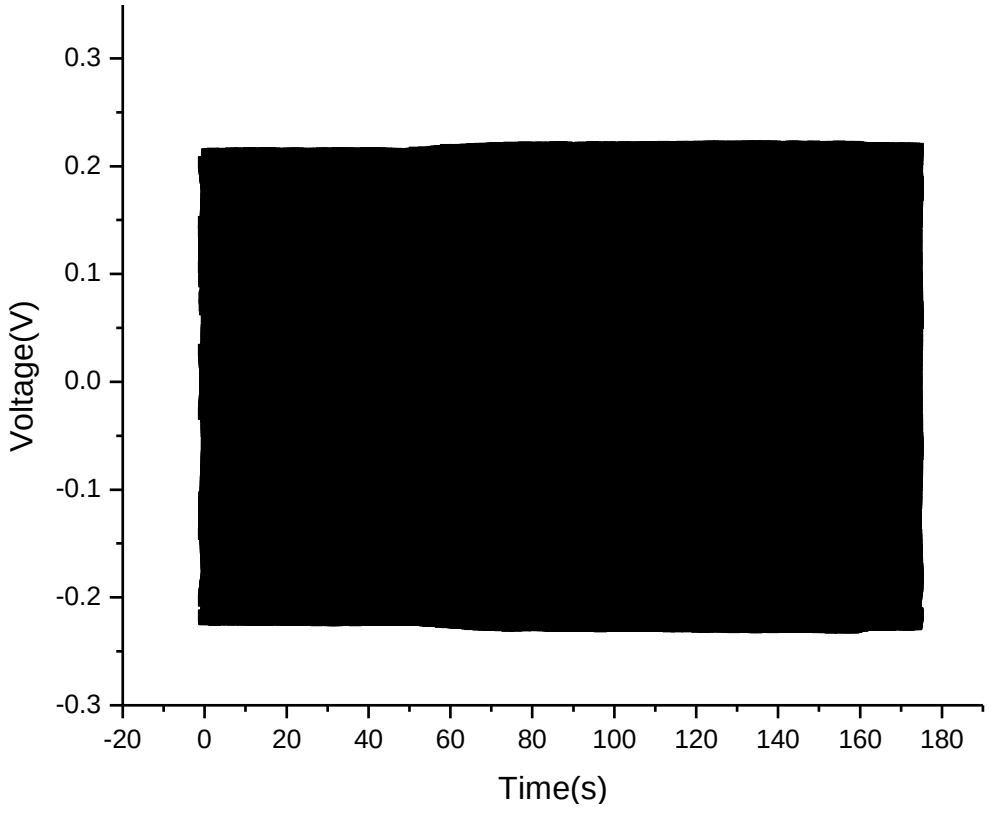


**Figure C 11:Demonstration of displacement-time data for maximum load experiment for NiTi SMA wire**

# Appendix D

## Shape memory alloy user material model code

```
      SUBROUTINE UMAT(STRESS, STATEV, DDSDDE, SSE, SPD, SCD,
     RPL,
     1 DDSDDT, DRPLDE, DRPLDT, STRAN, DSTRAN, TIME, DTIME, TEMP,
     DTEMP,
     2 PREDEF, DPRED, CMNAME, NDI, NSHR, NTENS, NSTATV, PROPS,
     NPROPS,
     3 COORDS, DROT, PNEWDT, CELENT, DFGRD0, DFGRD1, NOEL,
     NPT, LAYER,
     4 KSPT, KSTEP, KINC)

C
      INCLUDE 'ABA_PARAM.INC'
C
      CHARACTER*8 CMNAME
C
      DIMENSION STRESS(NTENS), STATEV(NSTATV), DDSDDE(NTENS,
     NTENS),
     1 DDSDDT(NTENS), DRPLDE(NTENS), STRAN(NTENS),
     DSTRAN(NTENS),
     2 PREDEF(1), DPRED(1), PROPS(NPROPS), COORDS(3), DROT(3, 3),
     3 DFGRD0(3, 3),
     DFGRD1(3,3),EACT(NTENS),EELAS(NTENS),ETH(NTENS)
      REAL EMOD,ENU,EBULK3,EG2,EG,EG3,ELAM,FLAG,MP0,AS,EMOD1,
     1 EBULK31,EG21,EG1,EG31,ELAM1,EA,EM,MS,MF

      INTEGER I,J

C     ELASTIC PROPERTIES----------------------------------------
      MP0=0.50
      QA = 0.0785
      AS = 67
      MF = 25
      MS = 58
      EMOD=70E3
      ENU=0.3
      EA = 70E3
      EM=28.3E3
```

```
      STRANMAX=6.0
      EBULK3=EMOD/(1.0-2.0*ENU)
      EG2=EMOD/(1.0+ENU)
      EG=EG2/2.0
      EG3=3.0*EG
      ELAM=(EBULK3-EG2)/3.0
C     TRAINING  STEP
      FLAG=ABS(STATEV(1))+ABS(STATEV(2))+ABS(STATEV(3))
C-----------------------------------------------------------------
      IF(TEMP.GT.500.AND.FLAG.LE.0)  THEN
C ELASTIC STIFFNESS
C
       DO I=1, NDI
         DO J=1, NDI
           DDSDDE(J,I)=ELAM
         END DO
          DDSDDE(I,I)=EG2+ELAM
       END DO
       DO I=NDI+1,  NTENS
        DDSDDE(I,I)=EG
       END DO
C
C CALCULATE STRESS
C
       DO I=1, NTENS
         DO J=1, NTENS
           STRESS(J)=STRESS(J)+DDSDDE(J,I)*DSTRAN(I)
         END DO
       END DO

         DO I=1,6
          STATEV(I)=DSTRAN(I)
         END DO
       END IF
C-----------------------------------------------------------------
C
C     ACTUATION  STEP
       IF(TEMP.LT.AS) THEN
        STATEV(7)=0.0
         ENDIF
```

```
      IF(FLAG.GT.0) THEN
        IF(TEMP.GE.AS.AND.TEMP.LT.200)STATEV(7)=(MP0*
     1  (1.0-(TANH(QA*(TEMP-AS)-1.0))))

C
C        VARIATION OF YOUNGS MODULUS WITH TEMPERATURE----------
------
       EMOD1=EA*(1.0-STATEV(7))+EM*STATEV(7)
       EBULK31=EMOD1/(1.0-2.0*ENU)
       EG21=EMOD1/(1.0+ENU)
       EG1=EG21/2.0
       EG31=3.0*EG1
       ELAM1=(EBULK31-EG21)/3.0
C
C       ELASTIC STIFFNESS-----------------------------------------
C
         DO I=1, NDI
        DO J=1, NDI
          DDSDDE(J,I)=ELAM1
        END DO
         DDSDDE(I,I)=EG21+ELAM1
      END DO
      DO I=NDI+1,  NTENS
       DDSDDE(I,I)=EG1
      END DO
C
C CALCULATE STRESS
C
      DO I=1, NTENS
       DO J=1, NTENS
         STRESS(J)=STRESS(J)+DDSDDE(J,I)*
     1 (DSTRAN(I)-STATEV(I)*STRANMAX*(STATEV(7)))

       END DO
      END DO
      END IF
C---------------------------------------------------------------
     RETURN
     END
```